Differential Rotation, Radiative Equilibrium, and Local Hydrodynamic Stability in Stellar Interiors

Andrea Caleo

Astrophysics Department

University of Oxford

A thesis submitted for the degree of

Doctor of Philosophy

November 2016

Il grande orologiaio non passa più,
e gli orologi li aggiustiamo noi.
Adesso costruiamo le macchine,
vedessi come sono belle, sai.
(R. Vecchioni)

The great watchmaker has stepped down,
so now we fix the clocks ourselves.
We move around by plane now,
if only you could see it...

Acknowledgements

This thesis would have never come to be without the many people who made me discover a passion for science. Most importantly, my parents; then, a number of very good maths and physics teachers (most importantly two Giuseppes, Pezzica and Ghelardini); and finally, the Italian Physics Olympiads.

More recently, the support received from my girlfriend Ashley, who also proofread this thesis, has been invaluable. Among my friends, Leslie and Mark helped me understand the changes in my life and direct my efforts and willpower towards fruitful directions. My colleagues, Andrea and Andre, went through this journey with me. Being able to vent to them has been important.

Thanks to William, the quality of the work presented here is much higher than what it would have otherwise been. I must thank him for criticising my approach during my first year, and the many discussions during my PhD. With his intelligence and positively skeptical approach, he will be amazingly successful in his future. He also gave me the template for this thesis.

Steven Balbus is both a good supervisor and an extremely gifted scientist; without him, this thesis would have been impossible. The intuition at the basis of the model presented here was his, not mine; and his continued help throughout these 3 years has made this all possible.

Among my professional collaborators, prof. Scilla Degl'Innocenti and Emanuele Tognelli at the University of Pisa have prepared the stellar models which I used in the analysis of Chapter 5. They have been extraordinarily patient with me. I also want to thank prof. Quataert, Mikhail Belyaev and Daniel Lecoanet for inviting me to visit UC Berkeley and having some useful exchanges, and Matteo Cantiello for my visit at UC Santa Barbara. I have also had useful discussions with Fabian Schneider in Oxford.

I have been supported by a departmental grant made possible by a donation from the Hintze Foundation, to which I am grateful. I have also been awarded a Senior Carreras scholarship by the Hertford college.

Abstract

Differential Rotation, Radiative Equilibrium, and Local Hydrodynamic Stability in Stellar Interiors

Andrea Caleo

Hertford College, University of Oxford

Submitted for the degree of Doctor of Philosophy

Michaelmas Term, 2016

The problem of angular momentum transport in the radiative zone of the Sun and other stars is currently one of the most discussed in stellar astrophysics. A wide range of local and global instabilities acting in differentially rotating stars have been studied and incorporated in stellar evolutionary codes. In this thesis, I revisit two of the hydrodynamic processes that are thought to operate, namely the Eddington-Sweet (ES) circulation and a global motion induced by the Goldreich-Schubert-Fricke (GSF) instability, and investigate stellar models in which these mechanisms are suppressed. In particular:

(a) The data from helioseismology show that the upper radiative zone of the Sun is in near-uniform rotation, but they have a significant uncertainty. I discuss the possibility of patterns of differential rotation compatible with the constraint of perfect radiative equilibrium, which implies the absence of ES circulation. I show that this constraint leads to a set of ordinary differential equations for the stellar rotation profile, which are solved numerically. I find that these models can be quite close to uniform rotation, and compatible with the data from helioseismology.

(b) I investigate the dynamical stability of these models. It is shown that while a naive approach would suggest that the GSF instability would distrupt the rotation of these stars, this does not happen in reality. I present a study of the local stability of stratified, weakly magnetized, differentially rotating fluids to non-axisymmetric perturbations with finite heat conductivity, kinematic viscosity, and resistivity. The models are found to be locally stable under rather general circumstances. Even if the molecular viscosity is very small compared to the heat conductivity, it suffices to suppress the GSF instability.

(c) I examine the onset of the GSF instability in the core of red giant stars, where, according to recent observations, strong differential rotation may be present. I derive constraints on the amount of shear necessary for the GSF instability to operate at different depths, and show that very strong shear is required. In general, the effectiveness of the GSF instability in transporting angular momentum is currently overstated.

Declaration of Authorship

Part of the original work in this thesis has been published in the following 3 papers:

Chapter 3 and section A.1 - Andrea Caleo, Steven A. Balbus, and William J. Potter, 2015, MNRAS, 448, 2077.
Chapter 4 - Andrea Caleo and Steven A. Balbus, 2016, MNRAS, 457, 1711.
Chapter 5 - Andrea Caleo, Steven A. Balbus, and Emanuele Tognelli, 2016, MNRAS, 460, 338.

I hereby certify that the work in this thesis is wholly my own, except for the contributions made by the aforementioned co-authors during the writing of the papers.

Contents

Chapter 1

Introduction: the observations

The content of this thesis concerns the physics of rotation and radiative energy transfer in stars. Although the original work presented here is of theoretical nature, my results involve the analysis of recent data on the Sun and other rotating stars. For this reason, this chapter gives a summary of recent observational techniques and of the results that will be analysed in the rest of the thesis. The purpose is not to introduce these concepts to the reader for the first time, but to refresh their memory about certain issues (e.g. limitations of the techniques, uncertainties in the Solar radiative zone) that will be important for what follows. Chapter 2 is an introduction to the theoretical results necessary for understanding the rest of the thesis, while chapters 3-5 present the original work contained in this thesis.

1.1 Historical overview of stellar rotation

The discussion on stellar rotation began around the year 1610, when astronomers from several western European countries observed the Sun by means of a new invention, the telescope. Among these astronomers was Galileo Galilei, who reported his results under the title "Istoria e Dimostrazioni intorno alle Macchie Solari e loro Accidenti" (literally "Stories and demostrations around the sun spots and their accidents"). Figure 1.1 shows two of the 38 drawings of the Solar surface that Galileo reproduced to study the motion of the sunspots. In this collection of letters, Galileo argues that the dark spots he observed are attached to the surface of the Sun, and their motion proves that our star rotates around an axis through its centre. A few years later Cristopher Scheiner, a German astronomer contemporary of Galileo, was able to study the motion of the sunspots and establish an approximate rotation period of 27 days, a remarkably accurate figure.

More than two centuries elapsed before new quantitative results on the Solar rotation were found. In the second half of the 19th century, Richard Carrington and Gustav Spörer studied long series of sunspots observations and noticed that the period of rotation of the Sun depends

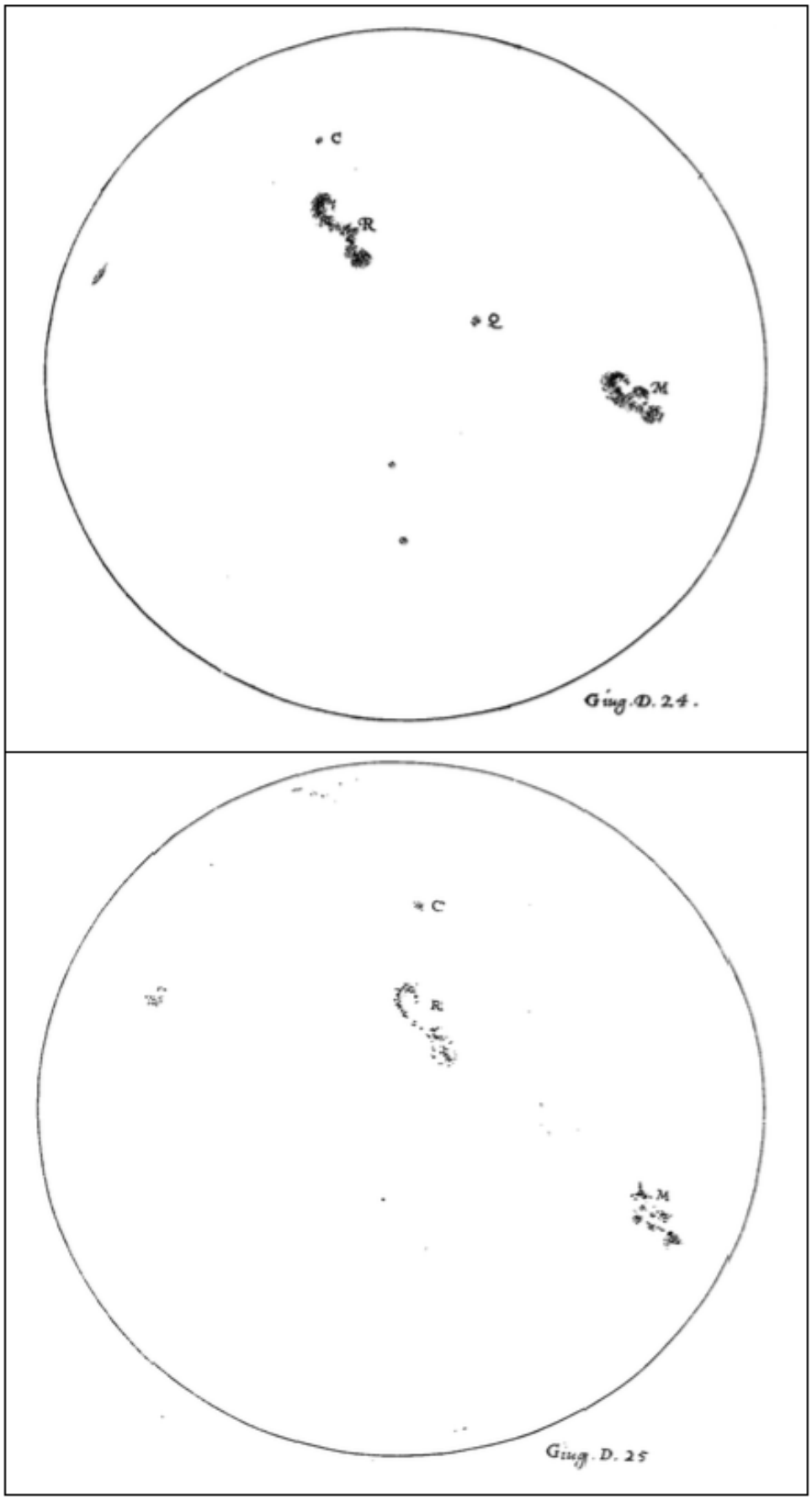

Figure 1.1: Sunspots observed by Galileo Galilei on 24/6/1612 and 25/6/1612. Figures extracted from Galilei et al. [1613].

on the distance from the equator. Hervé Faye approximated the observed angular rotation with the formula:

$$\Omega(\text{deg / day}) = 14^\circ 37' - 3^\circ 10' \sin^2\theta, \tag{1.1}$$

where θ is the latitude. This expression is equivalent to an expansion of Ω to the second Legendre polynomial, something very similar to what is still done today to describe the rotation of both the Solar surface and interior (usually Ω^2, not Ω, is now expressed in this way; see chapter 3).

With the invention of spectroscopy, the end of the 19th century saw the first studies of spectral line widths which eventually allowed astronomers to measure the rotation rate of other stars. The first successful systematic investigations were conducted in the late 1920s and early 1930s by a group led by Otto Struve, see e.g. Shajn and Struve [1929]. The measurements of $v \sin i$ showed that while the Sun rotates relatively slowly, with a velocity at the equator of about 2 km s^{-1}, many stars rotate much faster, with speeds up to a few hundred km s^{-1}. Over the years, many observations were collected and quantitative analyses of the results became possible.

The latest observational breakthrough comes from helio- and astero-seismology, the study of the pulsations of the stellar surface induced by resonant acoustic waves that propagate throughout its structure. One of the first reported observations is that by Deubner [1975]. The analysis of these pulsations allows us to gather information on the interior of the structure, and in some cases to determine the angular velocity well beneath the surface. In the last 30 years, the results from helioseismology have arguably revolutionised the field of Solar physics, and the recent advances in asteroseismology are such that the same is happening now to the more general field of stellar physics. The next section aims to provide a basic understanding of these techniques, while the rest of this chapter presents the data for the Sun and other stars.

The reader interested in the 20th century historical developments is referred to Tassoul [2000], from which part of the information reported here has been extracted and which contains a chapter dedicated to this topic.

1.2 Helioseismology and asteroseismology

There are numerous reviews on helioseismology and asteroseismology. The structure and content of this section follows the works of Howe [2009] and Gizon and Birch [2005], in addition to the other papers quoted in the text.

1.2.1 Stellar pulsations

The main purpose of helioseismology is to study the oscillations of the surface of the Sun. The data collected by the instruments are time series of measurements of the Doppler velocity of the resolved photosphere, collected over many consecutive months or even years. Figure 1.2

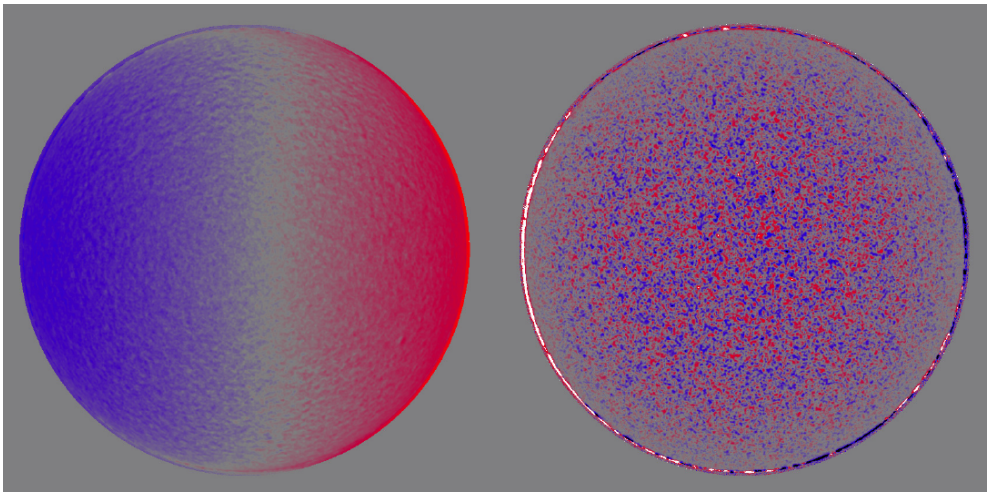

Figure 1.2: Doppler velocity image of the Solar photosphere (left), and the difference between that image and the one taken one minute earlier (right). Red and blue respectively correspond to motion away from and towards the observer. The figure is from Howe [2009]. The data are from the Global Oscillation Network Group.

shows a Doppler velocity image of the Sun with data from the Global Oscillation Network Group (hereafter GONG, see e.g. Harvey et al. 1996 and Hill and et al. 1996). GONG is a six-station network of sensitive, stable velocity imagers located around the Earth to monitor the surface of the Sun, and provides the data used in this thesis.

The Solar surface pulsates; the power spectrum peaks at a frequency which corresponds to a period close to 5 minutes. The discovery of these pulsations [Leighton et al., 1962] marked the initial research on helioseismology. The oscillations were soon interpreted as standing acoustic waves in the photosphere [Ulrich, 1970]. We now know that the oscillations are composed of a multitude of modes at discrete frequencies, thousands of which have been identified for the Sun. This wealth of information is our window into the interior of the Sun, which was considered unobservable before these discoveries. For an extensive reference on stellar pulsations see Christensen-Dalsgaard [2003]. To illustrate the five-minute oscillations, figure 1.3 shows an $l = 0$ time series of the velocity of the surface of the Sun (which is essentially given by the surface average of the data of figure 1.2).

The oscillations of the fluid elements of a star can be represented by a linear superposition of eigenmodes. Each mode is specified by three integer numbers: the radial order, n; the spherical harmonic degree, l; and the azimuthal order, m. The radial displacement of the fluid element can be expressed as:

$$\delta r(r,\theta,\phi,t) = \sum_{n,l} \sum_{m=-l}^{l} a_{nlm}\, \xi_{nl}(r)\, Y_l^m(\theta,\phi)\, e^{\mathrm{i}w_{nlm}t}, \tag{1.2}$$

where r is the radius, θ is the co-latitude, ϕ is the longitude, t is time, a_{nlm} is the amplitude of the mode with indices (n,l,m), ξ_{nl} is the radial eigenfunction of this mode, and w_{nlm} its frequency. n is the number of nodes of ξ_{nl}, l gives the number of nodal lines of $Y_l^m(\theta,\phi)$ on the

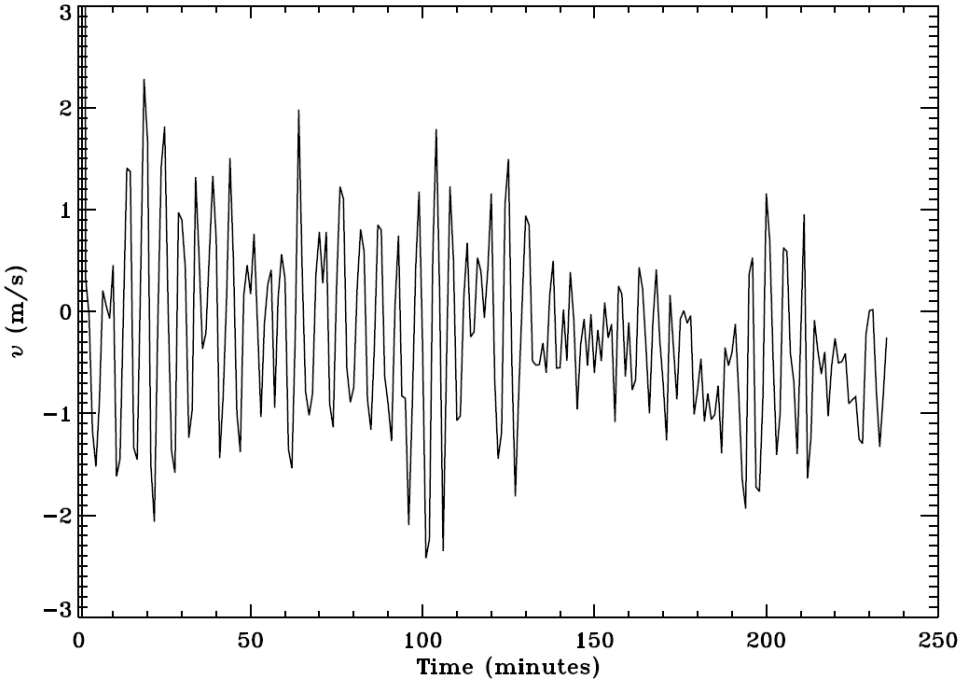

Figure 1.3: Segment of an $l = 0$ time series of Doppler velocity observations of the Solar photosphere, showing the appearance of the five-minutes oscillations. The figure is from Howe [2009]. The data are from the GONG.

surface of the sphere (i.e. the number of θ_is for which $Y_l^m(\theta_i, \phi) = 0$), and m indicates how many of these lines cross the equator. A spherically symmetric star would be characterized by a spectrum of azimuthally degenerate frequencies, so that w_{nlm} would not depend on m. However, rotation lifts this degeneracy, and the study of how w_{nlm} depends on m allows us to infer the internal rotation profile of the star.

Each mode corresponds to a standing acoustic wave that propagates beneath the photosphere and, as such, can be refracted in the medium. For this reason, different modes reach a different depth in the Sun. In particular, only modes with low l, and therefore a less rich angular structure, penetrate to the core of the star, while modes with high l (and therefore the only modes which can have high values of m) are confined to the outer layers. Unfortunately, only the latter provide information on the rotation of the star, as this affects only the m-dependence of the modes, as noted above. Moreover, modes with different values of m affect the surface at different latitudes, with modes with large $|m|$ having a smaller effect on the material near the poles of the star. For these reasons, the resolution of the rotation profile measured with these techniques will be better near the surface of the star than near its nuclear core, and will also be better near the equator than near the poles.

The modes described so far are called "p modes", because their restoring force is pressure; they are excited near the photosphere and for the most part suppressed or deflected when they propagate towards the interior. Another type of modes, known as "g modes", have gravity (buoyancy) as their restoring force, they have large amplitudes in the Solar core but are less likely to reach the surface of the star. Although astronomers have been trying to identify them for at least a decade, there is no confirmed detection of g modes for the Sun. However,

mixed modes, i.e. modes that are born as g modes in the stellar core and excite p modes in the outer convective layer, can and have been detected in other stars, including red giants (see Bedding et al. 2010, Beck et al. 2011) and white dwarfs [Charpinet et al., 2009]. In fact, the recent identification and still ongoing interpretation of mixed modes represents the most striking success of asteroseismology in the recent years, and is providing us with an unexpected amount of information on the internal structure and rotation of these stars.

1.2.2 The inversion problem

Once the frequencies of the surface oscillations have been detected and identified, one needs to use them to infer the internal rotation profile of the star. This is not an easy task. I illustrate here the difficulties involved in this process in order to better understand the limitations of helioseismology.

Consider a number M of helioseismological observations d_i, where $i = (n, l, m)$, from which we need to infer the stellar rotation profile $\Omega(r, \theta)$ (in this thesis, I always assume that the background structure and the rotation profile are azimuthally symmetric). Each d_i will depend on a correctly specified average of $\Omega(r, \theta)$ in the structure:

$$d_i = \int_0^{R_\odot} \int_0^{\pi} K_i(r, \theta)\ \Omega(r, \theta)\ dr d\theta + \epsilon_i, \tag{1.3}$$

where $R_\odot$ is the solar radius, ϵ_i the error on the measurement, and the weighing function $K_i(r, \theta)$ depends on the Solar model. K_i is called a *kernel* and expressions for K_i are given in the literature; see e.g. Schou et al. [1994]. The aim of the inversion problem is to express the inferred angular velocity profile $\bar{\Omega}(r, \theta)$ as a linear combination of the data points:

$$\bar{\Omega}(r_0, \theta_0) = \sum_{i=1}^{M} c_i(r_0, \theta_0) d_i, \tag{1.4}$$

where (r_0, θ_0) is the location at which we infer the angular velocity and the c_is are to be found.

Once the coefficients of the inversion problem have been calculated (see below), $\bar{\Omega}(r, \theta)$ can be expressed in terms of $\Omega(r, \theta)$ by combining equations (1.3) and (1.4) as:

$$\bar{\Omega}(r_0, \theta_0) = \int_0^{R_\odot} \int_0^{\pi} \kappa_i(r_0, \theta_0; r, \theta)\ \Omega(r, \theta)\ dr d\theta + \epsilon_0, \tag{1.5}$$

where

$$\kappa_i(r_0, \theta_0; r, \theta) = \sum_{i=1}^{M} c_i(r_0, \theta_0)\ K_i(r, \theta) \tag{1.6}$$

is known as the *averaging kernel* for the location (r_0, θ_0) and ϵ_0 is an error term. Equations (1.5) and (1.6) show that the inferred value at (r_0, θ_0) actually depends not just on $\Omega(r_0, \theta_0)$,

but also on the angular velocity in a region surrounding this point. The spatial scale, or resolution, of this region depends on that of κ_i. Therefore, while the formal uncertainty of the inferred profile may be expressed as:

$$\sigma^2[\bar{\Omega}(r_0,\theta_0)] = \sum_{i=1}^{M}[c_i(r_0,\theta_0)\sigma_i]^2, \tag{1.7}$$

where σ_i is the uncertainty on $c_i(r_0,\theta_0)$, spatial correlation of the errors makes the problem significantly more complicated than that.

For these reasons, the errors on the rotation profile inferred from helioseismology are not easy to determine. In particular, they are spatially correlated. Moreover, the finite resolution of the averaging kernels makes it impossible to resolve very steep changes of angular velocity, for example in a thin shear layer.

1.2.3 Solution of the inversion problem

The inversion problem is complex and many solutions have been proposed over the decades; I present here just one example. The reader interested in a more detailed discussion and a comparison of different techniques is referred to Christensen-Dalsgaard et al. [1990], Schou et al. [1994], and Aerts et al. [2010], on which the following discussion is based.

One of the procedures used to determine the inversion coefficients $c_i(r_0,d_0)$ is the technique of *optimally localized averages* (OLA), originally proposed by Backus and Gilbert [1970] for the study of Earth data. The idea is to select coefficients c_i to make the averaging kernels $\kappa_i(r_0,\theta_0;r,\theta)$ as similar as possible to a delta function $\delta(r-r_0,\theta-\theta_0)$. It is immediately clear from equation (1.5) that this would make $\bar{\Omega}(r_0,\theta_0)$ similar to $\Omega(r_0,\theta_0)$. This is achieved by determining the coefficients c_i such as to minimise:

$$\int(\boldsymbol{r}-\boldsymbol{r}_0)^2\kappa(\boldsymbol{r}_0,\boldsymbol{r})^2 d\boldsymbol{r} + \mu\sum_i c_i(\boldsymbol{r}_0)\sigma_i^2, \tag{1.8}$$

subject to the constraint

$$\int\kappa(\boldsymbol{r}_0,\boldsymbol{r})^2 d\boldsymbol{r} = 1, \tag{1.9}$$

where $\boldsymbol{r},\boldsymbol{r}_0$ are the vector positions of (r,θ), (r_0,θ_0) respectively, and μ is a regularisation parameter. The first term in equation (1.8) requires that κ does not deviate much from a δ function; the second term prevents the coefficients $c_i(\boldsymbol{r}_0)$ from assuming arbitrarily large values, which would increase the error on the final result, see equation (1.7).

The optimisation problem above can be reduced to a linear problem via the Lagrange multipliers technique. The principal difficulty of the OLA method is that it is computationally expensive; the references reported above discuss other techniques of more practical use.

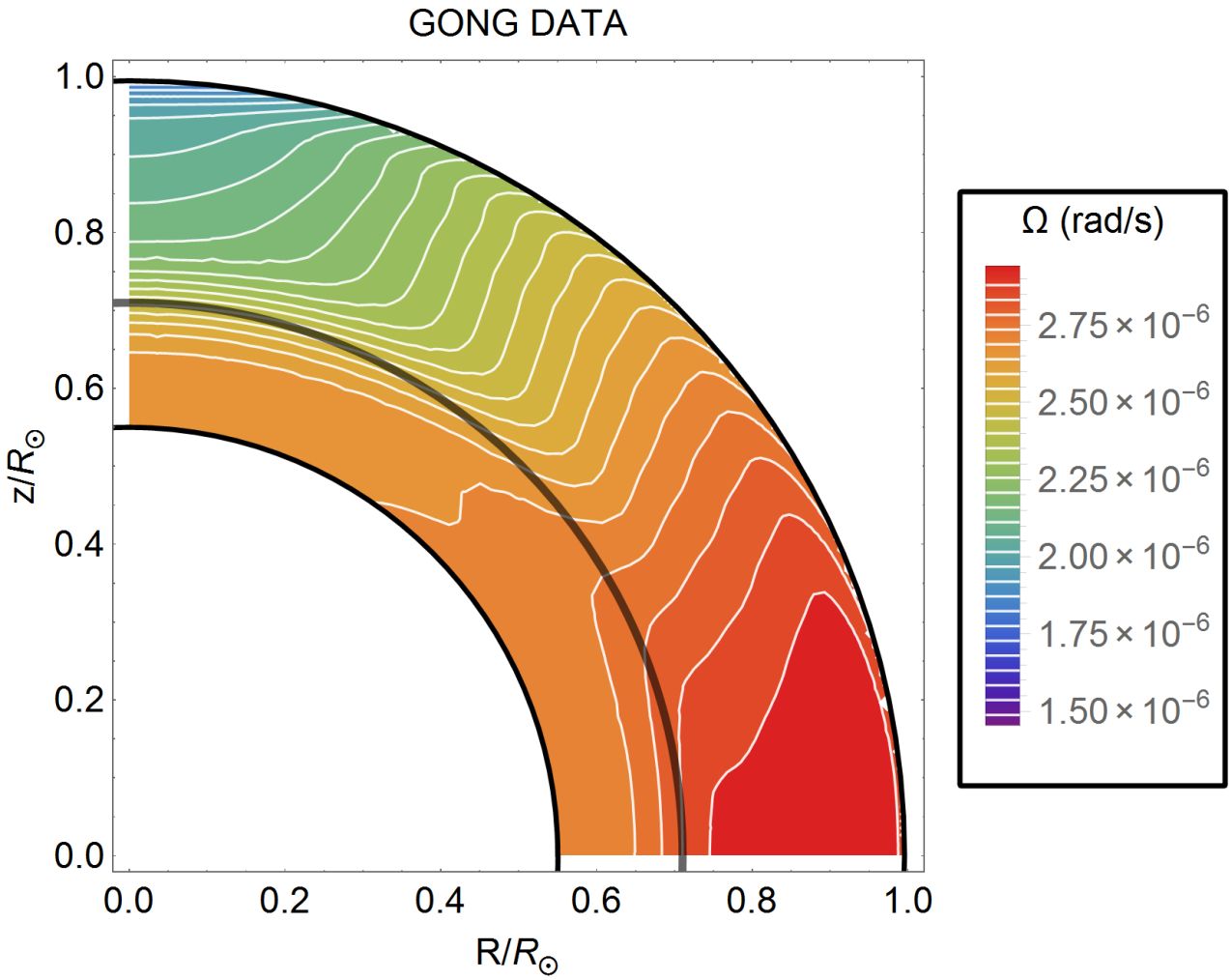

Figure 1.4: Angular velocity in a quarter of a meridional section of the Sun, at spherical radius $r > 0.55$ R$_\odot$. The axes show cylindrical coordinates (R, z), where $\hat{z}$ is the rotation axis. The thin white lines show the isocontours of angular velocity. The thick dark grey line marks the location of the tachocline (see section 1.3.2). GONG data courtesy of R. Howe.

1.3 The internal rotation of the Sun

The astronomers have been using helioseismology to understand the interior rotation of the Sun for more than 20 years, and most (but not all) of the results are now well established and commonly agreed upon. For this reason, there have been several reviews on this topic. I refer the reader to Howe [2009] and Thompson et al. [2003] for treatments which are unavoidably more detailed than that of this section, and for a historical overview of the observational results.

The angular velocity in the Sun for $r > 0.55$ R$_\odot$, where r is the distance from the centre of the star, is shown in figure 1.4. I will discuss some features of the data in three distinct regions: the convective zone, the tachocline, and the radiative zone.

1.3.1 The convective zone

As I discussed in section 1.2.2, the data from helioseismology are more accurate in the outer part of the Sun than in the deeper layers. For this reason, the results on the convective zone are the most reliable. The dynamics of this region has been studied extensively and it is now arguably the most understood.

When the data on the rotation of the convective zone started accumulating in the late 1990s, with results similar to those of figure 1.4, the astronomers were caught by surprise. They were expecting to find a pattern of rotation constant on cylinders parallel to the axis of rotation of the system (i.e., with the property $\partial_z \Omega = 0$, where $\hat{z}$ is the unit vector along the axis of rotation). This is mostly due to the Taylor-Proudman theorem, a well-known result of elementary fluid dynamics part of most standard textbooks, see e.g. Acheson [1990]. Early numerical experiments were also in general agreement with this constraint.

There is now no doubt that the rotation is, in fact, *not* constant on cylinders. The angular velocity in the convective zone shows a dependence on latitude which is similar to the one at the photosphere. At central latitudes Ω is approximately, but not quite, constant on lines of fixed co-latitude θ. However, this does not hold true near the equator and at the poles.

A theoretical explanation of these results has been given on the basis of an interplay between rotation and entropy-driven convection, see Balbus et al. [2009]. These authors recovered the shape of the isocontours with excellent precision, and showed that this can be done only if a crucial term $\boldsymbol{\nabla}\rho \times \boldsymbol{\nabla}P$ is carefully treated in the equations of fluid dynamics, where ρ and P are the density and pressure of the plasma. This term is typically small compared to other terms (the stratification in the convective zone is close to an adiabatic relation $P \cong C\rho^{\gamma}$, so that the vectors $\boldsymbol{\nabla}\rho$ and $\boldsymbol{\nabla}P$ are almost parallel), and for this reason it is difficult to capture this effect in numerical simulations, which in the past have for the most part reproduced patterns of rotation constant on cylinders. Nonetheless, recent hydrodynamic codes do give results that resemble the results of figure 1.4, at least qualitatively [Brun et al., 2011].

1.3.2 The tachocline

The *tachocline* is the thin layer of transition between the convective and radiative zone. Its name comes from the greek word "tachýs", fast, and was chosen to emphasize that this transition is particularly steep. Although its detection is due to helioseismology, the idea of a layer of strong shear between the two regions had been in the literature for many years before its observational discovery.

The location of the base of the convective zone and hence the upper part of the tachocline is generally quoted as $r = 0.713\ \mathrm{R}_{\odot}$ [Christensen-Dalsgaard and Thompson, 2007]. However, as previously discussed, the techniques of helioseismology are not ideal to detect shear layers which almost resemble a discontinuity. The resolution of the averaging kernels at the base of the convective zone is not excellent and this causes great uncertainty in the width of the

tachocline itself. Conservatively, the width is between 1% and almost 10% of the Solar radius (M. Miesch, private communication), though most estimates are in the 1% – 5% range (see Howe 2009). Special techniques that do not require standard inversion procedures have been designed to better investigate the thickness of the tachocline, and these seem to favour a very thin layer of width of about 1% $R_\odot$ [Antia and Basu, 2011], although the community is still cautious on accepting these results.

A range of theoretical issues are involved in modelling a layer of strong shear at the base of the convective zone. Most importantly, it has been proposed that the tachocline may be the region where the Solar magnetic field is generated, before it penetrates into the convective zone [Gough and McIntyre, 1998]. A complete understanding of the magnetohydrodynamic processes acting in this layer would contribute to solve problems that are many decades old.

Of particular interest to this thesis is the issue of the *spreading of the tachocline*. Not long after the detection of the tachocline, it was argued by Spiegel and Zahn [1992] that a thin shear layer at the base of the convective zone must eventually spread into the radiative zone and disrupt its uniform rotation. Theorists have been considering effects that would prevent the spreading of the tachocline; the candidate mechanisms include turbulent hydrodynamic processes, magnetic confinement, and gravity waves transport from the tachocline. Given its relevance to the work that will be presented here, the argument by Spiegel and Zahn [1992] is discussed further in section 2.3 of this thesis. One of the aims of my work is to present an alternative model for the rotation of the Solar radiative zone, one that is compatible with the data presented here and is not subject to the issue of the spreading of the tachocline.

Understanding the processes taking place in the tachocline would be very important to improve our comprehension of the Sun. For this reasons, considerable effort has gone into modelling this shear layer. A review entirely dedicated to this subject is the book edited by Hughes et al. [2007].

1.3.3 The radiative zone

Just as in the case of the convective zone, theorists had reasons to expect to find a pattern of rotation with $\partial_z \Omega = 0$ in the radiative zone too. This was in this case due to Goldreich-Schubert-Fricke instability, which will be discussed in sections 2.4 and 2.5 of this thesis. In fact, the observational results on the radiative zone and the nuclear core of the Sun are simply stated: they are compatible not just with rotation on cylinders, but with uniform rotation, with an angular velocity close to the mean value of Ω in the convective zone.

What is particularly relevant for this thesis, however, is an estimate of the errors. As mentioned above, the uncertainty is larger the greater the depth in the structure, and quoting a specific value for the error at a given location may be misleading because the errors are correlated. A conservative estimate is that the relative error on Ω beneath the tachocline is at least 10% (R. Howe, private communication), although some authors report errors of just a few percent in the upper part of the radiative zone. To illustrate how the errors increase

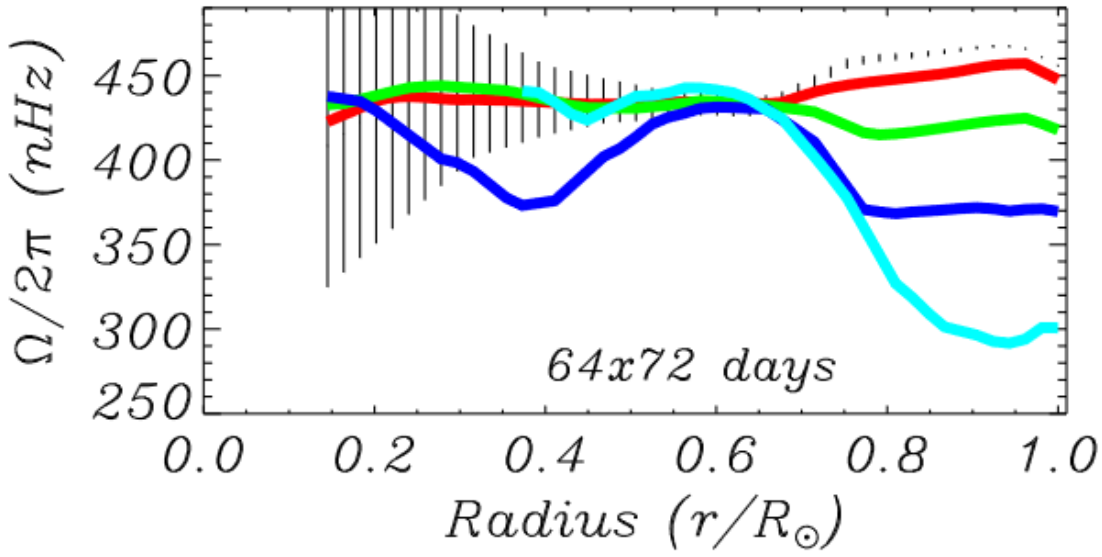

Figure 1.5: Rotational profile obtained from the inversions of a GONG data time series of 64 x 72 days. The red, green, dark-blue, and light-blue lines correspond to latitudes of 20, 40, 60, and 80°respectively. The centre of the vertical lines indicates the angular velocity at the equator (latitude of 0 °), while the lines itself are the respective error bars. GONG data, figure from Eff-Darwich and Korzennik [2013].

with depth, figure 1.5 shows a measurement of the angular velocity at various latitudes in the radiative zone, and the error bar for the value relative to the equator. Note that the error near the poles is always larger than at the equator, so that the figure effectively shows a lower bound for the error at mid-latitudes.

The error is undoubtedly large in the lower radiative zone and the nuclear core of the Sun, and the results concerning these regions are barely reliable. For this reason, I have not shown them in figure 1.4.

1.4 The internal rotation of other stars

1.4.1 Observed features

In the last decade, asteroseismology has allowed us to infer some information on the internal rotation of red giant stars and, more recently, subgiants. This was made possible by the detection and interpretation of mixed modes in the light curves of these stars. Mixed modes originate as gravity waves trapped in the radiative core of a star, and under favourable conditions they become coupled to p-modes that propagate in the convective envelope and reach the photosphere. Dupret et al. [2009] reports a theoretical study of these modes and discusses the possibility of detection in the light curves of red giants.

While detections of mixed modes from ground-based observatories had already been reported, the breakthrough occurred with the data from the satellite missions *Kepler*, see Bedding et al. [2010] and Beck et al. [2011], and CoRoT, see Mosser et al. [2010] and Mosser et al.

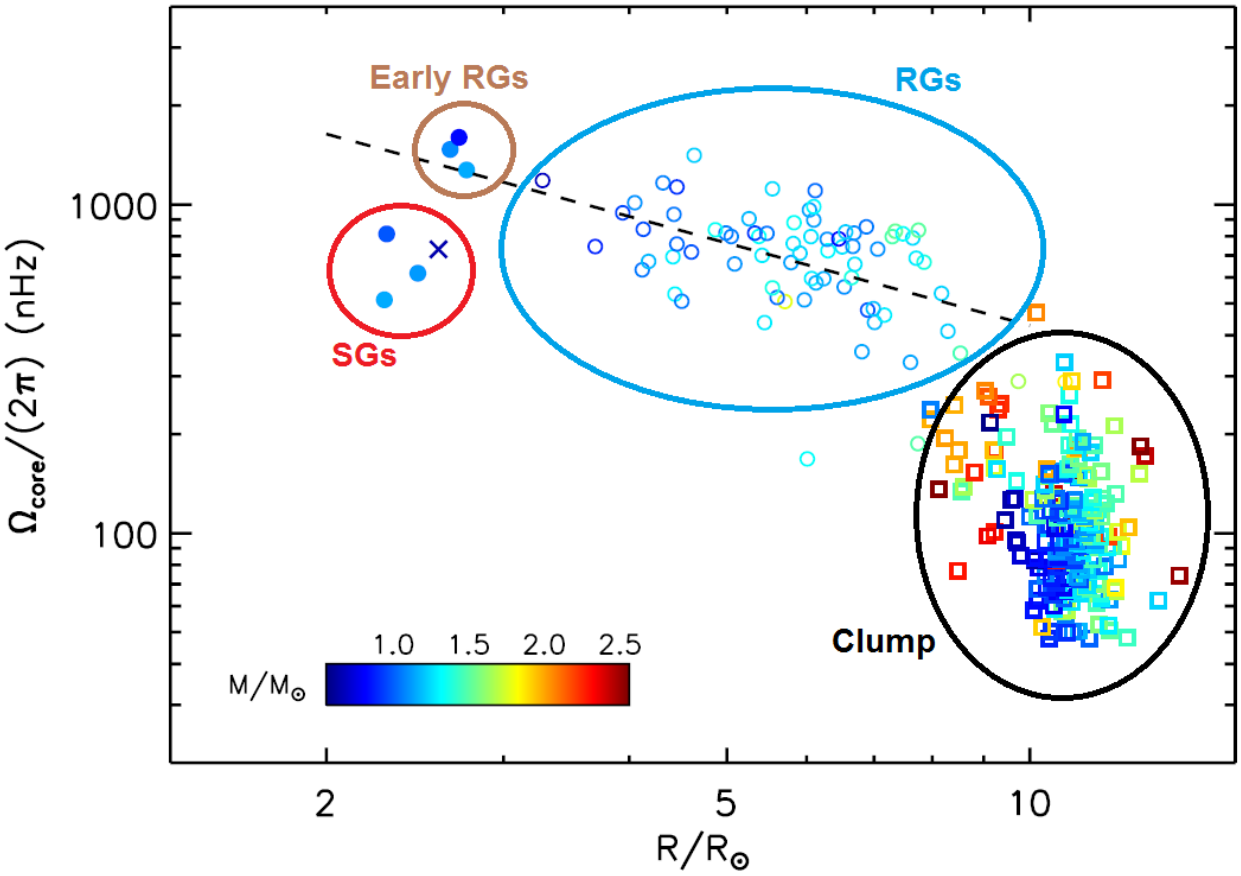

Figure 1.6: Core rotation rate as a function of the stellar radius. Original figure from Deheuvels et al. [2014]. Filled circles: subgiants and young red giants from that paper; cross: young red giant from Deheuvels et al. [2012]; open circles: red giants from Mosser et al. [2012]; open squares: clump stars from the same paper.

[2011]. The analysis of these data produces a scenario for the evolution of the angular velocity Ω_c of the core of these stars, which we summarise here. This field is so recent that, although a considerable amount of work has been done and some results are now well established, there is a scarcity of review articles on this subject. We refer the reader to Beck et al. [2012] and Mosser et al. [2012] for the results on red giant stars, and to Deheuvels et al. [2014] for those on subgiants.

In brief, the results show that the angular velocity of the core increases as a star becomes a subgiant, and then it progressively declines as the star ascends on the red giant branch. The angular velocity at the end of the evolution is one or two orders of magnitude lower than at its maximum, achieved on the subgiant phase. Figure 1.6 shows the measured values of Ω_c as a function of the stellar radius, which is related to its evolutionary stage, and illustrates these properties for subgiants, red giants, and clump stars[1].

It is important to stress here the limitations of the asteroseismological measurements. Unlike the Sun, the other stars are not resolved in our observations and what we can infer from the light curve is far less detailed. While the observations give an estimate for the angular velocity of the core Ω_c and that of the envelope Ω_e (which is naturally much lower), in

[1]Clump stars are cool horizontal branch stars, i.e. stars that are burning helium in their cores.

the vast majority of cases we do not have any additional information on the angular velocity pattern. Deheuvels et al. [2014] studied the seismic properties of six *Kepler* subgiants and young red giants to determine the most basic property of the rotation pattern: whether it is better approximated by a smooth transition from Ω_c in the core to Ω_e in the envelope, or by a discontinuous one (a step function in r). Intriguingly, they found that the discontinuous model provides a statistically better fit for two of the stars, but no claim can be made for the other models.

The most recent developments in asteroseismology include the study of hot main sequence stars. These stars have do not have an extended convective zone right beneath the photosphere, and this allows us to detect g-modes more easily than in the Sun. The first results on two of these stars do not show a significant difference between the rotation rate of the core and the surface (see Kurtz et al. 2014 and Saio et al. 2015).

1.4.2 Angular momentum of the core of red giants

It should not be surprising that, as a star moves towards the red giant branch, the angular velocity of its core increases. In fact, the core of the star is contracting during this evolutionary stage, and conservation of angular momentum (AM) implies that Ω_c will increase. What *is* surprising, however, is that the angular velocity inferred from asteroseismology is not compatible with AM conservation: while the angular velocity of stellar cores does increase as they contract, it does not increase as much as warranted by AM conservation, so that some processes must act to transfer AM from the core to the outer layers of the star.

AM appears to be definitely not conserved also during the rest of the evolution, which eventually leads to the formation of a white dwarf. White dwarfs are typically slow rotators (with periods ranging from several days to a few months), so that a significant amount of AM must be lost from the core of the star before the white dwarf is formed. The only seismic study to date of a white dwarf [Charpinet et al., 2009] did not detect any differential rotation in the star and this suggests that the AM is genuinely lost from the system, not hidden in internal layers.

The challenge for the theorist is to describe mechanisms of AM transport between the core and the envelope that are able to reproduce these findings. The processes that have been considered so far are generally included in one of three classes: (a) hydrodynamic instabilities and circulations, (b) magnetic torques, and (c) internal gravity (or mixed gravity-pressure) waves. Investigators are now trying to understand if, and how, these mechanisms contribute to the transfer of AM, and to incorporate them in codes of stellar evolution.

The hydrodynamic processes include, among many other effects, the Eddington-Sweet (ES) circulation (Eddington 1925, Kippenhahn 1974) and a circulation induced by the Goldreich-Schubert-Fricke (GSF) instability (Goldreich and Schubert 1967 and Fricke 1968). These mechanisms are the subject of investigation in the rest of this thesis, and are further discussed in chapter 2. The effect of the hydrodynamic processes on the AM is often modelled via a

diffusion-like equation so that they can be included in stellar evolution codes. A list of the various processes and their implementation is given by Heger et al. [2000]. Although these mechanisms contribute to removing AM from the core of the star, the angular velocity remains too high, so that other mechanisms are currently thought to be the main sources of AM loss.

The combined effect of differential rotation and a non-zero poloidal magnetic field in a stratified stellar region would cause a linear growth of the azimuthal component of the field. It is therefore natural to consider magnetic torques as a mechanism of AM transport. However, a process to sustain and grow the poloidal field ("close the dynamo loop") must be sought; the azimuthal field would otherwise grow until the magnetic energy overtakes the kinetic energy, which is not expected. The most promising dynamo candidate in strongly stratified layers is an instability first studied by Tayler [Tayler, 1973], and the resulting effect is known as Spruit-Tayler dynamo [Spruit, 2002]. Its implementation in terms of a diffusion-like equation is detailed by Heger et al. [2005]. However, while the occurrence of the instability is well established, its ability to sustain a dynamo is still debated and numerical simulations with contrasting results have been produced (see Braithwaite 2006 and Zahn et al. 2007). Other effects, including the magneto-rotational instability, might play the most prominent role in the redistribution of AM [Jouve et al., 2015].

Internal gravity waves extract energy and AM from the convective region of a star and deposit them in its radiative zone. Their contribution to the flow of AM has been debated for many years and they are thought to play a role in maintaining the near-uniform rotation of the Solar radiative core [Charbonnel and Talon, 2005b]. However, recent studies have concluded that neither progressive waves [Fuller et al., 2014] nor stationary modes [Belkacem et al., 2015a] seem to be sufficient to explain the current observations for subgiants and early RGs.

1.4.3 AM transport in stellar evolutionary codes

Stellar evolution codes generally incorporate the various mechanisms described above. Among these codes is MESAstar [Paxton et al., 2013], which currently incorporates several hydrodynamic processes thought to be induced by the differential rotation, together with magnetic AM transport based on the Tayler-Spruit dynamo. Each of these effects is reduced to a diffusive term in the equation for the evolution of the AM distribution. The joint consideration of these processes is still unable to reproduce the correct AM flux for subgiants and early RGs [Cantiello et al., 2014]. While the effect of internal gravity waves has not yet been taken into account in these models, the field is clearly moving towards more comprehensive codes and they might soon be included [Belkacem et al., 2015a]. This approach is very promising for the future, but the physics of the mechanisms that transport AM is often complicated and careful thought must be devoted to obtain a full understanding of each one of them.

Typical results are illustrated in figure 1.7 [Cantiello et al., 2014], obtained with MESAstar. The figure shows the evolution of the core rotation period, $P_c = 2\pi/\Omega_c$, during the early RGB for a 1.5 $M_\odot$ model when different mechanisms of AM transport are included. The models are

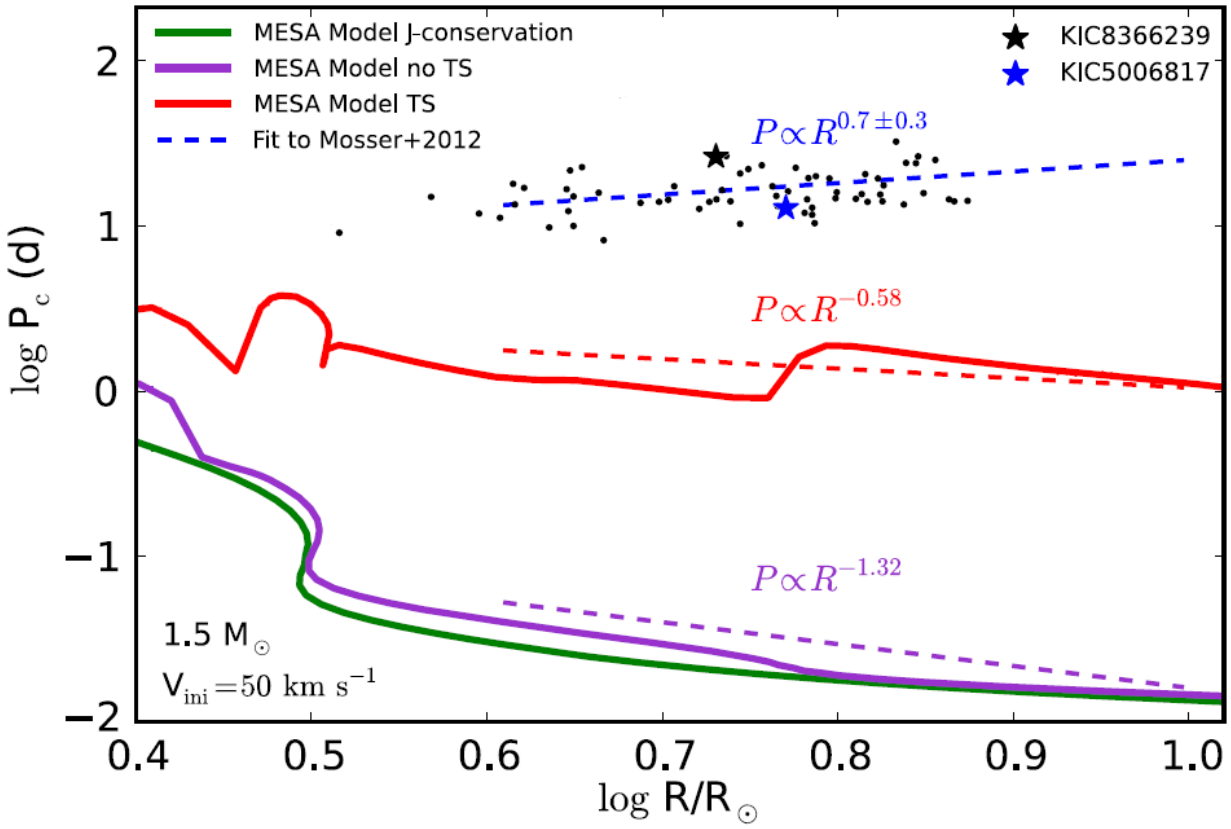

Figure 1.7: Evolution of the period of rotation of the core of a calculated stellar model as a function of radius of the star, in a 1.5 $M_\odot$ model initially rotating at 50 km s^{-1}. The green line corresponds to AM conservation, the purple line to the case of just hydrodynamic transport, the red line to the case of hydrodynamic and magnetic transport via the Taylor-Spruit (TS) process. The dashed lines indicate a linear fit to these curves during the early RGB phase. The black dots are the observational results for stars studied by Mosser et al. [2012]. The dashed blue line is a linear fit to these data. Original figure from Cantiello et al. [2014].

initially rigidly rotating at the beginning of their main sequence phase, with a surface velocity of 50 km s^{-1}. The value reported for P_c is a mass average of the period in the region below the maximum of the energy generation in the H-burning shell. The contraction of the core leads to different rates of angular acceleration for the different AM transport mechanisms considered. In any case, the calculated cores rotate between 1 and 3 orders of magnitude faster than the values inferred by asteroseismology.

1.5 Rotationally induced mixing in massive stars

In this thesis I question the existence or effectiveness of the two aforementioned hydrodynamic processes, the Eddington-Sweet circulation and the Goldreich-Schubert-Fricke instability. In addition to the role they play in AM transport, these mechanisms are also thought to induce chemical mixing in main sequence massive stars.

The literature on the chemical evolution of massive stars is vast. The arguments presented in this section are drawn from the comprehensive review by Langer [2012]. This author lists

indications that suggest the existence of rotational mixing. However, Langer himself concedes that they are at best indirect. Direct evidence, e.g. an observed correlation between the chemical enrichment of stellar surfaces and their period of rotation, is not very strong.

A proposed piece of evidence for rotational mixing is the observation that the surface of a number of massive main-sequence stars is enriched in nitrogen and poor in carbon (e.g. Przybilla et al. 2010). Rotational mixing has been proposed as the candidate process that operates to transport nitrogen throughout the outer radiative zone of these stars up to their surfaces. However, there is no obvious agreement between the observations and the current models of rotational mixing. Figure 1.8 shows an indicator of the surface nitrogen abundance and the apparent rotational velocity of a group of observed massive main sequence stars in the Large Magellanic Cloud. The coloured background shows the density of stars in the diagram calculated according to stellar models that include rotational mixing. While there is some similarity between the theoretical prediction and the observations, there is a significant number of enriched stars with very low rotation speed, as well as some that have high rotation period but very low enrichment. Both types of stars appear to contradict the predictions of rotational mixing in single stars.

In view of the weak corpus of evidence, why is rotation considered to be a good candidate for mixing of chemical elements? The answer resides in large part in the lack of alternatives. The mechanisms that may overshadow angular momentum transport by hydrodynamic processes, i.e. magnetic torques and waves, do so without transporting mass and are therefore unable to contribute to chemical mixing. The best alternative to rotational mixing is close binary evolution (in particular the possibility that enriched stars would be stellar mergers), which is far from well-understood. The degeneracy between the effects that rotation and binary evolution have on the surface chemical composition complicates the search of observational confirmation of rotational mixing.

In this chapter, I have reviewed recent observational and numerical studies on the effects of the ES circulation and the GSF instability on angular momentum diffusion and rotational mixing in differentially rotating stars. It should be clear at this point that there is no overwhelming evidence supporting the existence of the ES circulation and the GSF instability in stellar environments. In fact, the aim of this thesis is to consider stellar models in which these effects are not present altogether. In the next chapter, I will proceed to present the theoretical reasons for which the astronomers included the ES circulation and the GSF instability in their models, starting in the 1920s and 1970s respectively. This will also provide an opportunity to review the fundamental equations and techniques of stellar astrophysics and magnetohydrodynamics, which are essential for the original work presented in chapters 3 - 5.

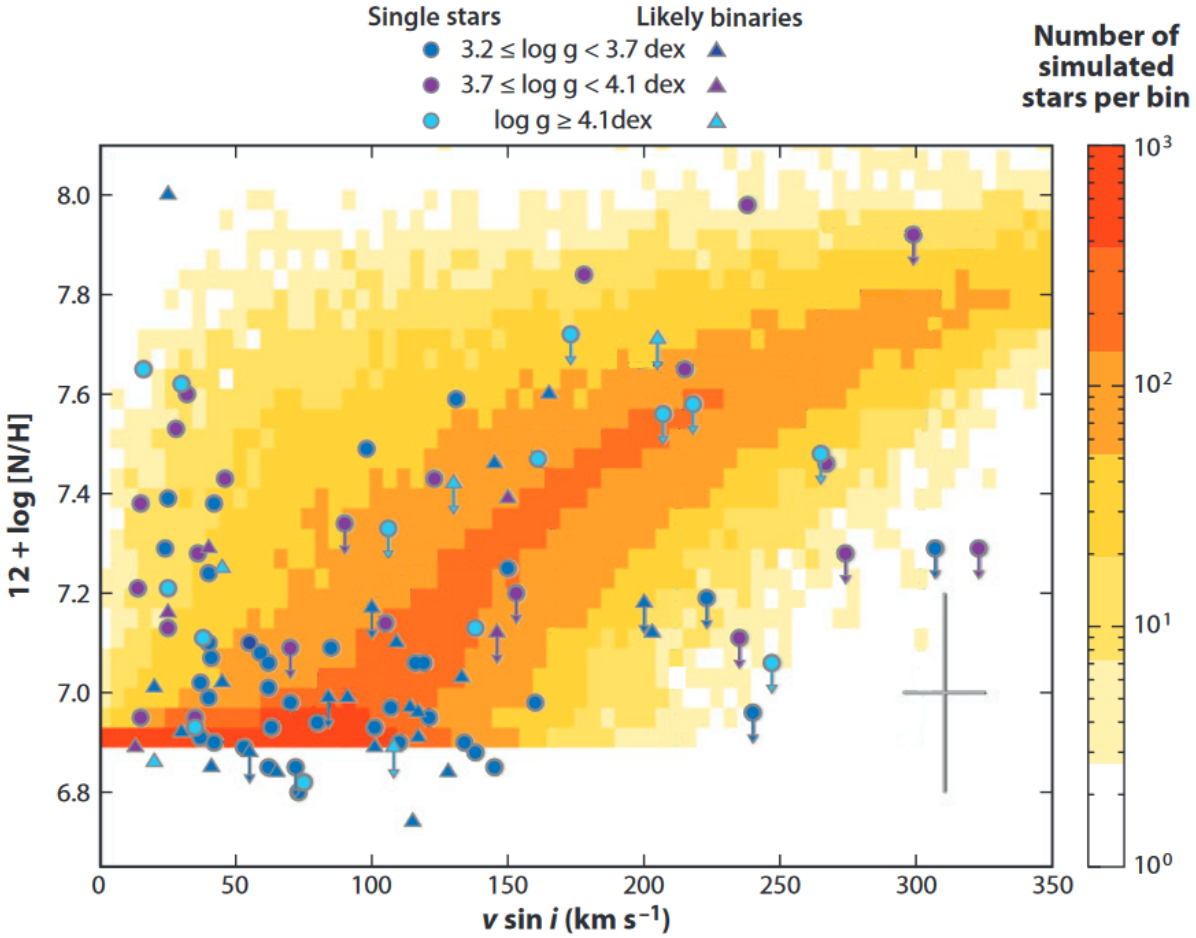

Figure 1.8: Nitrogen surface abundance and projected rotational velocity of early B-type stars in the Large Magellanic Cloud from the VLT-FLAMES Survey of Massive Stars. Single stars are shown as circles, binary stars as triangles. The colour of the symbol indicates the surface gravity of the star (see the legend at the top of the figure). The colours in the background represent the results of a population synthesis simulation based on single-star evolution models of stars of 13 $M_\odot$ with rotational mixing [Brott et al., 2011a]. The grey cross in the lower right corner shows the typical error on the observations. Figure adapted from Langer [2012], originally from Brott et al. [2011b].

Chapter 2

Introduction: the theory

The present chapter provides an introduction to several theoretical topics concerning the rotation of stellar radiative zones, necessary to understand the original work presented in this thesis. Although previous knowledge of stellar rotation theory is not essential to read this chapter, the reader should be familiar with basic concepts of stellar structure and evolution.

It is useful to start this discussion by laying down the four fundamental equations of stellar structure (see e.g. Kippenhahn et al. 2012). I list them here on the left-hand side of the page. On the right-hand side, I report their algebraic expressions in the simplest possible case of interest to us, that of a steady-state, non-rotating star in radiative equilibrium:

$$\text{equation of motion} \qquad -\frac{1}{\rho}\boldsymbol{\nabla} P - \boldsymbol{\nabla}\phi = 0, \tag{2.1}$$

$$\text{Poisson's equation} \qquad \boldsymbol{\nabla}^2\phi = 4\pi G\rho, \tag{2.2}$$

$$\text{equation of state} \qquad P = \frac{\rho}{\mu m_{\mathrm{P}}} k_{\mathrm{B}} T, \tag{2.3}$$

$$\text{equation of energy} \qquad \boldsymbol{\nabla}\cdot\boldsymbol{F}_{\mathrm{rad}} = 0. \tag{2.4}$$

Here, G is Newton's gravitational constant, m_{P} is the proton mass, k_{B} is Boltzmann's constant, ρ, P, ϕ, and T are respectively the density, pressure, gravitational potential, and temperature in the material, μ is the mean molecular weight (so that μm_{P} is the mean mass of a particle in the gas), $\boldsymbol{F}_{\mathrm{rad}}$ is the radiative energy flux. The latter is given by:

$$\boldsymbol{F}_{\mathrm{rad}} = -\frac{4acT^3}{3\rho\kappa}\boldsymbol{\nabla} T, \tag{2.5}$$

where a is the radiation constant, c is the speed of light, and κ is the Rosseland mean opacity, which depends on the density and temperature of the medium: $\kappa = \kappa(\rho, T)$. In the case of a non-rotating star, the equation of motion (2.1) is the condition of hydrostatic equilibrium.

In the rest of this chapter, I will consider changes to equations (2.1) - (2.4) to study the effect of rotation on the star.

2.1 The theorem of Von Zeipel

The theorem, or paradox, of Von Zeipel is one of the first results of stellar structure theory, and predates a large part of our knowledge on stellar evolution. The classic reference is von Zeipel [1924], although I present it here in a way that has become standard in the subsequent decades, see e.g. Schwarzschild [1958] and Kippenhahn et al. [2012].

The aim is to incorporate rotation in a stellar model described by equations (2.1) - (2.4). The most straightforward choice is to consider a uniformly rotating star and include a term due to the centrifugal acceleration in equation (2.1), with equations (2.2) - (2.4) unaltered, so that:

$$-\frac{1}{\rho}\boldsymbol{\nabla} P - \boldsymbol{\nabla}\phi + \Omega^2 \boldsymbol{R} = 0, \tag{2.6}$$

$$\boldsymbol{\nabla}^2 \phi = 4\pi G\rho, \tag{2.7}$$

$$P = \frac{\rho}{\mu m_{\mathrm{P}}} k_{\mathrm{B}} T, \tag{2.8}$$

$$\boldsymbol{\nabla}\cdot\boldsymbol{F}_{\mathrm{rad}} = 0, \tag{2.9}$$

where Ω is the angular velocity, the vector $\boldsymbol{R}$ is the cylindrical radius, and $\Omega^2 R$ is typically a small fraction of the gravity g in the star. The theorem of Von Zeipel states that this set of equations cannot be solved; in other words, it is said that *uniform rotation and radiative equilibrium are mutually incompatible in a chemically homogeneous star.*

It is useful to sketch here a proof of the theorem. The centrifugal acceleration in equation (2.6) can be written in terms of an effective potential, so that:

$$-\boldsymbol{\nabla}\phi + \Omega^2 \boldsymbol{R} = -\boldsymbol{\nabla}(\phi - \frac{1}{2}\Omega^2 R^2) = -\boldsymbol{\nabla}(\phi + \phi_{\mathrm{rot}}) = -\boldsymbol{\nabla} V, \tag{2.10}$$

where I have defined $\phi_{\mathrm{rot}} = -\Omega^2 R^2/2$ and $V = \phi + \phi_{\mathrm{rot}}$. The set of equations (2.6) - (2.9) is therefore similar to that of equations (2.1) - (2.4), the main difference being that the potential is not spherically symmetric. In fact, it is intuitive to recognise that the rotation will distort the shape of the equipotential curves in the star, making them oblate. I illustrate this point by considering the following toy model. Consider a spherically symmetric body of uniform density ρ. If I introduce a uniform angular velocity Ω in the model and assume that Ω is small, so that the gravitational field of the body is not affected by the small structural changes induced

by the rotation[1], the total (gravitational + rotational) potential in the body is given by:

$$V(r,R) = -\int \boldsymbol{g}\cdot d\boldsymbol{r} - \frac{1}{2}\Omega^2 R^2 = \int_0^r \frac{4\pi\rho r^3 G}{3r^2}dr - \frac{1}{2}\Omega^2 R^2 = \frac{2\pi G\rho}{3}r^2 - \frac{1}{2}\Omega^2 R^2, \tag{2.11}$$

where r, R are the spherical radius and cylindrical radius respectively, $\boldsymbol{g} = -g\hat{r}$ is the gravity in the body, and for convenience I set the zero of the gravitational and rotational potentials at $r = 0$. Using $r^2 = R^2 + z^2$, V can be written in terms of cylindrical coordinates only as:

$$V(R,z) = \frac{2\pi G\rho}{3}\Big((1 - \frac{3\Omega^2}{4\pi G\rho})R^2 + z^2\Big) \propto (1-Q)R^2 + z^2, \tag{2.12}$$

where the parameter Q is small if the rotation provides a small contribution to the effective gravity. Figure 2.1 shows the deformation of three equipotential lines in the case Q=0.2. In the more realistic case of a star with non-uniform density, a similar argument can be made to derive an analytical approximation for the shape of the equipotential surfaces [Schwarzschild, 1958]. The result is qualitatively similar to the one presented here.

To proceed with the proof of Von Zeipel's theorem, I note that equation (2.6) in the form $\boldsymbol{\nabla}P = -\rho\boldsymbol{\nabla}V$ implies that the gradient of P is parallel to the gradient of V at any point in the star. This means that these two quantities have the same isocontours. Therefore, P must be a function of V: $P = P(V)$. The same equation also gives:

$$\rho = \frac{|\boldsymbol{\nabla}P|}{|\boldsymbol{\nabla}V|} = \Big|\frac{\partial P}{\partial V}\Big|, \tag{2.13}$$

so that $\rho = \rho(V)$. Finally, if μ is uniform, equation (2.8) implies that $T = T(V)$. I also note that Poisson's equation gives a condition on the total potential V:

$$\boldsymbol{\nabla}^2 V = \boldsymbol{\nabla}^2\phi + \boldsymbol{\nabla}^2\phi_{\rm rot} = 4\pi G\rho - \frac{1}{2}\Omega^2\boldsymbol{\nabla}^2(R^2) = 4\pi G\rho - 2\Omega^2. \tag{2.14}$$

Finally, the radiative flux can be expressed as:

$$\boldsymbol{F}_{\rm rad} = -\frac{4acT^3}{3\rho\kappa}\boldsymbol{\nabla}T = -\frac{4acT^3}{3\rho\kappa}\frac{\partial T}{\partial V}\boldsymbol{\nabla}V \equiv H(V)\boldsymbol{\nabla}V, \tag{2.15}$$

where the last equality defines the function $H(V)$. The condition of radiative equilibrium (2.9)

[1]This approximation is commonly made and is sometimes known as the Cowling approximation [Cowling, 1941]. I will not discuss the validity of the Cowling approximation for each of the theoretical results presented in this introduction. I will also adopt this approximation in the original model presented in chapter 3 and refer the reader to appendix A for a detailed discussion of the effect of relaxing this assumption in that context.

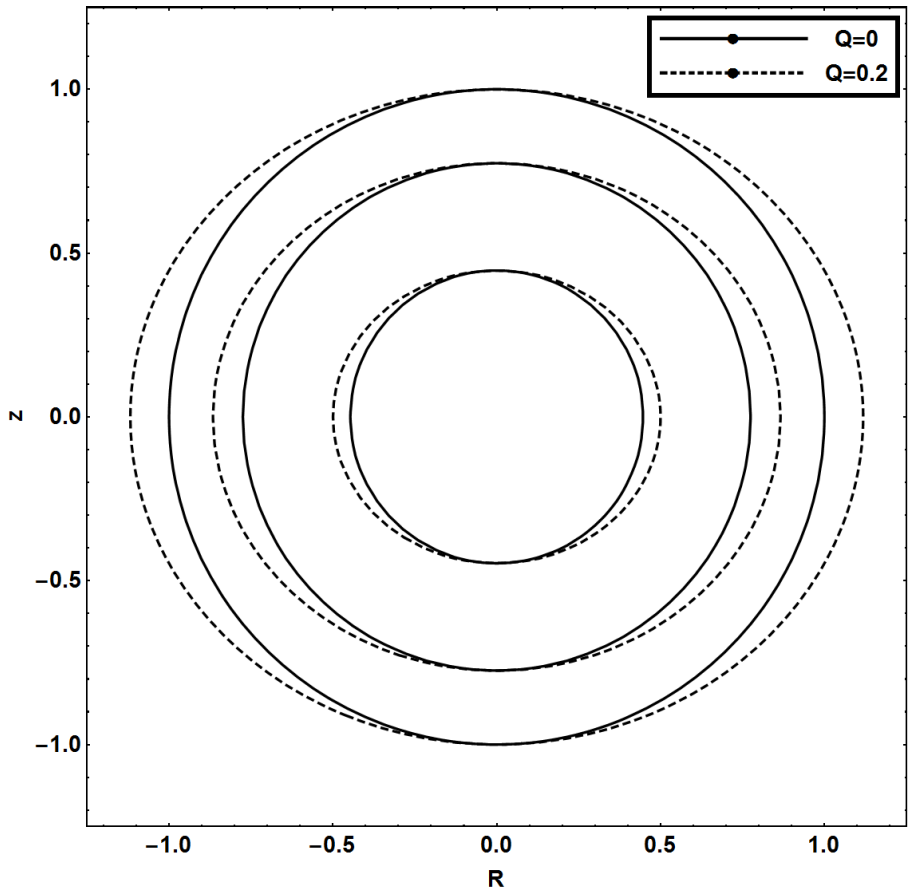

Figure 2.1: Isocontours of the function $f(R,z) = (1-Q)R^2 + z^2$ for $Q = 0$ (solid line) and $Q = 0.2$ (dashed line), corresponding to $f(R,z) = 0.2$, 0.6, and 1.0 respectively.

gives:

$$\boldsymbol{\nabla}\cdot\boldsymbol{F}_{\rm rad} = \frac{\partial H(V)}{\partial V}\boldsymbol{\nabla}V\cdot\boldsymbol{\nabla}V + H(V)\boldsymbol{\nabla}^2 V = \frac{\partial H(V)}{\partial V}|\boldsymbol{\nabla}V|^2 + H(V)(4\pi G\rho - 2\Omega^2) = 0, \quad (2.16)$$

where I made use of (2.14). Condition (2.16) cannot be satisfied at every point in the star: $\partial H(V)/\partial V$ and $H(V)(4\pi G\rho - 2\Omega^2)$ depend only on V, so that they are fixed on an isocontour of V, while $|\boldsymbol{\nabla}V|^2$ is larger at a point in which the isocontour meets the axis $R = 0$ than at a point at which it meets the plane $z = 0$, because any two isocontours, being oblate, are closer to each other along the z axis than along the radial direction. This concludes the proof.

The key point of this argument consisted in expressing the centrifugal acceleration in equation (2.6) in terms of the potential $\phi_{\rm rot}$. This is not only possible for uniform rotation, but also in the more general case in which $\Omega = \Omega(R)$ depends on the distance from the axis of rotation. In this case, the potential is:

$$\phi_{\rm rot} = -\int_0^R \Omega^2(s)s\, ds, \quad (2.17)$$

and a similar argument can be made. A pattern of rotation such that $\Omega = \Omega(R)$ is known as *barotropic*, one such that $\Omega = \Omega(R,z)$ depends on z is known as *baroclinic*. The more general

statement of Von Zeipel's theorem is that *barotropic rotation and radiative equilibrium are mutually incompatible in a chemically homogeneous star.*

2.2 The Eddington-Sweet meridional circulation

As a consequence of Von Zeipel's theorem, the astronomers were compelled to renounce either the assumption of uniform rotation or that of radiative equilibrium in the star. The favoured choice was to give up radiative equilibrium. Eddington [1925] proposed the following idea: while the energy is mostly transferred by radiation, a meridional circulation would also be present in the star, contributing to equation (2.4). The standard quantitative treatment is based on Sweet [1950]. This motion is now known as the Eddington-Sweet (ES) circulation.

2.2.1 ES circulation and ES time-scale

The ES meridional circulation is typically included in the model by means of transport terms in equation (2.4). The full set of equations in the case of uniform rotation can be expressed as:

$$-\frac{1}{\rho}\boldsymbol{\nabla} P - \boldsymbol{\nabla}\phi + \Omega^2 \boldsymbol{R} = 0, \tag{2.18}$$

$$\boldsymbol{\nabla}^2 \phi = 4\pi G \rho, \tag{2.19}$$

$$P = \frac{\rho}{\mu m_{\mathrm{P}}} k_{\mathrm{B}} T, \tag{2.20}$$

$$\boldsymbol{\nabla}\cdot\boldsymbol{F}_{\mathrm{rad}} = -\boldsymbol{\nabla}\cdot(\epsilon \boldsymbol{v}_{\mathrm{ES}}) - \boldsymbol{\nabla}\cdot(P \boldsymbol{v}_{\mathrm{ES}}), \tag{2.21}$$

where ϵ is the internal energy per unit volume, and $\boldsymbol{v}_{\mathrm{ES}}$ is the circulation velocity. The two terms on the right-hand side of (2.21) correspond to the advective transfer of energy by the velocity $\boldsymbol{v}_{\mathrm{ES}}$ and to the work done by the pressure on the moving fluid. These equations are solved by calculating $\boldsymbol{F}_{\mathrm{rad}}$ as in the proof of Von Zeipel's theorem, and then including a-posteriori the ES circulation. It is postulated that $v_{\mathrm{ES},\phi} = 0$ because of the azimuthal symmetry of the problem, so that two scalar relations are required to solve for $v_{\mathrm{ES},r}$ and $v_{\mathrm{ES},\theta}$; these are equation (2.21) and the continuity equation $\boldsymbol{\nabla}\cdot(\rho \boldsymbol{v}_{\mathrm{ES}}) = 0$.

Standard textbooks of stellar theory discuss the solution of equations (2.18) – (2.21). The approach involves expanding the structural quantities in a basis of functions in θ, usually Legendre polynomials, and is quite lengthy; the interested reader is referred to e.g. Kippenhahn et al. [2012] and Tassoul [2000]. For the sake of brevity, I report here an estimate of $v_{\mathrm{ES}} = |\boldsymbol{v}_{\mathrm{ES}}|$ based on a dimensional argument which is not rigorous but provides the correct result.

I express the radiative flux as $\boldsymbol{F}_{\rm rad} = \boldsymbol{F}_0 + \boldsymbol{F}_1$ where $\boldsymbol{F}_0$ is the flux in the non-rotating case and satisfies $\boldsymbol{\nabla}\cdot\boldsymbol{F}_0 = 0$, while $\boldsymbol{F}_1$ is a small correction due to the rotation. The order of magnitude of the correction is set by the rotational parameter $\eta = \Omega^2 R/g \ll 1$. I adopt the estimate $F_1 \sim \eta F_0$. For the left-hand side of equation (2.21) I then have:

$$\boldsymbol{\nabla}\cdot\boldsymbol{F}_{\rm rad} = \boldsymbol{\nabla}\cdot\boldsymbol{F}_1 \sim \frac{F_1}{L} \sim \eta\frac{F_0}{L}, \tag{2.22}$$

where L is the typical length scale in which the structural quantities change in the star (for example, $1/L = \partial \ln P/\partial r$), usually of order $0.1R_\odot$.

For what concerns the right-hand side of (2.21), one can expect ϵ and P to be of the same order of magnitude, and retain only the first term. One can estimate:

$$\boldsymbol{\nabla}\cdot(\epsilon\boldsymbol{v}) \sim \frac{\epsilon v_{\rm ES}}{L}. \tag{2.23}$$

It is now necessary to estimate ϵ as the total internal energy of the star divided by its total volume. I recall that the internal energy is of the same order of the gravitational potential energy (virial theorem), and neglecting numerical factors the result is:

$$\epsilon \sim \frac{GM^2}{R} \times \frac{1}{R^3} = \frac{GM^2}{R^4}, \tag{2.24}$$

where M and R are the mass and radius of the star respectively.

To estimate F_0, it is useful to remember that the time it would take for the star to radiate most of its energy from its surface if there were no nuclear energy generation in the centre is the Kelvin-Helmholtz time-scale $t_{\rm KH}$. Again neglecting numerical factors, this gives:

$$F_0 \times R^2 \times t_{\rm KH} \sim \frac{GM^2}{R}, \qquad \text{hence} \quad F_0 \sim \frac{GM^2}{R^3 t_{\rm KH}}. \tag{2.25}$$

Substituting the results of equations (2.22) - (2.25) into equation (2.21) and eliminating the common factors, one finds:

$$v_{\rm ES} \sim \eta\frac{R}{t_{\rm KH}}. \tag{2.26}$$

The ES time-scale, i.e. the time it takes for the circulation to cross a significant part of the star, is then given by:

$$t_{\rm ES} \sim \frac{R}{v_{\rm ES}} \sim \frac{t_{\rm KH}}{\eta}. \tag{2.27}$$

In the Solar radiative zone, $R \sim 10^{11}$ m, $\eta \sim 10^{-5}$ and $t_{\rm KH} \sim 10^7$ years, so that $v_{\rm ES} \sim 10^{-9}$ m s^{-1}, $t_{\rm ES} \sim 10^{12}$ years. The ES circulation velocity is tiny and $t_{\rm ES}$ is longer than the age of the Sun. For this reason, the ES circulation is considered to be unimportant in shaping the structure and evolution of the Sun. However, it should be noted that, in general, this does not

apply to other stars. Schwarzschild [1958] reports the critical velocity of rotation for a star of mass M and radius R as:

$$v_{\rm crit} = 52 \frac{M}{M_\odot} \frac{R_\odot}{R} \text{km s}^{-1}. \tag{2.28}$$

If the surface rotates with velocity $\Omega R > v_{\rm crit}$, the time-scale $\tau_{\rm ES}$ is of the comparable or shorter than the main-sequence lifetime of the star, so that the ES circulation is sufficiently fast to mix the material in the star and affect its chemical profile during its main sequence phase. Stars of type O, B, and A often rotate fast enough for this to occur.

2.2.2 ES circulation in a self-consistent model

While equations (2.18) – (2.21) can provide an estimate of $v_{\rm ES}$, they are *not self-consistent*. A correct treatment of the problem requires inclusion of the ES circulation velocity not just in the energy transfer equation, but also in the equation of motion. The full set of equations in this case is:

$$(\boldsymbol{v}\cdot\boldsymbol{\nabla})\boldsymbol{v} = -\frac{1}{\rho}\boldsymbol{\nabla}P - \boldsymbol{\nabla}\phi, \tag{2.29}$$

$$\boldsymbol{\nabla}^2\phi = 4\pi G\rho, \tag{2.30}$$

$$P = \frac{\rho}{\mu m_{\rm P}} k_{\rm B} T, \tag{2.31}$$

$$\boldsymbol{\nabla}\cdot\boldsymbol{F}_{\rm rad} = \boldsymbol{\nabla}\cdot(\epsilon\boldsymbol{v}) - \boldsymbol{\nabla}\cdot(P\boldsymbol{v}), \tag{2.32}$$

where $\boldsymbol{v}$ is the total velocity of the fluid, due to the rotation and the ES circulation, so that:

$$\boldsymbol{v} = \Omega R\hat{\phi} + \boldsymbol{v}_{\rm ES}. \tag{2.33}$$

The result of the previous section suggests that $|\boldsymbol{v}_{\rm ES}| \ll \Omega R$, so that the ES circulation velocity can be treated as a perturbation, retaining only first order terms in equation (2.29). The continuity equation is once again $\boldsymbol{\nabla}\cdot(\rho\boldsymbol{v}_{\rm ES}) = 0$.

To express the $\hat{\phi}$ component of equation (2.29) in terms of $\boldsymbol{v}_{\rm ES}$ I make use of the formulas valid in cylindrical coordinates (see e.g. Acheson 1990):

$$(\boldsymbol{v}\cdot\boldsymbol{\nabla}) = v_R\frac{\partial}{\partial R} + \frac{v_\phi}{R}\frac{\partial}{\partial\phi} + v_z\frac{\partial}{\partial z}, \tag{2.34}$$

and

$$\hat{\phi}\cdot\left[(\boldsymbol{v}\cdot\boldsymbol{\nabla})\boldsymbol{v}\right] = (\boldsymbol{v}\cdot\boldsymbol{\nabla})v_\phi + \frac{v_\phi v_R}{R}. \tag{2.35}$$

Using (2.33), this gives:

$$\hat{\phi}\cdot\left[(\boldsymbol{v}\cdot\boldsymbol{\nabla})\boldsymbol{v}\right] = v_{\mathrm{ES},R}(\Omega + \frac{\partial(\Omega R)}{\partial R}) + v_{\mathrm{ES},z}\frac{\partial(\Omega R)}{\partial z} = v_{\mathrm{ES},R}\frac{1}{R}\frac{\partial(\Omega R^2)}{\partial R} + v_{\mathrm{ES},z}\frac{1}{R}\frac{\partial(\Omega R^2)}{\partial z}. \quad (2.36)$$

The condition imposed by the $\hat{\phi}$ component of equation (2.29) is therefore:

$$\boldsymbol{v}_{\mathrm{ES}}\cdot\boldsymbol{\nabla} l = 0, \quad (2.37)$$

where $l = \Omega R^2$ is the angular momentum per unit mass due to the rotation.

The previous result holds for any pattern of rotation, either barotropic or baroclinic. In the simple case of uniform rotation, $\boldsymbol{\nabla} l = \boldsymbol{\nabla}(\Omega R^2) = 2\Omega R\hat{R}$, so that equation (2.37) gives $\boldsymbol{v}_{\mathrm{ES}}\cdot\hat{R} = 0$, i.e. $v_{\mathrm{ES},R} = 0$. In this case, the ES circulation velocity is along cylinders parallel to the rotation axis, and this contradicts the requirement of mass conservation. To see this, note that:

$$\boldsymbol{\nabla}\cdot(\rho\boldsymbol{v}_{\mathrm{ES}}) = \frac{1}{R}\frac{\partial(\rho R v_{\mathrm{ES},R})}{\partial R} + \frac{\partial(\rho v_{\mathrm{ES},z})}{\partial z} = \frac{\partial(\rho v_{\mathrm{ES},z})}{\partial z}, \quad (2.38)$$

so that the condition $\boldsymbol{\nabla}\cdot(\rho\boldsymbol{v}_{\mathrm{ES}}) = 0$ implies that the mass flow $\rho v_{\mathrm{ES},z}$ does not depend on z. But this means that there is a constant flow of mass from the northern hemisphere to the southern hemisphere if $\rho v_{\mathrm{ES},z} < 0$, or in the opposite direction if $\rho v_{\mathrm{ES},z} > 0$. The only possibility is that $\rho v_{\mathrm{ES},z} = 0$, in which case there is no circulation.

In the literature, this issue was first identified by Randers [1941], but it was largely ignored and, even nowadays, it is not always mentioned when the ES circulation is presented in courses on stellar structure and evolution. For wider criticisms related to the models with a circulation velocity and a list of references, see Tassoul [2000]. Several attempts have been made to solve the problem of self-consistency, and they typically require including other effects which appear as additional terms in equations (2.29) - (2.32). One possibility is to consider non-steady models, starting with Osaki [1972]. A non-steady model has been proposed more recently (though not quite to address the problem of self-consistency), and began the discussion of the spreading of the tachocline. This is the subject of the next section. Finally, another possibility is to consider large-scale magnetic fields, including the corresponding terms in the equation of motion. The work by Mestel [1999] discusses the magnetic models in great detail.

2.3 The spreading of the tachocline

The issue of the spreading of the tachocline, which provides motivation for the work done in this thesis, originates from trying to build a self-consistent model in an environment which is similar to that of the previous section. The original paper on the subject is Spiegel and Zahn [1992], while a more recent presentation was given by Zahn [2007]. The latter summarizes the essence of the problem with great clarity: “I recall here how latitude-dependent rotation

imposed by the solar convection zone on the top of the radiation zone would burrow deep into the interior, owing to thermal diffusion, in any laminar and purely hydrodynamic model. Since helioseismology has shown that this differential rotation remains confined in a thin boundary layer, the tachocline, it means that the radiative spread is inhibited by another physical process".

The aim of this section is to understand the argument behind this issue, with particular emphasis on the assumptions made by Spiegel and Zahn [1992], without reproducing the lengthy calculations reported in the original paper. The authors make use of the equations of stellar structure reported on the left-hand side of relations (2.1) - (2.4) in the tachocline, which is intended as a thin but not infinitesimal layer. I attempt to report the assumptions here in their completeness, but refer the reader to the original papers for further discussion:

(a) The magnetic field $\boldsymbol{B}$ is absent or negligible: $\boldsymbol{B} = 0$.

(b) Every quantity that appears in equations (2.1) - (2.4) is axisymmetric.

(c) The tachocline, or at least the part of the tachocline investigated in this analysis, is stably stratified. The effect of overshooting from the convective zone is neglected.

(d) The equation of state of the plasma is that of an ideal gas with uniform chemical composition.

(e) The angular velocity Ω is small, so that the model consists in imposing a perturbation on top of an originally non-rotating system. So, for example, the pressure may be expanded as $P(\boldsymbol{r}) = P_0(\boldsymbol{r}) + \hat{P}(\boldsymbol{r})$, where $\hat{P}$ is the small rotation-induced perturbation and $P_0(\boldsymbol{r}) = P_0(r)$ depends only on the spherical distance from the centre.

(f) The model features a circulation with velocity $\boldsymbol{v}_{\rm circ}$ contained in the meridional plane. This circulation is included self-consistently in equations (2.1) and (2.4).

(g) The radial variation scale of the perturbation functions (e.g. $\hat{P}$) is much smaller than both the radius r and the scale-height of the structural quantities of the non rotating model.

(h) The Rossby number of the system, which is given by the ratio of the inertial force to the Coriolis force, is small. This means that the contribution of the advective term $\boldsymbol{v}\cdot\boldsymbol{\nabla}\boldsymbol{v}$ can be neglected compared to the Coriolis force $\sim \boldsymbol{\Omega} \times \boldsymbol{v}$ in the $\hat{r}$ and θ components of Euler's equation.

(i) The flow is geostrophic. This means that the viscous forces are small compared to the Coriolis force. Nevertheless, only small terms appear in the $\hat{\phi}$ component of Euler's equation, and therefore advective and viscous terms are retained in it.

(j) The time-scales of the evolution of ρ and T are much shorter than that of Ω. The partial derivatives $\partial_t\rho$, $\partial_t T$, and $\partial_t\Omega$ appear respectively in the continuity equation, in the energy equation, and in the equation of motion.

Because of assumption (j), the authors investigate the state of the system after the relaxation of ρ and T has occurred, i.e. they set

$$\frac{\partial \rho}{\partial t} = 0, \text{ and } \frac{\partial T}{\partial t} = 0. \tag{2.39}$$

Although the formalism is different, and the viscosity is also included (but eventually found to play only a marginal role), Spiegel and Zahn solve equations (2.29) - (2.32) with just one additional term, which is proportional to $\partial_t \Omega$ and appears in the $\hat{\phi}$ component of equation (2.29). They then proceed to solve the equations with boundary conditions that impose uniform rotation in the tachocline at $t = 0$. Since I have just demonstrated that those equations cannot be solved self-consistently when $\partial_t \Omega = 0$, it is unavoidable that the solution will require $\partial_t \Omega \neq 0$. Spiegel and Zahn have therefore solved the problem originating from angular momentum conservation in a star with meridional circulation by allowing for a time-dependent angular velocity.

The perturbations to the structural quantities $\hat{P}$, $\hat{\rho}$, $\hat{T}$, and the angular velocity Ω, are expanded in the form:

$$\hat{P}(r, \theta) = \sum_i \tilde{P}_i(r) f_i(\cos\theta), \tag{2.40}$$

where r, θ are the spherical radius and co-latitude, and f_i is a set of basis functions, for example Legendre polynomials. When this is done and the previous assumptions hold, an equation for the evolution of $\tilde{\Omega}$ is derived:

$$\frac{\partial \tilde{\Omega}}{\partial t} + \kappa \Big(\frac{2\Omega}{N}\Big)^2 \Big(\frac{r_0}{\lambda}\Big)^2 \frac{\partial^4 \tilde{\Omega}}{\partial r^4} - \nu \frac{\partial^2 \tilde{\Omega}}{\partial r^2} = 0, \tag{2.41}$$

where N is the Brunt-Väisälä frequency, r_0 is the radius of the tachocline, λ is a dimensionless parameter of order unity, ν is the kinematic viscosity in the vertical direction, and $\kappa = \chi / \rho C_P$ where χ is the thermal conductivity and C_P is the specific heat at constant pressure. In the Sun, $\nu/\kappa \sim 10^{-6}$, so that the spreading of the tachocline is mainly due to the second term of equation (2.41), which is referred to as the "hyperdiffusion" term because of the appearance of a fourth spatial derivative. Spiegel and Zahn solved equation (2.41) and found that the differential rotation would extend to the radiative zone within a time comparable with the age of the Sun, so that, by now, the tachocline would stretch down to $r \sim 0.3 R_\odot$. This clearly contradicts the data presented in chapter 1 of this thesis.

In the next chapter, I will propose an alternative Solar model which is not affected by this issue, showing that baroclinic patterns of rotation $\Omega = \Omega(R, z)$ can be independent of time and compatible with the data from helioseismology. Most authors have not followed this approach, but rather looked to maintain a uniform angular velocity in the radiative zone and identify another mechanism to prevent the spreading of the tachocline. A comprehensive review of the efforts in this direction is given by the book edited by Hughes et al. [2007]; see also Gough [2015] for a more recent discussion.

In the same paper in which the problem was noted, Spiegel and Zahn [1992] proposed a counteracting mechanism that was purely hydrodynamic, based on horizontal turbulence in the tachocline. This turbulence would contribute to advecting angular momentum by suppressing the latitudinal shear imposed onto the layer. It is not clear whether this mechanism is actually effective, and it has been disputed, see e.g. Elliott [1997] and McIntyre [2003].

Another possibility, arguably the most popular to date, is the model proposed by Gough and McIntyre [1998], in which a large-scale magnetic field, possibly primordial, is present in the upper radiative zone and contributes to halting the spreading of the tachocline. This model features a complex balance between the magnetic field, the meridional circulation, and the downflow and upflow of material between the tachocline and convective zone. Numerical simulations have given contrasting results on this issue, with the earlier (but more numerous) works being unsuccessful in using magnetic fields to contain the differential rotation to the tachocline, see among others Brun and Zahn [2006], Strugarek et al. [2011], and Acevedo-Arreguin et al. [2013].

Finally, other authors have considered angular momentum transport to and from the tachocline due to internal gravity waves. The most prominent work on the subject was produced by Charbonnel and Talon [2005a], who showed that the rate of angular momentum transfer due to waves could suffice to explain the rotation profile of the Sun and the other stars. However, it should be noted that this model ignores the differential rotation in latitude, as most other works based on wave transport do [Zahn, 2007]. More recent efforts have gone into creating a better theoretical framework for wave transport of energy and angular momentum and incorporating this effect into codes of stellar evolution; see Fuller et al. [2014] and Belkacem et al. [2015a,b].

2.4 Local stability of differentially rotating stars

As I have already indicated, chapter 3 presents a Solar model with a baroclinic rotation profile in the upper radiative zone and the tachocline which is compatible with the data from helioseismology and the condition of exact radiative equilibrium. To be viable, however, such a model must be stable, and the rest of this thesis consequently deals with the issue of stability. The current section provides a brief review of the literature on the local stability of differentially rotating stars. The next section will then treat in some more detail the Goldreich-Schubert-Fricke (GSF) instability, and illustrate why this can be expected to be the main process disrupting any baroclinic pattern of rotation. Chapter 4 presents a fairly general stability analysis of the Solar baroclinic rotation profile. Finally, chapter 5 studies the onset of the GSF instability not just in the Sun, but also in red giant stars, whose internal rotation profile is now being probed by asteroseismological means.

It needs to be emphasized that only issues of local stability will be discussed in this thesis. An example of a global flow that would alter the state of the fluid is the appearance of an Eddington-Sweet circulation; this may not affect the baroclinic patterns of rotation that I will

describe, since they are by construction devoid of it, but other mechanisms might operate. Moreover, only linear processes are treated in this work. Another example of a process that is not covered by this analysis is provided by the non-linear shear instability that, in either local or global form, has now been present in the literature for decades [Zahn, 1975]. While a full understanding of this instability remains elusive [Menou and Le Mer, 2006], some astronomers consider it to be one of the mechanisms that could contribute to the transfer of angular momentum in stars.

The literature on the local stability of differential rotation, which in astrophysics is also relevant to the study of accretion discs and accretion flows in general, is vast. The problem is difficult to treat in its full generality, i.e. with the inclusion of (a) a background magnetic field, (b) all the relevant diffusive terms (thermal diffusion, viscosity, and resistivity), and (c) allowing for non-axisymmetric perturbations. The importance of each of these components will be illustrated in the following discussion. Here I use both standard spherical coordinates (r, θ, ϕ) as well as cylindrical coordinates (R, ϕ, z). The background rotation profile is azimuthally symmetric, but otherwise arbitrary: $\Omega = \Omega(r, \theta)$ or $\Omega = \Omega(R, z)$.

2.4.1 Axisymmetric perturbations

The stability conditions for adiabatic, axisymmetric perturbations in a non-magnetic star are derived by applying linear perturbations to the fluid equations in a shearing fluid. They constitute a classic result in the linear theory of shearing flows, historically attributed to Solberg and Høiland (see e.g. Tassoul 2000), and can be expressed in many equivalent ways. Among these is the following: the Solberg-Høiland criteria state that such systems are stable only if:

$$N^2 + \frac{1}{R^3}\frac{\partial l^2}{\partial R} > 0, \tag{2.42}$$

$$(-\frac{\partial P}{\partial z})(\frac{\partial l^2}{\partial R}\frac{\partial \sigma}{\partial z} - \frac{\partial l^2}{\partial z}\frac{\partial \sigma}{\partial R}) > 0, \tag{2.43}$$

where N^2 is the usual Brunt-Väisälä frequency

$$N^2 = -\frac{1}{\gamma\rho}\frac{dP}{dr}\frac{d\sigma}{dr}, \tag{2.44}$$

and $\sigma = \ln(P\rho^{-\gamma})$ is a dimensionless entropy variable. Finally, γ is the adiabatic index, ρ the mass density in the star, P the pressure, and l the specific angular momentum:

$$l = \Omega R^2. \tag{2.45}$$

Note that these conditions are reduced to the familiar Schwarzschild criterion $N^2 > 0$ in the non-rotating case.

An important modification of this result comes from introducing a finite thermal diffusivity. The destabilising effect of thermal diffusion was studied by Goldreich and Schubert [1967] (hereafter GS67) and Fricke [1968], who considered axisymmetric perturbations in a non-magnetic star with a finite thermal diffusion coefficient $\xi_{\rm rad}$ and kinematic viscosity ν. The authors found that if the heat leakage due to thermal diffusion from a perturbed fluid element is sufficiently rapid, the restoring effect of buoyancy is lost. I will discuss this in detail in the next section; for now, it suffices to say that the introduction of even small diffusivities often plays a key role in altering the conditions required for stability.

As a remnant of their formation, the Sun and the other stars are expected to have an internal magnetic field of indeterminate strength in their radiative zones. The diffusion time-scale of such a fossil magnetic field is very long (see e.g. Parker 1979 and Mestel 1999). Developments in the last decades, stemming from the studies of accretion disc stability, have made it clear that consideration of even weak magnetic fields is often essential for an understanding of the dynamics of shearing fluids (see e.g. the magneto-rotational instability (MRI), Balbus and Hawley 1991). The effects of toroidal magnetic fields in the context of differentially rotating stars had already been discussed by Acheson [1978], who had noted that the presence of such weak fields can change the results by GS67. Balbus [1995] has derived the dispersion relation for linear adiabatic axisymmetric perturbations in a weakly magnetized non-diffusive star. For even very weak background magnetic fields, the conditions for stability are essentially independent of the magnetic field itself:

$$N^2 + \frac{\partial \Omega^2}{\partial \ln R} > 0, \tag{2.46}$$

$$(-\frac{\partial P}{\partial z})(\frac{\partial \Omega^2}{\partial R}\frac{\partial \sigma}{\partial z} - \frac{\partial \Omega^2}{\partial z}\frac{\partial \sigma}{\partial R}) > 0, \tag{2.47}$$

i.e., the same as equations (2.42) and (2.43) but with the angular velocity replacing the specific angular momentum. The range of magnetic field strength for the validity of the stability criteria (2.46) and (2.47) depends on the diffusion coefficients (see section 2.4 of Balbus 1995 for a discussion). For typical solar values, the criterion is valid for $B > 10^2$ G. The bottom line is that even weak magnetic fields are essential to any careful stability analysis and profoundly affect the final result.

More recently, a general analysis of axisymmetric modes in a magnetised star including the effect of thermal diffusivity $\xi_{\rm rad}$, viscosity ν, and magnetic resistivity η was conducted by Menou et al. [2004]. They derived a fifth-order dispersion relation and discussed necessary stability conditions in the limit in which one of the three diffusivities is zero, analytically recovering several of the conditions described above. They have then applied the full dispersion relation to the upper radiative zone of the Sun, finding that the addition of a third, weak diffusivity is often able to stabilise an unstable double-diffusive situation. They showed that the radiative zone of the Sun would likely be subject to unstable axisymmetric modes if

moderate or strong radial gradients of angular velocity were present. This is clearly not the case, at least in the bulk of the radiative zone, which helioseismology showed to be in near-uniform rotation. In another recent work, Menou and Le Mer [2006] have used the same dispersion relation to survey the axisymmetric stability of the early (faster rotating) Sun, and have showed that it may have been more prone to rotational instabilities than the current Sun. In particular, these authors have found that at least in the early Sun, magnetic modes are likely more efficient at transporting angular momentum than hydrodynamic instabilities.

2.4.2 Non-axisymmetric perturbations

Historically, studies of stability of differentially rotating stars have often been restricted to axisymmetric perturbations. This is primarily due to the complications associated with the behaviour of non-axisymmetric fluid displacements, which in general cannot be described by a local plane wave dispersion relation. The following discussion briefly illustrates why this is the case. For a recent, more detailed study of the local linear behaviour of three-dimensional fluid displacements in a shearing and stratified background medium, the reader can be directed to Balbus and Schaan [2012] (the more classic "shearing-sheet" reference is Goldreich and Lynden-Bell 1965).

The linear evolution of the perturbations can be studied using Lagrangian cylindrical coordinates (R', ϕ', z', t'), locally comoving with the fluid, and related to the Eulerian coordinates (R, ϕ, z, t) by:

$$R' = R, \qquad \phi' = \phi - \Omega t, \qquad z' = z, \qquad t' = t, \tag{2.48}$$

with $\Omega = \Omega(R, z)$. In the well-known Wentzel–Kramers–Brillouin (hereafter WKB) limit, when written in Lagrangian coordinates[1] the perturbations have the familiar plane wave spatial dependence:

$$\exp[i(k'_R R' + m\phi' + k'_z z')], \tag{2.49}$$

where $\boldsymbol{k}' = (k'_R, m/R, k'_z)$ is the wave vector, and m is a dimensionless number. Here k'_R, m, and k'_z are constants. The WKB approximation is valid when the wavelengths $1/k'_R$, R/m, and $1/k'_z$ are smaller than the scale-heights of the structural quantities that appear in the same equations. In the Sun, these are typically of order 0.1 $\mathrm{R}_\odot$, where $\mathrm{R}_\odot$ is the Solar radius.

The equations of fluid dynamics are often more conveniently written in terms of the Eulerian coordinates, and contain partial derivatives in time and space. The partial derivatives with respect to the Eulerian coordinates (R, ϕ, z, t) are related to those in the Lagrangian coordinates by:

$$\frac{\partial}{\partial R} = \frac{\partial}{\partial R'} - t\frac{\partial \Omega}{\partial R}\frac{\partial}{\partial \phi'}, \tag{2.50}$$

[1] It is important to note that the usual WKB prescription, which consists of studying the different Fourier modes separately, only makes sense in the Lagrangian frame. In the Eulerian frame, plane waves are affected by the shear. The current section illustrates that this effectively amounts to changing the wave vector $\boldsymbol{k}$ over time: the motion remains wave-like, but $\boldsymbol{k}$ is not constant.

$$\frac{\partial}{\partial \phi} = \frac{\partial}{\partial \phi'}, \tag{2.51}$$

$$\frac{\partial}{\partial z} = \frac{\partial}{\partial z'} - t\frac{\partial \Omega}{\partial z}\frac{\partial}{\partial \phi'}, \tag{2.52}$$

$$\frac{\partial}{\partial t} = \frac{\partial}{\partial t'} - \Omega\frac{\partial}{\partial \phi'}. \tag{2.53}$$

When these derivatives act on the perturbed quantities, they are immediately seen to act as if these had a plane wave behaviour, with a time dependent Eulerian wave vector with components

$$k_R(t) = k'_R - mt\frac{\partial \Omega}{\partial R}, \qquad k_z(t) = k'_z - mt\frac{\partial \Omega}{\partial z}, \tag{2.54}$$

with m unchanged. Since I have shown that the Eulerian wavenumbers depend on time, the coefficients in the governing evolutionary fluid equations must depend on time as well, and simple harmonic wave solutions of the form $e^{\mathrm{i}\omega t}$ do not exist. Of course, it must be possible to formulate the same problem and obtain the same result entirely in Eulerian coordinates; however, this is less straightforward and in my view less natural.

The Eulerian wave vector $\boldsymbol{k}$ is constant either when $m = 0$, which is the axisymmetric case, or when

$$\frac{\partial \Omega}{\partial R} = 0 \qquad \text{and} \qquad \frac{\partial \Omega}{\partial z} = 0, \tag{2.55}$$

i.e., the case of uniform rotation. In these two instances, a dispersion relation for the evolution of the perturbations can be derived. Balbus and Schaan [2012] discuss the dispersion relation for non-axisymmetric displacements in the case of uniform rotation. They note that in some instances, "*the pure m modes are more unstable than are modes contaminated by poloidal wavenumber components*". In particular, it is possible to find that the axisymmetric perturbations are stable, whereas high m modes are not. It is therefore of great importance to consider the full 3-dimensional case.

Several studies (e.g. Acheson 1978, Masada et al. 2007, and Kagan and Wheeler 2014) have neglected the time-dependence of k_R and k_z in the non-axisymmetric case. This restricts their range of validity. The latter two papers explicitly note that the analysis is valid only when the axisymmetric component of the wave vector is small enough not to be significantly sheared with time. However, it is not entirely clear how this approximation is included in their analyses, and my view is that their results may be correct only to zeroth order in m, i.e. the axisymmetric limit. In particular, Kagan and Wheeler [2014] (see also Parfrey and Menou 2007) study the growth rate of the MRI in the upper radiative and convective regions of the Sun and suggest that the unstable MRI modes may play a dominant role in the generation of the toroidal magnetic field near the tachocline. However, this conclusion is based upon the behaviour of their fastest growing modes, which are, in fact, fully non-axisymmetric. This rich problem merits a fully self-consistent non-axisymmetric local analysis.

2.5 The Goldreich-Schubert-Fricke instability

Before presenting the technical details of the GSF instability, it is interesting to note the historical context in which it was first studied.

In the 1960s, long before the era of helioseismology, the community of stellar theorists became very interested in differentially rotating stars. The reason is the following: some authors (in particular Dicke 1964) noted that the main observational support for the theory of general relativity was at the time given by the precession of the perihelion of Mercury. They argued that this phenomenon could instead be due to the gravitational field of the Sun, which is distorted because of the oblate shape of the structure, in turn caused by its rotation. The rotation of the Solar surface is too slow to explain the precession of the perihelion of Mercury; however, if the nuclear or radiative core were rotating approximately one order of magnitude faster than the surface, this model would be viable. The contribution of Goldreich and Schubert [1967] and Fricke [1968] was to identify an instability that would make any stellar model with such strong differential rotation unfeasible.

Despite the widespread popularity it had at the time and more generally its historical importance, most standard textbooks of stellar physics do not discuss the GSF instability (the notable exception is Kippenhahn et al. 2012). It is therefore useful to provide a brief presentation of it in what follows.

2.5.1 The dispersion relation of the GSF instability

Goldreich and Schubert studied axisymmetric perturbations applied to the radiative zone of a differentially rotating star. They found that thermal diffusion from the displaced fluid element can counterbalance the stabilising effect of entropy stratification. A simple physical interpretation of the onset of the stability is given by Menou et al. [2004]: "The mechanism is analogous to "salt fingering" in the oceans. In this process, warm salty water overlying cool fresh water, naively a stable configuration, is destabilized by heat transfer. Warm fingers of salty water, penetrating into the cooler waters below, diffuse heat outward more rapidly than they diffuse salt, and thereby lose their buoyancy. In the stellar case, a downwardly displaced fluid element is adiabatically heated and is normally warmer than its ambient surroundings. This results in a restoring buoyant force. But if thermal diffusion causes sufficiently rapid heat leakage, the buoyant force is diminished, and destabilizing angular momentum gradients are then able to operate."

Goldreich and Schubert performed a WKB analysis of modes of wavelength $\lambda \ll R$ allowing for finite thermal diffusion and kinematic viscosity in the medium. The perturbations depend on space and time as:

$$\exp[q\Omega t + i(k_R R + k_z z)], \tag{2.56}$$

where i is the imaginary unit, t is time, q is in general a complex number, and $\boldsymbol{k} = (k_R, 0, k_z)$ is the wave vector. I present here their results, without their derivation. The technical steps

are similar to those involved in the perturbation study which constitutes chapter 4 of this thesis.

The system is unstable if the dispersion relation has solutions with a positive real part of q. For convenience, I report here the dispersion relation that describes the evolution of the modes in a compact form (see also equation (32) of GS67):

$$q^3 + A(\boldsymbol{k})q^2 + B(\boldsymbol{k})q + C(\boldsymbol{k}) = 0, \tag{2.57}$$

where

$$A(\boldsymbol{k}) = \frac{k^2}{\Omega}\Big(2\nu + \frac{1}{\gamma}\chi\Big), \tag{2.58}$$

$$B(\boldsymbol{k}) = -\Big(\frac{k_z}{k}\Big)^2\Big[\frac{1}{\gamma\Omega^2\rho}(\widetilde{D}P)(\widetilde{D}\sigma) + \frac{2}{\Omega R}\widetilde{D}l\Big] + \frac{2}{\gamma}\Big(\frac{\chi k^2}{\Omega}\Big)\Big(\frac{\nu k^2}{\Omega}\Big), \tag{2.59}$$

$$C(\boldsymbol{k}) = -\Big(\frac{k_z}{k}\Big)^2\Big(\frac{\nu k^2}{\Omega}\Big)\Big[\frac{1}{\gamma\Omega^2\rho}(\widetilde{D}P)(\widetilde{D}\sigma)\Big] - \Big(\frac{k_z}{k}\Big)^2\Big(\frac{\chi k^2}{\Omega}\Big)\Big[\frac{2}{\gamma\Omega R}\widetilde{D}l\Big] + \frac{1}{\gamma}\Big(\frac{\chi k^2}{\Omega}\Big)\Big(\frac{\nu k^2}{\Omega}\Big)^2. \tag{2.60}$$

In these equations, ρ is the density of the fluid, P its pressure, T its temperature, ν the kinematic viscosity, $\sigma = \ln(P\rho^{-\gamma})$ the entropy variable, γ the adiabatic index, χ the heat conductivity, $l = \Omega R^2$ the angular momentum per unit mass, and $k^2 = k_R^2 + k_z^2$. I have introduced the differential operator [Balbus, 1995]:

$$\widetilde{D} = \frac{k_R}{k_z}\frac{\partial}{\partial z} - \frac{\partial}{\partial R}. \tag{2.61}$$

Inspection of equation (2.57) immediately shows that there is at least one real positive solution for q if $C(\boldsymbol{k}) < 0$ for any $\boldsymbol{k}$. A necessary stability criterion is therefore $C(\boldsymbol{k}) > 0$. Goldreich and Schubert studied this requirement in the small Prandtl number case: $\mathrm{Pr} = \nu/\chi \to 0$. In this case, it is immediately seen that the stability condition reduces to $\widetilde{D}l < 0$. Since the ratio k_R/k_z can assume any value, this condition can then hold only if

$$\frac{\partial l}{\partial R} > 0 \qquad \text{and} \qquad \frac{\partial \Omega}{\partial z} = 0, \tag{2.62}$$

or, in other words, the angular momentum increasing outward and the angular velocity fixed on cylinders. The latter constraint is very strong: any barotropic rotation pattern would be subject to an exponentially growing instability. A naive application of equation (2.57) with $\nu = 0$ to the upper radiative zone of the Sun gives a growth time-scale of less than 10 years (this result is recovered in section 4.4 and figure 4.1 of this thesis). Models with Ω fixed at a given spherical distance from the centre, $\Omega = \Omega(r)$ ("shellular" rotation, see Meynet and

Maeder 1997) are often used in modern stellar codes, see e.g. Paxton et al. [2013]; all these structures would be unstable unless the star rotates as a rigid body.

It should now be clear why the GSF instability is of particular interest to this thesis, which studies rotating stars in radiative equilibrium. As I have discussed, Von Zeipel's theorem shows that a star with a barotropic rotation profile (i.e., $\partial_z \Omega = 0$) cannot be in radiative equilibrium; on the other hand, Goldreich and Schubert argued that if the rotation profile is baroclinic (i.e. $\partial_z \Omega \neq 0$), the structure is unstable! It would appear, therefore, that rotation and radiative equilibrium are always incompatible.

However, a feature of the analysis by GS67, though noted early on (e.g. Acheson 1978, Knobloch and Spruit 1982, and Menou et al. 2004), has often been ignored. Conditions (2.62) apply only when $\nu/\xi_{\rm rad}$ is sufficiently small. Small compared to what? A careful analysis shows that being small compared to unity is not sufficient: $\nu/\xi_{\rm rad}$ must be small compared with the squared ratio of Ω over the Brunt-Väisälä frequency. This condition is not met in much of the radiative zone. It is therefore necessary to retain the viscosity ν when studying the behaviour of these local perturbations. I will discuss this issue in detail in chapter 5.

2.5.2 AM redistribution due to the GSF instability

In the non-viscous case, how efficient would the GSF instability be in redistributing the angular momentum in a star that does not comply with equation (2.62)? The answer to this question is not simple. While solving the dispersion relation gives a growth time-scale of order 10 years, it was soon recognised that the consequences of the GSF instability would not be as dramatic as suggested by these results. Kippenhahn [1969] argued that a displaced fluid element that starts moving in a star with $\partial_z \Omega \neq 0$ would soon be torn apart by the shear and therefore short lived. This author was the first to suggest that the effect of the GSF instability would therefore be reduced to a meridional circulation in the star. It has also been suggested that a small compositional gradient could render the fluid stable [Knobloch and Spruit, 1983].

James and Kahn [1970] studied the readjustment of the structure at the onset of the GSF instability and also concluded that the displaced fluid elements are quickly destroyed; however, they identify the main process with a "sliding instability" rather than the shear. These authors then proceeded to adopt a diffusion-like approximation to estimate the rate of AM transport due to the resulting meridional circulation [James and Kahn, 1971]. This rate is found to be moderately low, of the same order or slightly higher than that due to the Eddington-Sweet circulation[1]. The analysis by James and Kahn is relatively involved and contains important approximations; in particular that the fluid is inviscid. There seem to be no simulations that confirm or contradict the existence of the GSF circulation and test its effectiveness in transporting angular momentum in a star. Their formula was then taken up by Endal and Sofia [1978] for the first evolutionary study of rotating stars with time-dependent

[1]The usual prescription of AM transport due to the Eddington-Sweet circulation is given by Kippenhahn [1974]. As I have discussed above, the Eddington-Sweet circulation itself is a complex physical process and important assumptions are often made to describe it.

redistribution of angular momentum. Since then, it has become a standard component of many evolutionary codes.

Incidentally, it should also be noted here that equations (2.57) - (2.60) have been derived under the assumption that no energy is generated in the material; i.e. the energy equation is $\boldsymbol{\nabla \cdot F}_{\rm rad} = 0$, where $\boldsymbol{F}_{\rm rad}$ is the radiative flux. The equations are therefore not strictly correct in the nuclear core of a star. It is occasionally argued that any corrective term would affect the perturbations on the nuclear time-scale of the star, which is long. For this reason, equations (2.57) - (2.60) and the diffusion-like approximation for the transport of AM have often been applied to any stably stratified zone of the star, independently of the energy generation processes taking place there.

Chapter 3

Differential rotation and radiative equilibrium in the Sun

We have seen that the combination of barotropic rotation and radiative equilibrium are mutually incompatible in stars. However, the Sun's internal rotation is far from barotropic, which allows at least the theoretical possibility that the Sun's thermal balance is one of radiative equilibrium in the region of the tachocline near the outer boundary of the radiative zone. I will show here that (i) the constraint of radiative equilibrium leads to a straightforward ordinary differential equation for the Sun's rotation profile, and (ii) solutions of this equation can be found that, to within current levels of accuracy, closely resemble the rotation profile deduced from helioseismology. More generally, I will calculate how large a baroclinic deviation from uniform rotation is required to maintain radiative equilibrium without meridional circulation throughout the bulk of the radiative zone. I will show that very little deviation is required, well below detectability. The feasibility of radiative equilibrium for the tachocline suggests that the issue of the spreading of the tachocline may be less severe than previously thought.

3.1 Introduction

Since the availability of helioseismological data has allowed the reconstruction of the details of the internal rotation of the Sun, significant effort has been directed towards understanding what sustains the observed rotation rate $\Omega(r, \theta)$. The shape of the iso-rotation curves in the bulk of the convective zone was found to be well described by the characteristic solutions of the thermal wind equation [Balbus et al., 2009]. In contrast, the physics of the solar tachocline is still largely uncertain.

The theorem of Von Zeipel states that a star in uniform rotation cannot be in radiative equilibrium. This is generally applied well within radiative cores, where any residual thermal energy imbalance is thought to be compensated by means of a mean velocity flow, the

Eddington-Sweet circulation. However, Balbus and Schaan [2012] have noted that matters are not so simple near the outer boundary of the radiative zone in a Sun-like star. I report here their argument. The steady entropy equation, allowing for advection and radiative diffusion, is:

$$P(\boldsymbol{u}\cdot\boldsymbol{\nabla})\sigma = -(\gamma-1)\boldsymbol{\nabla}\cdot\boldsymbol{F}, \tag{3.1}$$

where P is the pressure, $\boldsymbol{u}$ is the circulation velocity, $\sigma = \log(P\rho^{-\gamma})$ is the entropy variable, γ is the adiabatic index and $\boldsymbol{F}$ is the radiative flux. The radial, dominating component of $\boldsymbol{\nabla}\sigma$ is positive in the radiative zone and negative in the convective zone as for the Schwarzschild criterion, so that it has to go through zero at the radiative-convective boundary. In this case, even if $\boldsymbol{u}$ is not zero, equation (3.1) reduces to $\boldsymbol{\nabla}\cdot\boldsymbol{F} = 0$, the condition of radiative equilibrium.

The Eddington-Sweet circulation velocity in the radiative zone of stars has a prominent role in the literature for solving the problem of energy transfer under conditions of uniform rotation. However, the inclusion of meridional circulation in the equations of stellar structure generates further complications, which were discussed at length in chapter 2. In brief, the problem originates from the time-steady azimuthal component of the Euler equation of motion:

$$(\boldsymbol{v}\cdot\boldsymbol{\nabla})\boldsymbol{v} = -\frac{1}{\rho}\boldsymbol{\nabla}P + \boldsymbol{g}, \tag{3.2}$$

which, for $\boldsymbol{v} = \Omega R\hat{\phi} + \boldsymbol{u}$, where Ω is the angular velocity, R the cylindrical radius and $\hat{\phi}$ the azimuthal direction, gives

$$\boldsymbol{u}\cdot\boldsymbol{\nabla}(\Omega R^2) = 0, \tag{3.3}$$

i.e. for a star in uniform rotation, the circulation is along cylindrical surfaces at fixed distance from the rotation axis. This is incompatible with a model that is steady and symmetric with respect to the equatorial plane, as material would accumulate onto such a plane due to the circulation velocity. One is then compelled to consider non-steady models or to introduce an accommodating magnetic field structure that would change equation (3.3). Building a simple, comprehensive model for rotating stars when meridional circulation is included is not straightforward.

For these reasons, it is interesting to ask whether the current data on the rotation of the outer part of the radiative zone of the Sun are compatible with a model in *strict radiative equilibrium.* Even in the bulk of the radiative zone, which is in near uniform rotation, the current accuracy of the data certainly does not allow one to say that it is rotating *exactly* as a rigid body. A small amount of differential rotation could be present. Would this undetected deviation from uniformity be enough for the Sun to be in radiative equilibrium?

The accuracy of the data of helioseismology decreases with depth in the Sun, and it is particularly difficult to study the properties of a narrow transition layer like the tachocline, whose thickness may appear to be broader than it actually is because of the resolution of the inversion techniques involved in the data analysis. There are several different estimates of the width of the tachocline (see section 1.3.2), mostly in the range $1\% - 5\%$ $R_\odot$; the analysis by

Antia and Basu [2011] suggests the possibility of a significant dependence of the tachocline width on solar latitude, with an average value not larger than 0.03 $R_\odot$ but a strong uncertainty for the value at mid-latitudes (see their figure 2). This is thinner than the transition apparent from the data used in this thesis. It is likely that the structure of the tachocline is still substantially unresolved. Any direct comparison of theory with the data must therefore be considered as a test of the plausibility of the model, not as a precision attempt to reproduce the actual $\Omega(R, z)$ in the interior of the Sun.

Although a thorough estimate of the errors in the outer radiative zone is not available, it is likely to be intermediate between the convective zone and the core, with a relative uncertainty that is perhaps of order 10%; if one is conservative, possibly more (R. Howe, private communication).

With these caveats in mind, I construct here a model of the outer Solar radiative zone under the assumption of radiative equilibrium, use this constraint to compute the rotation profile itself, and compare the resulting angular velocity curves with the observed differential rotation of the Sun. I will show that this model is compatible with the current data.

3.1.1 The spreading of the tachocline

It is worth mentioning again the influential analysis conducted by Spiegel and Zahn [1992] (see also Zahn 2007) at a time when the early results of helioseismology showed that the rotation of the Sun turned from strongly differential to uniform in a thin, unresolved transition at the radiative-convective boundary. As we have seen, these authors considered the standard equations of stellar structure, including the effect of circulation velocity. A time-dependent, initial-value problem with boundary conditions at the tachocline emerged. In the Spiegel & Zahn calculation, the term that offset the advection of angular momentum in equation (3.3) above was $\partial\Omega/\partial t$, the time-explicit inertial derivative in the azimuthal equation of motion. Time-dependence thus played an essential role in the analysis from the start.

The inclusion of this term led to the conclusion that the tachocline transition must spread with time. Specifically, Spiegel and Zahn [1992] showed that under these assumptions, a time-dependent diffusion-like equation for the angular velocity followed, implying ongoing penetration of the differential rotation into the radiative core of the Sun on a time-scale of $\tau \sim 10^9$ yr, significantly shorter than the age of the Sun. This posed a fundamental problem: why is the tachocline so thin?

The differential rotation of the Sun has been examined by numerical hydrodynamic and magnetohydrodynamic solar models, and important results have been obtained in reproducing rotation profiles for the convective zone that qualitatively resemble the results of helioseismology. Miesch et al. [2006] imposed ad-hoc entropy boundary conditions at the base of the convective zone, and more recently there have been 2D [Rogers, 2011] and 3D [Brun et al., 2011] simulations of the coupled convective and radiative regions. The simulations are limited

by the necessity of including artificially large diffusivities, which prevent an accurate force balance in the interior and in the tachocline, and coping with a wide range of time-scales, from those of convection and internal gravity waves to the predicted long time-scale of tachocline spreading. The results of Rogers [2011] (who finds that hydrodynamic processes can significantly slow down the spreading of the tachocline) and Brun et al. [2011] (who find a very fast spreading of the tachocline but relate it to a large viscous diffusivity), while significant on their own terms, may not fully capture the true dynamics of the radiative-convective boundary.

The result by Spiegel and Zahn [1992] implies that a thin (nearly discontinuous) tachocline, with initial and boundary conditions for the base of the convective zone drawn from helioseismology, is not a steady solution for the Sun, but instead gives rise to "burrowing" by differential rotation. This does not rule out the existence of a model of a steady, thin tachocline with a self-consistent angular velocity differing from the Spiegel and Zahn [1992] profile, but nevertheless compatible with the present helioseismology data. In this chapter, I present such a model.

3.2 Description of the model

3.2.1 Equations of stellar equilibrium

The steady equations of stellar equilibrium in the outer radiative zone for an inviscid flow are given by:

$$(\boldsymbol{v}\cdot\boldsymbol{\nabla})\boldsymbol{v} = -\frac{1}{\rho}\boldsymbol{\nabla}P + \boldsymbol{g}, \tag{3.4}$$

$$P = \frac{\rho}{\mu m_{\mathrm{P}}} k_{\mathrm{B}} T, \tag{3.5}$$

$$\boldsymbol{\nabla}\cdot\boldsymbol{F}_{\mathrm{rad}} = 0, \tag{3.6}$$

$$\boldsymbol{F}_{\mathrm{rad}} = -\frac{4acT^3}{3\rho\kappa}\boldsymbol{\nabla}T, \tag{3.7}$$

where $\boldsymbol{v}$ is the rotation velocity, ρ the density, P the gas pressure, $\boldsymbol{g}$ the (self) gravitational field, m_{P} the atomic mass unit, μ the mean molecular mass, T the temperature, $\boldsymbol{F}_{\mathrm{rad}}$ the radiative flux, a the radiation constant, c the speed of light, and κ the Rosseland mean opacity. For a given chemical composition κ is a function of the local density and temperature: $\kappa = \kappa(\rho, T)$.

I denote the rotational velocity in spherical coordinates (r, θ, ϕ) by $\boldsymbol{v} = \Omega(r,\theta) r \sin\theta \hat{\boldsymbol{\phi}}$, introducing the angular velocity Ω. The rotation is considered to be a small perturbation to a static spherical structure, so that the equations can be linearized in the Eulerian perturbation

variables δP, $\delta\rho$, $\delta\boldsymbol{g}$. The result is:

$$\Omega^2 r\sin^2\theta - \frac{1}{\rho}\frac{\partial\delta P}{\partial r} - \frac{g}{\rho}\delta\rho + \delta g_r = 0, \tag{3.8}$$

$$\Omega^2 r\sin\theta\cos\theta - \frac{1}{r\rho}\frac{\partial\delta P}{\partial\theta} + \delta g_\theta = 0, \tag{3.9}$$

$$\boldsymbol{\nabla}\cdot\left(\frac{ac}{3\rho\kappa}\left(\boldsymbol{\nabla}(4T^3\delta T) - \left(\frac{\delta\kappa}{\kappa}+\frac{\delta\rho}{\rho}\right)\boldsymbol{\nabla}T^4\right)\right) = 0, \tag{3.10}$$

$$\frac{\delta T}{T} = \frac{\delta P}{P} - \frac{\delta\rho}{\rho}, \tag{3.11}$$

where the first two equations are the $\hat{\boldsymbol{r}}$ and $\hat{\boldsymbol{\theta}}$ components of the Euler force balance equation. The unsubscripted ρ, P and T quantities refer now to the unperturbed, nonrotating spherical equilibrium solution, and the perturbed Rosseland opacity $\delta\kappa$ is given by:

$$\delta\kappa = \left(\frac{\partial\kappa}{\partial\rho}\right)_T\delta\rho + \left(\frac{\partial\kappa}{\partial T}\right)_\rho\delta T. \tag{3.12}$$

In the following analysis, I will neglect the self-gravity perturbations δg_r, δg_θ in equations (3.8) and (3.9), following the Cowling approximation [Cowling, 1941]. The validity of this approximation is discussed at length in Appendix A, together with a procedure to include values of δg_r and δg_θ that are more realistic, though still not entirely self-consistent.

3.2.2 Expansion in $\cos\theta$

To solve equations (3.8)-(3.11) in the variables Ω^2, $\delta\rho$, δP and δT, it is convenient to expand these quantities in even powers of $\cos\theta$. The solar angular velocity given by the GONG data [Hill and et al., 1996] in the outer part of the radiative zone is very well approximated by a function of the form:

$$\Omega^2(r,\theta) \cong \Omega_0^2(r) + \Omega_2^2(r)\cos^2\theta. \tag{3.13}$$

The accuracy of this fit may be seen in figures 3.1 and 3.2 (the figures are reported at the end of the chapter for readability). Figure 3.1 shows the angular velocity isocontours of the Sun according to the GONG data (upper figure), and an expansion of the form (3.13) for $r < 0.76R_\odot$ in which $\Omega_0^2(r)$, $\Omega_2^2(r)$ are 5th order polynomials in r optimised to fit the data (lower figure). Figure 3.2 shows the same quantities just in the outer radiative zone of the Sun, providing a slightly magnified view of the data and the fit. The functions $\Omega_0^2(r)$ and $\Omega_2^2(r)$ are shown as the solid lines in figures 3.3, 3.4. I have used an expansion of the type (3.13) for the model of the radiatively sustained angular velocity curves.

It has been noted by Balbus and Schaan [2012], see their equation (85), that if $\Omega^2(r,\theta)$ can be expressed in terms of the first n powers of $\cos^2\theta$, the equations of equilibrium can only be satisfied if the perturbations of the structural variables δP and $\delta\rho$ have terms up to $n+2$ in their expansion. I will therefore require that:

$$\delta P(r,\theta) = \sum_{n=0,2,4} P_n(r)\cos^n\theta, \tag{3.14}$$

$$\delta\rho(r,\theta) = \sum_{n=0,2,4} \rho_n(r)\cos^n\theta. \tag{3.15}$$

3.2.3 Solutions of the model in radiative equilibrium

Expressions (3.13), (3.14), and (3.15) can be substituted into equations (3.8) to (3.10) (in which δT is expressed in terms of δP, $\delta\rho$ by means of (3.11)) and the sum of all the terms proportional to the same power of $\cos\theta$ must be zero. Equation (3.9) then yields for $n = 2,\ 4$:

$$P_n(r) = -\frac{1}{n} r^2 \rho \Omega^2_{n-2}(r), \tag{3.16}$$

and equation (3.8) gives, again for $n = 2,\ 4$:

$$\rho_n(r) = \frac{1}{g}\left(\rho r(\Omega^2_n(r) - \Omega^2_{n-2}(r)) - \frac{dP_n(r)}{dr}\right). \tag{3.17}$$

The perturbations in the pressure and density can therefore be expressed in terms of the functions $\Omega^2_n(r)$ from the expansion of $\Omega^2(r,\theta)$, except for the spherically symmetric terms $P_0(r)$, $\rho_0(r)$. Knowledge of those terms is not required to impose radiative equilibrium, and they can ultimately be considered as absorbed into the non rotating, spherically symmetric solution.

We may eliminate Ω^2_n from the above, obtaining a relation between ρ_n and P_n:

$$r\rho_n = \frac{1}{r}\left[nP_n - (n+2)P_{n+2}\right] - \frac{dP_n}{dr}. \tag{3.18}$$

The same technique applied to the radiative equilibrium equation (3.10) leads to the rather cumbersome form

$$\begin{aligned}
&\frac{5C}{\rho r^2}\frac{d}{dr}\left(\frac{\rho_n}{\rho}\right) - \frac{4C}{Pr^2}\frac{d}{dr}\left(\frac{P_n}{P}\right) + \frac{1}{r^2}\frac{d}{dr}\left\{\frac{r^2T^4}{\rho\kappa}\left[\left(\frac{P_n}{P}\right)' - \left(\frac{\rho_n}{\rho}\right)'\right]\right\} + \\
&+ \frac{C}{r^2}\frac{d}{dr}\left\{\frac{1}{\kappa}\left[\rho_n\frac{\partial\kappa}{\partial\rho} + T\frac{\partial\kappa}{\partial T}\left(\frac{P_n}{P} - \frac{\rho_n}{\rho}\right)\right]\right\} + \\
&+ \frac{T^4}{r^2\rho\kappa}(n+1)\left[(n+2)\left(\frac{P_{n+2}}{P} - \frac{\rho_{n+2}}{\rho}\right) - n\left(\frac{P_n}{P} - \frac{\rho_n}{\rho}\right)\right] = 0
\end{aligned} \tag{3.19}$$

where the constant

$$C = \frac{3L_\odot}{16\pi ac}, \tag{3.20}$$

has been introduced, where $L_\odot$ is the Solar luminosity, and I have used prime notation $(X)'$ for dX/dr to aid readability. This equation holds for $n = 2, 4$, with the understanding that $P_6 = 0$, $\rho_6 = 0$. Equations (3.18) and (3.19), with proper boundary conditions, are coupled ordinary differential equations that uniquely determine the solution of our problem. In practice, the best way to proceed is to express $P_n(r)$, $\rho_n(r)$ in terms of $\Omega_0^2(r)$, $\Omega_2^2(r)$ via equations (3.16) and (3.17) and use equation (3.19) for $n = 2, 4$ to obtain a set of two lengthy, coupled ordinary differential equations for Ω_0^2, Ω_2^2. This is a straightforward procedure. To report the result in a compact form, one defines the functions:

$$X_0(r) = \rho\Omega_0^2(r), \qquad X_2(r) = \rho\Omega_2^2(r), \tag{3.21}$$

so that:

$$P_2(r) = -\frac{1}{2}r^2 X_0(r), \qquad P_4(r) = -\frac{1}{4}r^2 X_2(r), \tag{3.22}$$

$$\rho_2(r) = \frac{r}{g}(X_2(r) - X_0(r)) + \frac{1}{2g}\frac{d(r^2X_0(r))}{dr}, \qquad \rho_4(r) = -\frac{r}{g}X_2(r) + \frac{1}{4g}\frac{d(r^2X_2(r))}{dr}. \tag{3.23}$$

These expressions can be plugged into equation (3.19), which I reproduce here for $n = 2, 4$:

$$\begin{aligned}
&\frac{5C}{\rho r^2}\frac{d}{dr}\Big(\frac{\rho_2}{\rho}\Big) - \frac{4C}{Pr^2}\frac{d}{dr}\Big(\frac{P_2}{P}\Big) + \frac{1}{r^2}\frac{d}{dr}\Big\{\frac{r^2T^4}{\rho\kappa}\Big[\Big(\frac{P_2}{P}\Big)' - \Big(\frac{\rho_2}{\rho}\Big)'\Big]\Big\} + \\
&+ \frac{C}{r^2}\frac{d}{dr}\Big\{\frac{1}{\kappa}\Big[\rho_n\frac{\partial\kappa}{\partial\rho} + T\frac{\partial\kappa}{\partial T}\Big(\frac{P_2}{P} - \frac{\rho_2}{\rho}\Big)\Big]\Big\} + \\
&+ 3\frac{T^4}{r^2\rho\kappa}\Big[4\Big(\frac{P_4}{P} - \frac{\rho_4}{\rho}\Big) - 2\Big(\frac{P_2}{P} - \frac{\rho_2}{\rho}\Big)\Big] = 0,
\end{aligned} \tag{3.24}$$

$$\begin{aligned}
&\frac{5C}{\rho r^2}\frac{d}{dr}\Big(\frac{\rho_4}{\rho}\Big) - \frac{4C}{Pr^2}\frac{d}{dr}\Big(\frac{P_4}{P}\Big) + \frac{1}{r^2}\frac{d}{dr}\Big\{\frac{r^2T^4}{\rho\kappa}\Big[\Big(\frac{P_4}{P}\Big)' - \Big(\frac{\rho_4}{\rho}\Big)'\Big]\Big\} + \\
&+ \frac{C}{r^2}\frac{d}{dr}\Big\{\frac{1}{\kappa}\Big[\rho_4\frac{\partial\kappa}{\partial\rho} + T\frac{\partial\kappa}{\partial T}\Big(\frac{P_4}{P} - \frac{\rho_4}{\rho}\Big)\Big]\Big\} + \\
&- 20\frac{T^4}{r^2\rho\kappa}\Big(\frac{P_4}{P} - \frac{\rho_4}{\rho}\Big) = 0.
\end{aligned} \tag{3.25}$$

Equations (3.24) and (3.25) with P_2, P_4, ρ_2, ρ_4 expressed in terms of $X_0(r)$, $X_2(r)$ constitute a set of two ordinary differential equations that can be solved jointly. $\Omega_0^2(r)$ and $\Omega_2^2(r)$ are then immediately derived from $X_0(r)$ and $X_2(r)$ dividing by ρ. Boundary conditions must be specified for Ω_0^2, Ω_2^2 and their first and second derivatives at some radius r_0.

	Best fit	Model a	Model b
$\Omega_0^2(r_0)$	$7.4 \cdot 10^{-12}$	$7.4 \cdot 10^{-12}$	$7.4 \cdot 10^{-12}$
$d\Omega_0^2(r_0)/dr$	$3.9 \cdot 10^{-23}$	$2.0 \cdot 10^{-23}$	$7.8 \cdot 10^{-23}$
$d^2\Omega_0^2(r_0)/dr^2$	$-4.5 \cdot 10^{-33}$	$-2.3 \cdot 10^{-33}$	$-9.1 \cdot 10^{-33}$
$\Omega_2^2(r_0)$	$-2.4 \cdot 10^{-13}$	$-2.4 \cdot 10^{-13}$	$-2.4 \cdot 10^{-13}$
$d\Omega_2^2(r_0)/dr$	$-5.9 \cdot 10^{-23}$	$-3.0 \cdot 10^{-23}$	$-1.2 \cdot 10^{-22}$
$d^2\Omega_2^2(r_0)/dr^2$	$-1.2 \cdot 10^{-32}$	$-0.6 \cdot 10^{-32}$	$-2.4 \cdot 10^{-32}$

Table 3.1: Boundary conditions imposed at $r_0 = 0.60$ R$_\odot$ for the solutions of figures 3.3, 3.4. The units are in cgs and have been omitted to aid readability.

3.3 Application to the outer radiative zone

In the following analysis, the equilibrium variables P, ρ and g have been extracted from the solar model of Bahcall et al. [2005]. The Rosseland opacity $\kappa(\rho, T)$ and its derivatives have been interpolated from the OPAL table for solar composition [Iglesias and Rogers, 1996].

My approach is to solve the coupled equations for Ω_0^2 and Ω_2^2 for comparison with the rotational GONG data. I set the boundary conditions for Ω^2 and its first and second radial derivatives at $r_0 = 0.60 R_\odot$, where the rotation rate is approximately uniform, and integrate outwards. I adjust the spatial derivatives within the constraint of interior quasi-uniform rotation, and fit the curve to the GONG data. The fit has been executed by performing a χ^2 minimization around an initial, exploratory solution. The resulting boundary conditions imposed at $r_0 = 0.60$ R$_\odot$ are shown in table 3.1. The angular velocity terms $\Omega_0^2(r)$, $\Omega_2^2(r)$ of equation (3.13) for this radiative solution are shown as the dashed lines in figures 3.3, 3.4 along with the GONG data.

Figures 3.3, 3.4 indicate that solutions of the model in radiative equilibrium can be found which fit the data well and match closely to a uniformly rotating interior. I have shown illustrative 5% and 10% error bars for the values of Ω_0^2, Ω_2^2 in figures 3.3, 3.4. It is clear that the model fits well to the data within the expected uncertainties. This result raises the possibility that a very small deviation from uniform rotation might be sufficient to allow the deeper stellar interior to be in baroclinic radiative equilibrium.

It should be noted that although the data from helioseismology impose a constraint on the values of $\Omega_0^2(r_0)$, $\Omega_2^2(r_0)$, they are too uncertain to constrain the values of the derivatives of Ω_0^2, Ω_2^2 deep in the radiative zone. It is therefore not possible to compare the derivative boundary conditions imposed here with those derived from helioseismology. A test of the robustness and sensitivity of the solutions can be performed by noting how they change when the unconstrained boundary conditions $d\Omega_0^2(r_0)/dr$, $d^2\Omega_0^2(r_0)/dr^2$, $d\Omega_2^2(r_0)/dr$, $d^2\Omega_2^2(r_0)/dr^2$ are varied. I report in figures 3.3, 3.4 the solutions for the case in which the spatial derivatives of Ω_0^2, Ω_2^2 are a factor of 2 smaller (model a) and larger (model b) than those of the best fit. The respective boundary conditions for each model are shown in table 3.1. From figures (3.3) and (3.4), it is clear that the validity of the assumption of radiative equilibrium is not acutely sensitive to possible future moderate revisions of the angular velocity profile.

$\Omega_0^2(r_0)$	$7.5 \cdot 10^{-12}$ s^{-2}
$d\Omega_0^2(r_0)/dr$	0
$d^2\Omega_0^2(r_0)/dr^2$	0
$\Omega_2^2(r_0)$	0
$d\Omega_2^2(r_0)/dr$	0
$d^2\Omega_2^2(r_0)/dr^2$	0

Table 3.2: Boundary conditions imposed at $r_0 = 0.65$ R$_\odot$ for the solution of figure 3.5.

3.4 Deviation from uniform rotation

As a more general investigation to determine what amount of differential rotation is required for a star to be in radiative equilibrium, I have applied the model to a Solar-like star, i.e. a star with the same pressure, density and temperature profiles as the model by Bahcall et al. [2005] but a different rotation profile. I integrate towards the deep interior with boundary conditions at $r_0 = 0.65 R_\odot$ locally resembling uniform rotation, using a value of $\Omega(r_0)$ close to the average angular rotation rate of the radiative zone of the Sun. The boundary conditions are shown in table 3.2.

The model is able to maintain nearly uniform rotation down to a significant depth in the radiative zone. $\Omega_2^2(r)$ is identically zero, while the solution for $\Omega_0^2(r)$ is shown in figure 3.5. The solution starts to deviate more strongly only at a significant depth (with a deviation of 4% at $r \sim 0.4$ R$_\odot$). It appears that a star could be in near-uniform rotation in large part of its radiative zone, without the need for meridional circulation.

3.5 Conclusion

Meridional circulation is generally seen as a means to maintain thermal energy balance in rotating stars. However, the purpose of meridional circulation is to maintain uniform or barotropic rotation; if the rotation is baroclinic, it might well be compatible with radiative equilibrium. Nevertheless, small circulation velocities are usually invoked even in baroclinic flows to maintain thermal balance.

While solving one problem, meridional circulation seems to create another: starting with the influential study of Spiegel and Zahn [1992], circulation-induced diffusive spreading of the tachocline has been viewed as a major problem for understanding solar rotation. In this chapter, I have taken a step back by arguing that since baroclinic solar rotation is a reality, one should investigate what sort of rotation profiles emerge when the constraint of strict radiative equilibrium is applied, without the benefit (or complications) of circulation velocities. I have shown that it is easy to find solutions that fit well to the observed rotation profiles. Indeed, it is not clear that even the deep radiative interior is free of baroclinic rotation at the small level needed to influence radiative balance.

The most striking feature of the model presented here is its simplicity. It is devoid of meridional circulation currents, magnetic fields, viscosity and compositional gradients, effects

often invoked to explain the physics of the tachocline. It is by far the simplest interpretation that is compatible with the current data from helioseismology. Interestingly, however, the problem of time dependence might still implicitly be present in this model, since I have not yet addressed the all important question of the stability of the baroclinic rotation profiles. We have seen in chapter 2 that the stability of stellar rotation curves is complex because the criteria are significantly affected by such subtleties as the presence of even weak magnetic fields [Balbus, 1995], the thermal diffusion of the displaced fluid elements [Goldreich and Schubert, 1967], viscosity [Acheson, 1978], and even resistivity [Menou et al., 2004]. One advantage of the model presented here is that it is simple enough to lend itself to a rigorous linear stability analysis. If such study shows that the profiles are stable, this would go some way to alleviating the problem of the spreading of the tachocline. It is to this analysis that we now turn.

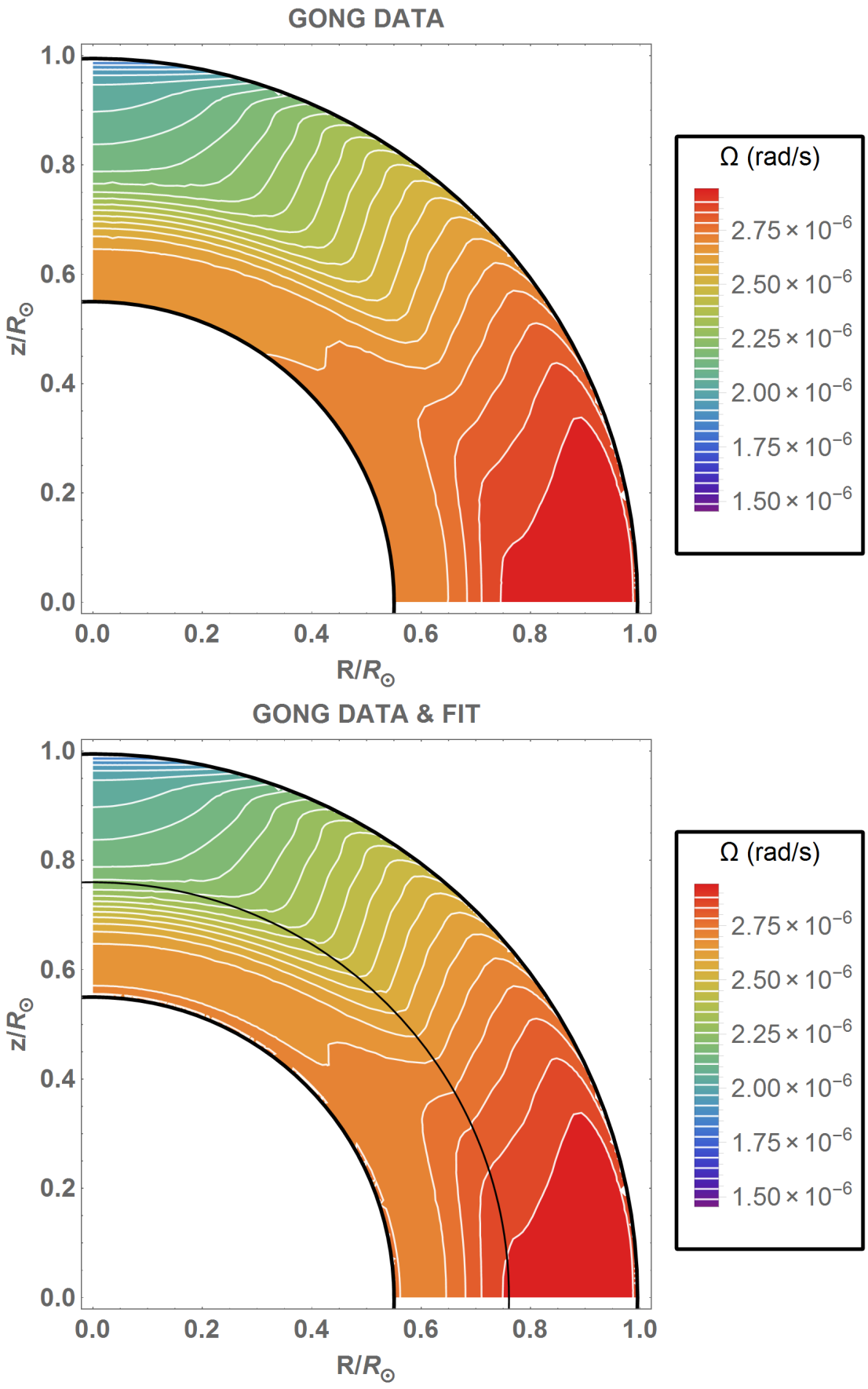

Figure 3.1: Isocontours of the angular velocity $\Omega(r,\theta)$ for $0.55R_\odot < r < R_\odot$. The upper panel shows the GONG data. The lower panel shows the best fit of the form (3.13) for the data interior to $r < 0.76R_\odot$, joined with the actual GONG data for $r > 0.76R_\odot$ (the surface $r = 0.76R_\odot$ is shown as a black line). Figure 3.2 shows a more detailed comparison of the values in the interval $0.55R_\odot < r < 0.76R_\odot$.

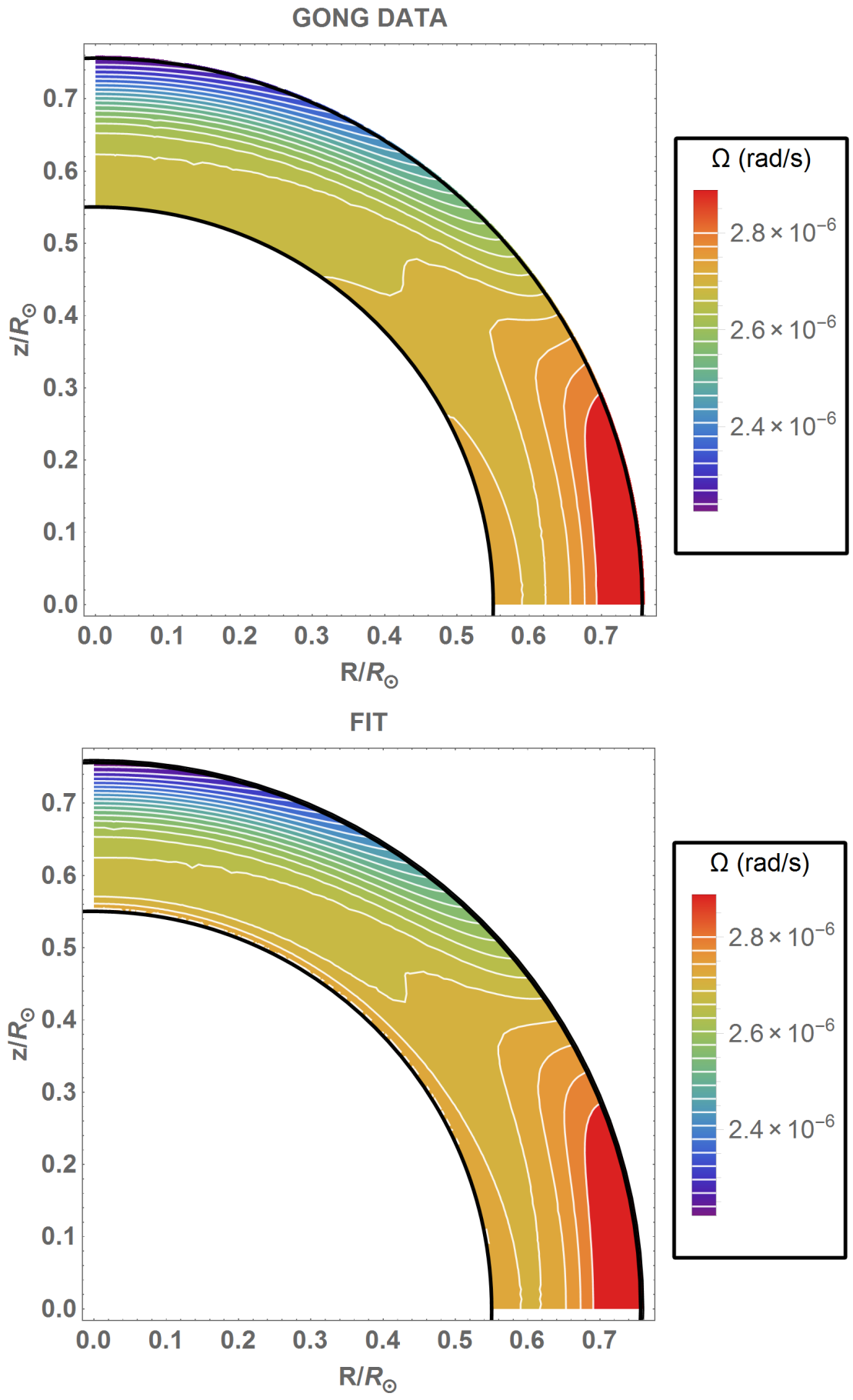

Figure 3.2: Isocontours of the angular velocity $\Omega(r,\theta)$ for $0.55R_\odot < r < 0.76R_\odot$. The upper panel shows the GONG data, while the lower panel shows the best fit of the form (3.13) for the data.

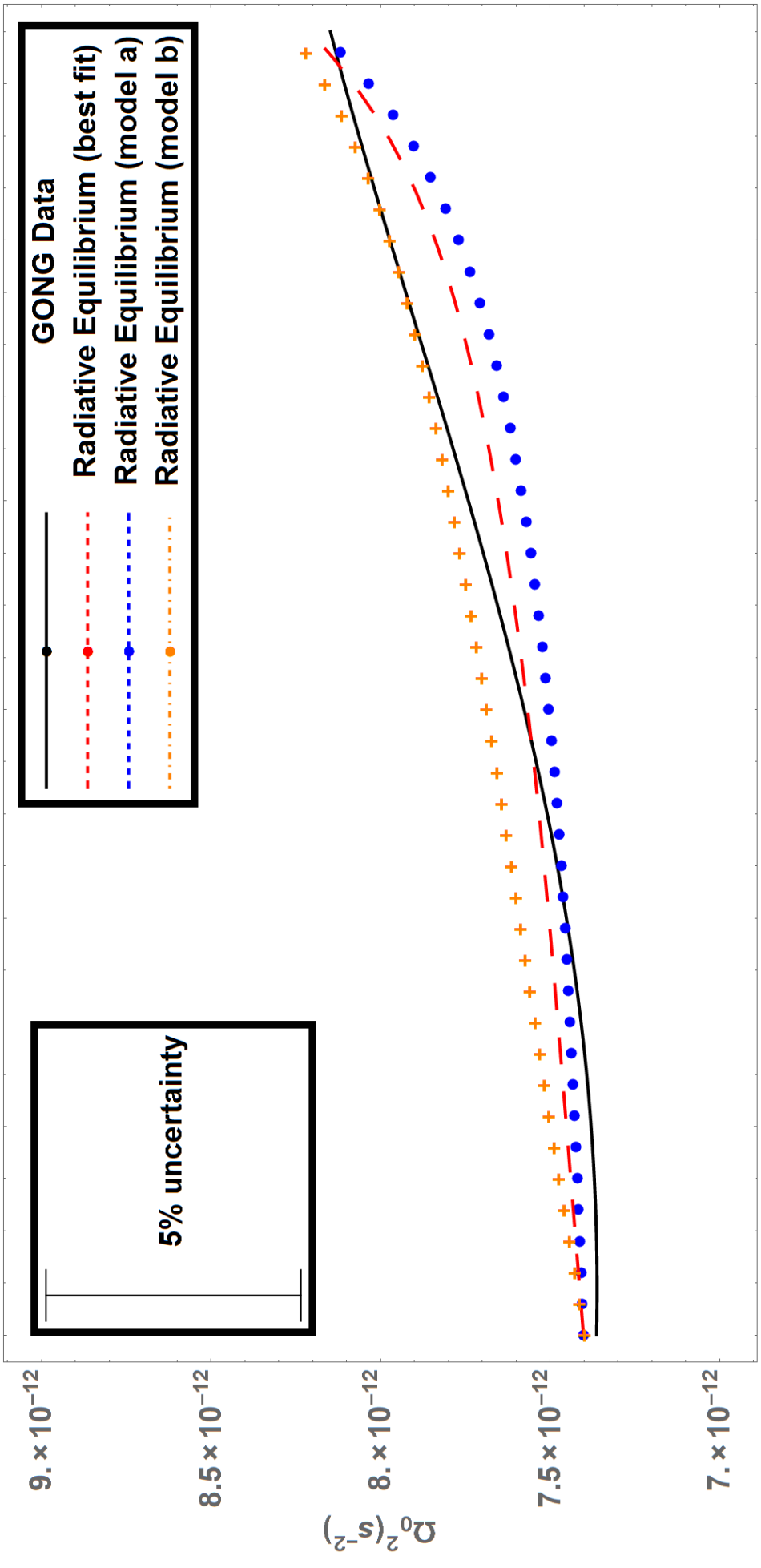

Figure 3.3: Angular velocity term $\Omega_0^2(r)$ of equation (3.13) in the outer part of the radiative zone according to the GONG data (solid line), to the model in radiative equilibrium that best fits the data (dashed line), and to models a (dots) and b (crosses); see description in the text. The boundary conditions at $r_0 = 0.60$ $R_\odot$ are illustrated in table 3.1. An error bar corresponding to a relative uncertainty of about 5% at the tachocline is shown, although the actual error is probably larger.

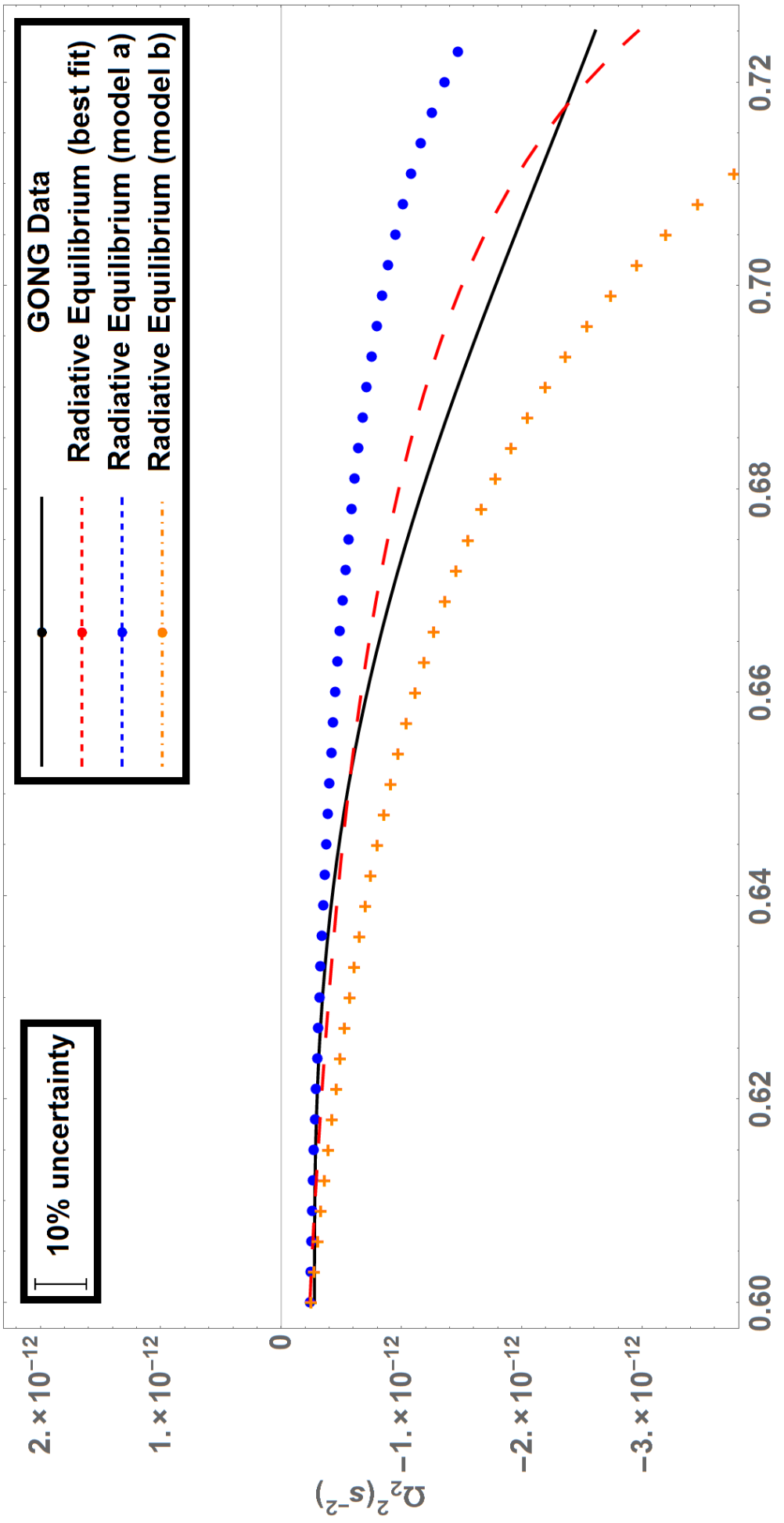

Figure 3.4: Angular velocity term $\Omega_2^2(r)$ of equation (3.13) in the outer part of the radiative zone according to the GONG data (solid line), to the model in radiative equilibrium that best fits the data (dashed line), and to models a (dots) and b (crosses); see description in the text. The boundary conditions at $r_0 = 0.60$ $R_\odot$ are illustrated in table 3.1. An error bar corresponding to a relative uncertainty of about 10% at the tachocline is shown, although the actual error is probably larger.

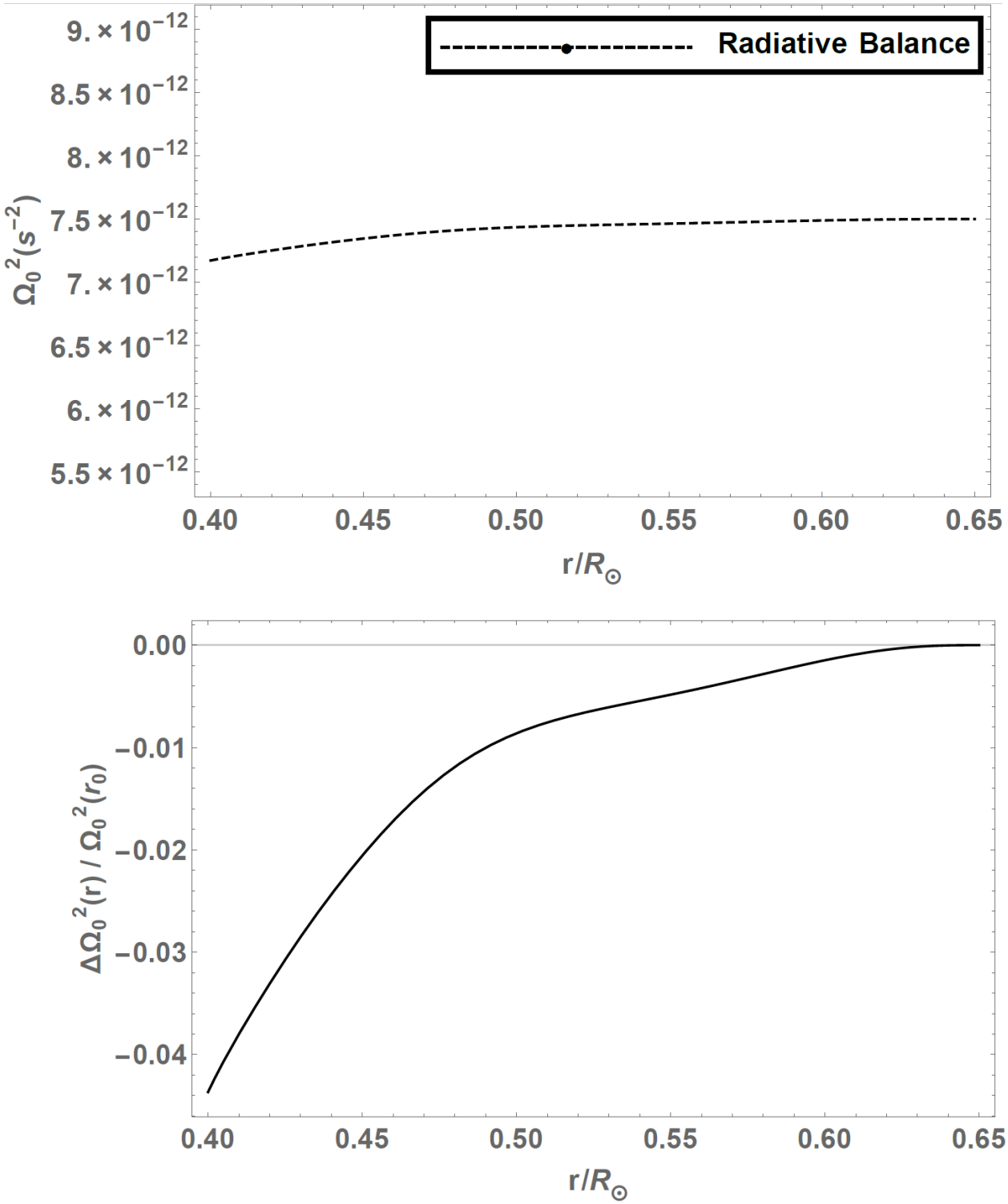

Figure 3.5: Upper panel: angular velocity $\Omega_0^2(r)$ in a Sun-like star, obtained imposing the boundary conditions of table 3.2 at $r_0 = 0.65R_\odot$. Lower panel: deviation from uniform rotation expressed as $(\Omega_0^2(r) - \Omega_0^2(r_0))/\Omega_0^2(r_0)$.

Chapter 4

Stability of baroclinic patterns of differential rotation

We have seen that barotropic rotation and radiative equilibrium are mutually incompatible in stars. Addressing this issue by allowing for a meridional circulation is also not devoid of theoretical complications. In the previous chapter, I have presented models of Solar rotation which maintain strict radiative equilibrium. To investigate the dynamical behaviour of these solutions, I study here the local stability of stratified, weakly magnetized, differentially rotating fluids to non-axisymmetric perturbations. Finite heat conductivity, kinematic viscosity, and resistivity are all included.

I will show that the evolution of local embedded perturbations is governed by a set of coupled, ordinary differential equations with time-dependent coefficients. In particular, I consider two baroclinic models of rotation for the upper radiative zone and tachocline: (i) an interpolation based on helioseismology data, and (ii) a theoretical solution directly compatible with radiative equilibrium. I study the growth of the local Goldreich-Schubert-Fricke axisymmetric instability, which appears to be suppressed, largely because of the viscosity. An extensive exploration of wavenumber space is also carried out, with and without a magnetic field, following the evolution of a total of approximately 2×10^6 modes.

The analysis reveals neither unstable solutions, nor even solutions featuring a large transient growth. Whilst my result does not rule out larger scale or nonlinear instabilities, nor have I rigorously proven local stability, it suggests that rotational configurations in close agreement with the observations, generally thought to be vulnerable to the classic local Goldreich-Schubert-Fricke instability, are very likely to be locally stable under rather general circumstances.

4.1 Introduction

In chapter 3, I have calculated models in radiative equilibrium for the upper radiative zone and tachocline. These models are time-steady and feature a baroclinic deviation from uniform rotation. To be viable, however, such models must be stable. Are these solutions actually stable? I present here an investigation of this question, by studying the local stability behaviour of such configurations and, more generally, of models compatible with the helioseismology data.

An overview of the astrophysical literature on the local stability of differential rotation has been given in sections 2.4 and 2.5, for both the axisymmetric and non-axisymmetric case. There I argued that the inclusion of a background magnetic field, diffusive terms, and non-axisymmetry can all play an important role, even when these effects would appear to be negligible at a first glance. I develop here a general diffusive treatment, deriving a set of equations for the time-evolution of embedded local linear perturbations under conditions in which the equilibrium is both shearing and stratified. This requires a Lagrangian approach, using coordinates tied to the background flow. The work presented here extends the study of stability to axisymmetric perturbations by Menou et al. [2004, hereafter MBS2004], by considering non-axisymmetric modes. These techniques are then applied to two patterns of rotation that are compatible with the data from helioseismology.

Once again, I use both standard spherical coordinates (r, ϕ, θ) as well as cylindrical coordinates (R, ϕ, z). The background rotation profile is azimuthally symmetric, but otherwise arbitrary: $\Omega = \Omega(r, \theta)$ or $\Omega = \Omega(R, z)$.

4.2 Local linear growth of perturbations in a shearing fluid

I present here the equations for the local linear growth of incompressible WKB perturbations in a weakly magnetized, shearing fluid in the triple-diffusive case for a generic Lagrangian wave vector $\boldsymbol{k}'_R = (k'_R, k'_\phi, k'_z)$. The axisymmetric limit of this is presented in MBS04, while the adiabatic limit is presented in Balbus and Schaan [2012]. The azimuthal component of the wave vector, expressed henceforth as k'_ϕ, is related to the notation of section 2.4 by $k'_\phi = m/R$.

4.2.1 The fluid equations

The governing MHD equations are:

$$\frac{\partial \rho}{\partial t} + \boldsymbol{\nabla}\cdot(\rho \boldsymbol{v}) = 0, \tag{4.1}$$

$$\rho\frac{D\boldsymbol{v}}{Dt}+\boldsymbol{\nabla}\left(P+\frac{B^2}{8\pi}\right)-\frac{1}{4\pi}(\boldsymbol{B}\cdot\boldsymbol{\nabla})\boldsymbol{B}-\rho\boldsymbol{g}-\rho\nu\nabla^2\boldsymbol{v}=0, \tag{4.2}$$

$$\frac{\partial\boldsymbol{B}}{\partial t}-\boldsymbol{\nabla}\times(\boldsymbol{v}\times\boldsymbol{B})-\eta\nabla^2\boldsymbol{B}=0, \tag{4.3}$$

$$\frac{P}{\gamma-1}\frac{D\sigma}{Dt}-\chi\nabla^2T=0, \tag{4.4}$$

where $\boldsymbol{v}$ is the velocity of the fluid, ρ its density, P its pressure, $\boldsymbol{B}$ the magnetic field, $\mathbf{g}$ the gravitational field, ν the kinematic viscosity, η the resistivity, $\sigma=\log\left(P\rho^{-\gamma}\right)$, γ the adiabatic index, χ the heat conductivity, and T the temperature. The Lagrangian derivative D/Dt in its Eulerian form is as usual:

$$\frac{D}{Dt}=\frac{\partial}{\partial t}+(\boldsymbol{v}\cdot\boldsymbol{\nabla}). \tag{4.5}$$

As in MBS04, I neglect the spatial dependence of the diffusion coefficients, which is appropriate for a local WKB analysis. I also neglect the resistive and viscous dissipation terms in equation (4.4), as they appear only at higher order; see Appendix A1 of MBS04.

I consider Eulerian perturbations (denoted by a prefix δ) of a background medium. The perturbations have a local WKB plane wave spatial dependence in the Lagrangian frame, as described in section 2.4, with Lagrangian wave vector $\boldsymbol{k}'=(k'_R,k'_\phi,k'_z)$ and corresponding Eulerian wave vector $\boldsymbol{k}(t)=(k_R(t),k_\phi,k_z(t))$ where $k_R(t)$ and $k_z(t)$ are given by:

$$k_R(t)=k'_R-Rk'_\phi t\frac{\partial\Omega}{\partial R},\qquad k_z(t)=k'_z-Rk'_\phi t\frac{\partial\Omega}{\partial z}, \tag{4.6}$$

with k_ϕ unchanged.

The equilibrium state rotation is given by $\boldsymbol{\Omega}=\Omega(R,z)\hat{z}$ along the z-axis. I neglect any bulk circulation in the star. I also neglect the effects our perturbations have on the gravitational potential of the star (Cowling approximation). For the magnetic field, I make the weak field approximation, assuming that the magnetic field plays no role in the background equilibrium state, but it can still be important for the evolution of perturbations with large wavenumbers. I will explicitly state whenever I neglect a magnetic term when equations (4.2) - (4.4) are perturbed.

I restrict the analysis to nearly incompressible modes, adopting the Boussinesq approximation (Spiegel and Veronis 1960, Kundu et al. 2012). This involves replacing the linearised continuity equation (4.1) with the simpler condition:

$$\boldsymbol{\nabla}\cdot\delta\boldsymbol{v}=0, \tag{4.7}$$

and neglecting perturbations in the density in equations (4.2) - (4.4), except when ρ is multiplied by the gravity $\boldsymbol{g}$, and in the entropy equation where it dominates over pressure pertur-

bations δP. In this problem, equation (4.7) translates to

$$\boldsymbol{k}\cdot\delta\boldsymbol{v} = 0. \tag{4.8}$$

In this equation and in those that follow, it is understood that $\boldsymbol{k}$ always refers to the Eulerian, time-dependent wave vector. I also of course require the magnetic field to be divergence-free:

$$\boldsymbol{k}\cdot\delta\boldsymbol{B} = 0. \tag{4.9}$$

It should be noted that if equation (4.9) holds at time $t = 0$, equation (4.3) implies that it will also hold at $t > 0$.

4.2.2 First-order expansion of (4.2)

With a linear perturbation added to the velocity field, I set $\boldsymbol{v} = \Omega R\hat{\phi} + \delta\boldsymbol{v}$ in equation (4.2). The leading order linear terms are given by

$$\delta\left(\frac{D\boldsymbol{v}}{Dt}\right) = \left(\frac{D\delta v_R}{Dt} - 2\Omega\delta v_\phi\right)\hat{R} + \left(\frac{D\delta v_\phi}{Dt} + \Omega\delta v_R + \delta\boldsymbol{v}\cdot\boldsymbol{\nabla}(\Omega R)\right)\hat{\phi} + \left(\frac{D\delta v_z}{Dt}\right)\hat{z}. \tag{4.10}$$

To express the first-order approximation of the second term of equation (4.2), I define the total (gas + magnetic) pressure in the plasma as:

$$P_t = P + \frac{B^2}{8\pi}. \tag{4.11}$$

The result is:

$$\delta\left(\boldsymbol{\nabla}P_t\right) \cong \left(i\frac{k_R}{\rho}\delta P_t\right)\hat{R} + \left(i\frac{k_\phi}{\rho}\delta P_t\right)\hat{\phi} + \left(i\frac{k_z}{\rho}\delta P_t\right)\hat{z}. \tag{4.12}$$

Assuming the equilibrium magnetic field and its spatial derivatives to be small, I neglect the $(\delta\boldsymbol{B}\cdot\boldsymbol{\nabla})\boldsymbol{B}$ term in the first-order expression of the third term of equation (4.2) relative to spatial gradients of $\delta\boldsymbol{B}$. The result is:

$$\frac{1}{4\pi}(\boldsymbol{B}\cdot\boldsymbol{\nabla})\delta\boldsymbol{B} \cong \frac{1}{4\pi}i(\boldsymbol{k}\cdot\boldsymbol{B})(\delta B_R\hat{R} + \delta B_\phi\hat{\phi} + \delta B_z\hat{z}) \tag{4.13}$$

I note that the azimuthal component of the background magnetic field B_ϕ is not independent of time, but satisfies the induction equation:

$$\frac{\partial B_\phi}{\partial t} = R(\boldsymbol{B}\cdot\boldsymbol{\nabla})\Omega, \tag{4.14}$$

which gives

$$B_\phi = B'_\phi + tR(\boldsymbol{B}\cdot\boldsymbol{\nabla})\Omega, \tag{4.15}$$

where B'_ϕ is the initial azimuthal component of the magnetic field. Computing the dot product $\boldsymbol{k}\cdot\boldsymbol{B}$ by means of equations (4.6) and (4.15), one obtains:

$$\boldsymbol{k}(t)\cdot\boldsymbol{B}(t) = (k'_R - Rk'_\phi t\frac{\partial\Omega}{\partial R})B_R + k'_\phi(B'_\phi + tR(B_R\frac{\partial\Omega}{\partial R} + B_z\frac{\partial\Omega}{\partial z})) + (k'_z - Rk'_\phi t\frac{\partial\Omega}{\partial z})B_z, \tag{4.16}$$

which reduces to $\boldsymbol{k}(t)\cdot\boldsymbol{B}(t) = k'_R B_R + k'_\phi B'_\phi + k'_z B_z = \boldsymbol{k}'\cdot\boldsymbol{B}'$. The quantity $\boldsymbol{k}\cdot\boldsymbol{B}$ is thus independent of time. I will make use of this result in later sections.

Adopting the standard Cowling approximation, I neglect the changes to the gravitational potential caused by linear perturbations. The buoyancy term in $\delta\rho\,\boldsymbol{g}$ is retained when perturbing equation (4.2). Assuming hydrostatic equilibrium and axisymmetry for the background state, we have:

$$\boldsymbol{g} = \frac{1}{\rho}\frac{\partial P_t}{\partial R}\hat{R} + \frac{1}{\rho}\frac{\partial P_t}{\partial z}\hat{z}. \tag{4.17}$$

Therefore:

$$\delta(\rho\boldsymbol{g}) = (\delta\rho)\boldsymbol{g} = \Big(\frac{\delta\rho}{\rho}\frac{\partial P_t}{\partial R}\hat{R} + \frac{\delta\rho}{\rho}\frac{\partial P_t}{\partial z}\hat{z}\Big). \tag{4.18}$$

Finally, the first-order approximation of the last term of equation (4.2) is:

$$-\rho\nu\nabla^2\boldsymbol{v} \simeq \rho\nu k^2(\delta v_R\hat{R} + \delta v_\phi\hat{\phi} + \delta v_z\hat{z}). \tag{4.19}$$

The resulting equations for the three components of equation (4.2) are:

$$\frac{D\delta v_R}{Dt} = 2\Omega\delta v_\phi + \frac{\delta\rho}{\rho^2}\frac{\partial P_t}{\partial R} - \frac{ik_R}{\rho}\delta P_t + \frac{i(\boldsymbol{k}\cdot\boldsymbol{B})}{4\pi\rho}\delta B_R - k^2\nu\delta v_R, \tag{4.20}$$

$$\frac{D\delta v_\phi}{Dt} = -\Omega\delta v_R - \delta\boldsymbol{v}\cdot\boldsymbol{\nabla}(\Omega R) - \frac{ik_\phi}{\rho}\delta P_t + \frac{i(\boldsymbol{k}\cdot\boldsymbol{B})}{4\pi\rho}\delta B_\phi - k^2\nu\delta v_\phi, \tag{4.21}$$

$$\frac{D\delta v_z}{Dt} = \frac{\delta\rho}{\rho^2}\frac{\partial P_t}{\partial z} - \frac{ik_z}{\rho}\delta P_t + \frac{i(\boldsymbol{k}\cdot\boldsymbol{B})}{4\pi\rho}\delta B_z - k^2\nu\delta v_z. \tag{4.22}$$

4.2.3 First-order expansion of (4.3)

In the first-order expansion of equation (4.3), I neglect the term $(\delta\boldsymbol{v}\cdot\boldsymbol{\nabla})\boldsymbol{B}$ by the weak field assumption. Proceeding as above, the components of the perturbed equation are found to be:

$$\frac{D\delta B_R}{Dt} - i(\boldsymbol{k}\cdot\boldsymbol{B})\delta v_R + \eta k^2\delta B_R = 0, \tag{4.23}$$

$$\frac{D\delta B_\phi}{Dt} - i(\boldsymbol{k}\cdot\boldsymbol{B})\delta v_\phi - R\big((\delta\boldsymbol{B}\cdot\boldsymbol{\nabla})\Omega\big) + \eta k^2 \delta B_\phi = 0, \tag{4.24}$$

$$\frac{D\delta B_z}{Dt} - i(\boldsymbol{k}\cdot\boldsymbol{B})\delta v_z + \eta k^2 \delta B_z = 0. \tag{4.25}$$

4.2.4 First-order expansion of (4.4)

To compute the first-order expansion of equation (4.4), I make the standard assumption that the displaced fluid element is in near pressure equilibrium with its surroundings, because the time-scale to reach such equilibrium is much shorter than any other relevant time-scale.

$$\delta\sigma = \delta \log\left(P\rho^{-\gamma}\right) = \frac{\delta P}{P} - \gamma\frac{\delta\rho}{\rho} \simeq -\gamma\frac{\delta\rho}{\rho}. \tag{4.26}$$

I also assume a perfect gas equation of state,

$$P = \frac{\rho}{\mu m_{\mathrm{P}}} k_{\mathrm{B}} T, \tag{4.27}$$

where μ is the average chemical weight, m_{P} is the mass of the proton, and k_{B} is Boltzmann's constant. Assuming a uniform chemical composition, I relate the perturbations in the pressure, density, and temperature by:

$$\frac{\delta T}{T} = \frac{\delta P}{P} - \frac{\delta\rho}{\rho} \cong -\frac{\delta\rho}{\rho}. \tag{4.28}$$

Proceeding as in section 4.2.2, the perturbed entropy equation is found to be:

$$\frac{D}{Dt}\left(\frac{\delta\rho}{\rho}\right) - \frac{1}{\gamma}\left(\delta v_R \frac{\partial\sigma}{\partial R} + \delta v_z \frac{\partial\sigma}{\partial z}\right) + \frac{\gamma-1}{\gamma}\chi k^2 \frac{T}{P}\frac{\delta\rho}{\rho} = 0. \tag{4.29}$$

4.2.5 Reduction to real, coupled equations

I aim to reduce the perturbed equations to a set of real, coupled ordinary differential equations. By multiplying equations (4.23), (4.24), and (4.25) by the imaginary unit i, the magnetic field perturbation $\delta\boldsymbol{B}$ always appears with a factor of i in the perturbed equations. This is equivalent to a simple change of phase by $\pi/2$. To obtain a set of real equations, I work with the variable

$$\delta\boldsymbol{C} = i\delta\boldsymbol{B}, \tag{4.30}$$

in preference to $\delta\boldsymbol{B}$ itself.

I make use of equations (4.8) and (4.9) to replace δv_ϕ and δC_ϕ:

$$\delta v_\phi = -\frac{1}{k_\phi}(k_R \delta v_R + k_z \delta v_z), \tag{4.31}$$

$$\delta C_\phi = -\frac{1}{k_\phi}(k_R \delta C_R + k_z \delta C_z). \tag{4.32}$$

It is also necessary to compute the Lagrangian time derivative of equation (4.31), since the term $D\delta v_\phi/Dt$ appears in equation (4.21). The result is:

$$\frac{D\delta v_\phi}{Dt} = -\frac{1}{k_\phi}\left(k_R \frac{D\delta v_R}{Dt} + k_z \frac{D\delta v_z}{Dt}\right) + R(\delta \boldsymbol{v}\cdot\boldsymbol{\nabla})\Omega. \tag{4.33}$$

4.2.6 Governing equations

My strategy is to eliminate δv_ϕ and δC_ϕ in equations (4.20)-(4.25) and (4.29). It is then possible to solve for

$$i\frac{1}{\rho}\delta P_t \tag{4.34}$$

in equation (4.21) and substitute this into equations (4.20) and (4.22). Finally, I rearrange equations (4.20) and (4.22) to isolate the Lagrangian derivatives of δv_R and δv_z. The procedure is quite lengthy, but entirely straightforward. Defining the Alfvén velocity:

$$\boldsymbol{v}_A = \frac{\boldsymbol{B}}{\sqrt{4\pi\rho}}, \tag{4.35}$$

the final form of the equations is:

$$\begin{aligned}\frac{D\delta v_R}{Dt} &- \frac{\boldsymbol{k}\cdot\boldsymbol{v}_A}{\sqrt{4\pi\rho}}\delta C_R + 2\Omega\frac{k_\phi^2 + k_z^2}{k_\phi k^2}(k_R\delta v_R + k_z\delta v_z) - \\ &- 2\frac{k_\phi k_R}{k^2}(\delta\boldsymbol{v}\cdot\boldsymbol{\nabla})(\Omega R) + \frac{\delta\rho}{\rho^2}\left(\frac{k_z^2}{k^2}\widetilde{D}P - \frac{k_\phi^2}{k^2}\frac{\partial P}{\partial R}\right) + \nu k^2 \delta v_R = 0,\end{aligned} \tag{4.36}$$

$$\begin{aligned}\frac{D\delta v_z}{Dt} &- \frac{\boldsymbol{k}\cdot\boldsymbol{v}_A}{\sqrt{4\pi\rho}}\delta C_z - 2\Omega\frac{k_R k_z}{k_\phi k^2}(k_R\delta v_R + k_z\delta v_z) - \\ &- 2\frac{k_\phi k_z}{k^2}(\delta\boldsymbol{v}\cdot\boldsymbol{\nabla})(\Omega R) - \frac{\delta\rho}{\rho^2}\left(\frac{k_R k_z}{k^2}\widetilde{D}P + \frac{k_\phi^2}{k^2}\frac{\partial P}{\partial z}\right) + \nu k^2 \delta v_z = 0,\end{aligned} \tag{4.37}$$

$$\frac{D\delta C_R}{Dt} + \eta k^2 \delta C_R + \sqrt{4\pi\rho}(\boldsymbol{k}\cdot\boldsymbol{v}_A)\delta v_R = 0, \tag{4.38}$$

$$\frac{D\delta C_z}{Dt} + \eta k^2 \delta C_z + \sqrt{4\pi\rho}(\boldsymbol{k}\cdot\boldsymbol{v}_A)\delta v_z = 0, \tag{4.39}$$

$$\frac{D}{Dt}\left(\frac{\delta\rho}{\rho}\right) - \frac{1}{\gamma}\left(\delta v_R\frac{\partial\sigma}{\partial R} + \delta v_z\frac{\partial\sigma}{\partial z}\right) + \frac{\gamma-1}{\gamma}\chi k^2\frac{T}{P}\frac{\delta\rho}{\rho} = 0. \tag{4.40}$$

In these equations, I have introduced once again the $\widetilde{D}$ operator [Balbus, 1995]:

$$\widetilde{D} = \frac{k_R}{k_z}\frac{\partial}{\partial z} - \frac{\partial}{\partial R}, \tag{4.41}$$

and the coordinates of the Eulerian wave vector $\boldsymbol{k}$ are given by:

$$k_R(t) = k_{R0} - k_{\phi 0} R t \frac{\partial \Omega}{\partial R}, \tag{4.42}$$

$$\frac{m}{R} \equiv k_\phi = k_{\phi 0} = \text{constant}, \tag{4.43}$$

$$k_z(t) = k_{z0} - k_{\phi 0} R t \frac{\partial \Omega}{\partial z}, \tag{4.44}$$

where k_{R0}, $k_{\phi 0}$, and k_{z0} are the initial values of the wave vector components (corresponding to k'_R, k'_ϕ, and k'_z in the notation of chapter 2). Finally, the azimuthal components of $\delta\boldsymbol{v}$ and $\delta\boldsymbol{C}$ are given by equations (4.31) and (4.32). Equations (4.36) - (4.40) constitute a set of five ordinary differential equations with time-dependent coefficients in the variables δv_R, δv_z, δC_R, δC_z, and $\delta\rho$. Given the appropriate initial conditions, they can be solved numerically.

4.3 The rotation of the upper radiative zone of the Sun

4.3.1 Model parameters

I use equations (4.36) - (4.40) to analyse the local stability of the upper radiative zone of the Sun. As in chapter 3, the background state is given by a standard, non-rotating solar model (Bahcall et al. 2005). I have extracted local values for the background structural variables P, ρ, and T and calculated the gravitational field in the star from the mass distribution. The background state in effect satisfies equation (4.2) with $\boldsymbol{v} = 0$ and $\boldsymbol{B} = 0$. Just as with the magnetic field, the rotation does not influence hydrostatic equilibrium at a significant level, but it is important for the behaviour of perturbations.

Observational constraints on the angular velocity are provided by helioseismology and have been discussed in section 1.3; the data show a pattern of approximately uniform rotation throughout much of the radiative zone, but with significant shear near the convective boundary. The uncertainty on Ω depends on latitude, with values at the poles being relatively less reliable. It may be estimated to be of order 10% at the depth of the radiative zone. The situation is more difficult to assess in the tachocline, which is not particularly well-resolved. Models exist for the physics of the upper radiative zone yielding rotation curves compatible with the helioseismology data, but neither the models nor the observations must abide to the strict GSF local stability criterion of Ω being fixed on cylinders, $\partial_z \Omega = 0$. In the rest of this chapter,

I investigate the local stability behaviour of two such "GSF-violating" patterns of differential rotation with $\partial_z \Omega \neq 0$, which will be referred to as models A and B:

- Model A is the interpolation of a recent set of helioseismology data by the GONG group [Hill and et al., 1996]. The data and isorotation contours are shown in figure 1.4. I approximate $\Omega(r, \theta)$ with a function of the form:

$$\Omega^2(r, \theta) \cong \Omega_0^2(r) + \Omega_2^2(r) \cos^2 \theta, \tag{4.45}$$

  where fifth-order polynomials are used for $\Omega_0^2(r)$ and $\Omega_2^2(r)$. This approximation reproduces the helioseismology data very accurately, as discussed in section 3.2.2. $\Omega_0^2(r)$ and $\Omega_2^2(r)$ are shown as black solid lines in figures 3.3 and 3.4 respectively.

  While the Sun may or may not be in static radiative equilibrium depending on fine rotational details, this model would, strictly speaking, require some form of circulation or evolution to maintain radiative equilibrium. This would not immediately affect my analysis, which is concerned with time-scales much shorter than the Kelvin-Helmholtz time-scale.

- Model B is the radiative rotation curve described in chapter 3 (see the red dashed lines in figures 3.3 and 3.4). This curve, which also provides a good fit to the GONG data, is derived by imposing the requirement of *exact* radiative equilibrium $\boldsymbol{\nabla \cdot F}_{\rm rad} = 0$ in the radiative zone and in the tachocline. Model B represents an alternative to the standard uniform rotation model with thermal equilibrium maintained by meridional circulation. It describes a time-steady, circulation-free state of strict radiative equilibrium, both in the bulk of the radiative zone (where the differential rotation is tiny) and in the tachocline (where it is significant). Model A and model B are both compatible with the data at the current level of accuracy.

As already demonstrated, models A and B are numerically similar, although their physical interpretation is different. I report here just the angular velocity and its first derivatives at $r = 0.7 R_\odot$ and $\theta = 45^\circ$ for the two models:

$$\Omega_A = 2.7 \times 10^{-6} \text{ rad s}^{-1}, \qquad \Omega_B = 2.7 \times 10^{-6} \text{ rad s}^{-1}, \tag{4.46}$$

$$\left(\frac{\partial \ln \Omega}{\partial \ln R}\right)_A = -0.11, \qquad \left(\frac{\partial \ln \Omega}{\partial \ln R}\right)_B = -0.15, \tag{4.47}$$

$$\left(\frac{\partial \ln \Omega}{\partial \ln z}\right)_A = -0.24, \qquad \left(\frac{\partial \ln \Omega}{\partial \ln z}\right)_B = -0.26. \tag{4.48}$$

For comparison, $(N/\Omega)^2 \cong 1.6 \times 10^5$ in both models[1].

The diffusivities are estimated in the same manner as MBS04. I denote by χ the coefficient so denoted by the same letter by MBS04. This differs from χ as used by Goldreich and Schubert [1967, hereafter GS67], even dimensionally. The latter is related to the coefficient $\xi_{\rm rad}$ of MBS04 by:

$$\xi_{\rm rad} = (\gamma - 1)\chi_{GS}, \tag{4.49}$$

where χ_{GS} is the quantity denoted as χ by GS67. Dimensionally, $[\chi] = MLT^{-3}K^{-1}$, $[\xi_{\rm rad}] = [\chi_{GS}] = L^2T^{-1}$, where M, L, T, and K respectively represent mass, length, time, and temperature.

The thermal diffusion coefficients in the radiative zone of the Sun are given by (see e.g. Schwarzschild 1958):

$$\chi = \frac{16T^3\sigma_{\rm SB}}{3\kappa\rho}, \tag{4.50}$$

$$\xi_{\rm rad} = \frac{\gamma - 1}{\gamma}\frac{T}{P}\chi, \tag{4.51}$$

where $\sigma_{\rm SB}$ is the Stefan-Boltzmann constant and κ is the radiative opacity. I have interpolated the Rosseland opacity $\kappa(\rho, T)$ from the OPAL table for solar composition [Iglesias and Rogers, 1996]. The kinematic viscosity is taken from Spitzer [1962], $\nu_d \simeq 21$ cm^2 s^{-1}. An expression for the radiative viscosity is given by e.g. GS67 and yields a small contribution to the total viscosity; with the current solar model and the Rosseland opacity interpolated from the OPAL table for solar composition, I have determined $\nu_r \simeq 2$ cm^2 s^{-1}. I adopt the same value of MBS04 for the resistivity η. Finally, the values I adopt for the diffusivities at $r = 0.70R_\odot$ are: $\xi_{rad\odot} = 1.4 \times 10^7$ cm^2 s^{-1}, $\nu_\odot \simeq 23$ cm^2 s^{-1}, and $\eta_\odot = 596$ cm^2 s^{-1}.

Since $\partial_z\Omega \neq 0$, the naive expectation is that the GSF instability should be present. In what follows, I discuss the occurrence of this instability in the upper radiative zone of the Sun in section 4.4. I will then present in section 4.5 the evolution of a variety of non-axisymmetric solutions of equations (4.36) - (4.40).

4.3.2 The magnetic field in the radiative zone of the Sun

If a magnetic field with finite poloidal components B_R, B_z and finite derivatives of angular velocity $\partial_R\Omega$, $\partial_z\Omega$ are present at the same time, the azimuthal component of the background field $\boldsymbol{B}$ might increase linearly with time. This of course is also encountered in classical accretion disc theory of the magnetorotational instability (MRI). It makes no difference to the analysis so long as the background field remains weak. In disc theory, the rapid breakdown

[1]This shows that the stability criterion (2.46) is not violated at this depth and latitude. It is interesting to note that there are locations near the tachocline with $\partial \ln \Omega^2/\partial \ln R < 0$, and N^2 goes through zero at the radiative - convective boundary, so that there must be a region in which equation (2.46) is not satisfied. However, this region is very narrow in the current standard Solar model and becomes immediately convectively unstable.

of the flow into MHD turbulence renders moot the problem of a progressive linear build-up of the azimuthal field.

In the stellar case, this could be an issue in principle for an ostensibly stable rotation profile. Of course this is true for *any* model analysis that does not have $\boldsymbol{B} \cdot \boldsymbol{\nabla}\Omega = 0$, and stability issues can arise (see e.g Braithwaite 2009). The Sun is not in a state of uniform rotation, and it is magnetised. After 4.5 billion years it is not unreasonable to assume that the magnetic field lies very nearly in constant Ω surfaces. Since my findings of local stability are not sensitive to field geometry, I will ignore the problem of strong field build-up, assuming that in regions of the Sun that are not actively turbulent and dissipating magnetic field, such strong growth is not occurring. It is worth noting, however, that effects connected to a growing B_ϕ have been considered as angular momentum transport mechanisms in stellar interiors, as we have seen in section 1.4.2.

Finally, it must be noted that the process driving the Solar dynamo might affect the work presented here. It is well known that the a time-dependent magnetic field is present at the surface of the Sun; the detailed mechanism that generates it is not understood. The present analysis may be unaffected by the Solar dynamo if it is due to processes acting in the convective zone; it would likely be affected if the dynamo is located at the tachocline, and most certainly so if the dynamo is located deeper in the radiative zone.

4.4 Axisymmetric perturbations: the GSF instability in the upper radiative zone of the Sun

The GSF instability affects axisymmetric perturbations in a rotating medium if the angular velocity is not constant on cylinders, i.e. $\partial_z\Omega \neq 0$, and a finite thermal diffusion coefficient $\xi_{\rm rad}$ is present. I study here the evolution of perturbations under such conditions, at first in the inviscid case and then allowing for the introduction of a finite viscosity ν.

Analytically, the unstable modes may be identified by determining the sign of the last term of the dispersion relation of GS67, equation (2.60) of this thesis: whenever it is negative, the equation has an unstable solution. In the $\nu = 0$ case, it is easy to see that unstable modes will be found whenever $\partial_z\Omega \neq 0$, independently of the value of $\xi_{\rm rad}$. In this case, the region of the $k_R - k_z$ space corresponding to the unstable models is, by the classical GSF criterion,

$$\frac{\partial l}{\partial R} - \frac{k_R}{k_z}\frac{\partial l}{\partial z} > 0, \tag{4.52}$$

where $l = R^2\Omega$, the specific angular momentum. For $r = 0.7R_\odot$, $\theta = 45^\circ$, there are unstable modes only when k_R and k_z have opposite signs. Figure 4.1 shows the region of the $k_R < 0, k_z > 0$ plane where unstable modes exist, for a large range of values of k_R and k_z, for an

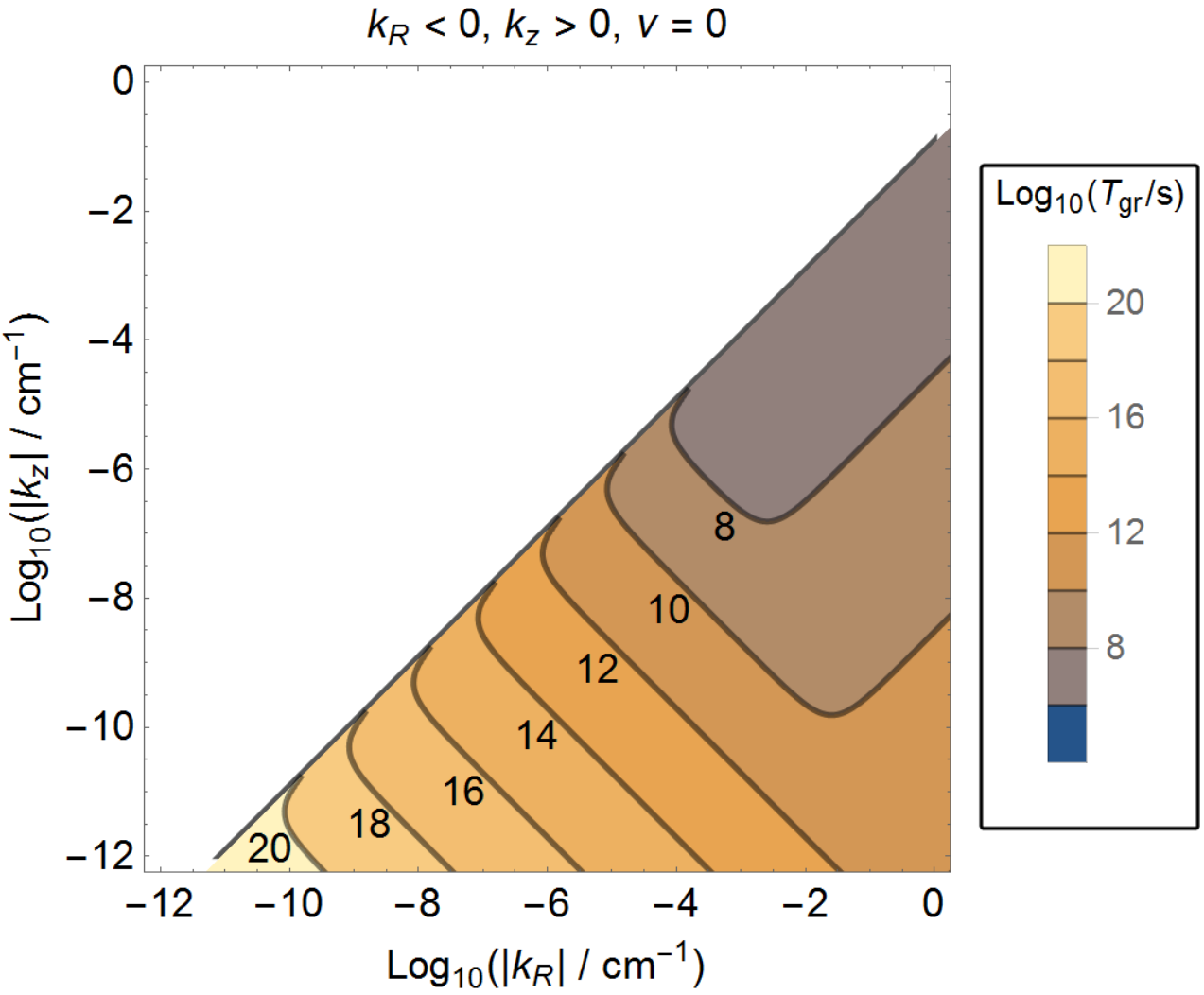

Figure 4.1: Region of the $k_R < 0, k_z > 0$ plane where the GSF axisymmetric instability occurs in the Sun, for $r = 0.7R_\odot$, $\theta = 45°$, in case of no viscosity, for an angular velocity pattern corresponding to model A. The growth time-scale $T_{\rm gr}$ of the instability is also shown. The numbers next to the iso-contours correspond to the value of $\log_{10}(T_{\rm gr})$ with $T_{\rm gr}$ expressed in seconds.

angular velocity pattern corresponding to model A. The figure also reports the growth rate $T_{\rm gr}$ of the axisymmetric perturbations, derived from the dispersion relation by GS67.

Matters are quite different when a finite viscosity is taken into account. As discussed in section 2.5, some authors noted that even a small viscosity $\nu \ll \xi_{\rm rad}$ has a stabilising effect on the GSF instability. I have solved the GS67 axisymmetric dispersion relation in the viscous case. As the equation is quite lengthy, I shall not reproduce it here again, but refer the reader to the original paper or section 2.5 of this thesis. Over the range of k_R, k_z shown in figure 4.1 with $\nu = \nu_\odot$, I have found no unstable behaviour: all the axisymmetric modes appear to be stable.

Performing the same analysis for values of the co-latitude θ in the $5° - 85°$ range, I have found stability for all θ. I have also performed the same analysis for the angular velocity pattern corresponding to model B, which is numerically similar to model A, and have found very little behavioural difference for $\nu = 0$ and no difference for $\nu = \nu_\odot$. Finally, I have

explored the case $\nu = 0.5\nu_\odot$, to determine whether an order unity uncertainty on the value of ν would bear any consequence on this analysis. Once again, even with this reduced value of the viscosity, there are no unstable modes. Evidently, the axisymmetric GSF instability does not occur in the Sun, even if its pattern of rotation features a moderate gradient of angular velocity, compatible with the data from helioseismology.

Although the Sun's rotation profile does not appear to be vulnerable to the axisymmetric GSF instability, conditions in other stars may be, and it is of interest to pursue equations (4.36) - (4.40) to study the behaviour of a fluid which is axisymmetrically unstable in the presence of finite viscosity, allowing for the presence of a magnetic field and finite k_ϕ. A more general study of the onset of the GSF instability in the Sun and other stars is presented in chapter 5.

4.5 Stability of the upper radiative zone of the Sun

The main point of the work presented here is the study of the local stability of non-axisymmetric displacements in a differentially rotating background, which requires the solution of a set of ordinary differential equations not reducible to an algebraic dispersion relation. Since the wavenumber is varying, this approach seems more prudent than trying to incorporate an intrinsically time-dependent wavenumber into a dispersion relation formalism (e.g. Kagan and Wheeler 2014).

As seen from equations (4.42) - (4.44), perturbations with $k_\phi \neq 0$ become asymptotically axisymmetric as $t \to \infty$, provided that $\boldsymbol{\nabla}\Omega \neq 0$, though the time dependence of $\boldsymbol{k}$ is not lost. A general stability analysis of the models of rotation of the upper radiative zone described in section 4.3 requires the full solution of equations (4.36) - (4.40) for any given initial wave vector $\boldsymbol{k}_0$, initial conditions $\delta\boldsymbol{v}_0$, $\delta\rho_0$, and $\delta\boldsymbol{B}_0$. Non-modal problems with similar features have recently been discussed for the onset of the MRI in discs. Here, transient growths of (eventually) stable modes are of particular significance. Squire and Bhattacharjee [2014] discuss this topic and the relevant methods in some detail. (See Trefethen and Embree 2005 for a rigorous mathematical presentation.) This method is computationally demanding and lies outside the scope of the current work.

Here, I present a study of the transient evolution of a variety of modes for an arbitrary set of initial conditions, both systematically and randomly selected. My aim is to identify regions of instability (or large transient growth) in the $k_R - k_\phi - k_z$ space, if any exist. As we have seen, the GSF instability occurs in a broad section of the $k_R - k_z$ plane when viscosity is ignored. It is in principle possible that nonaxisymmetry might also tip the balance. In fact, however, I find no large transient growth. I caution that the limitations of my approach do not allow me to make a definitive claim for the absolute stability of the models, as a complete exhaustive study of parameters (particularly the initial conditions) has not been performed, for the reasons presented above. However, my results definitely signal stability. If these models are unstable, something more elaborate than simple GSF behaviour is involved,

and the instability must depend anomalously on the initial conditions of the perturbation or be confined to a very narrow region of the $k_R - k_\phi - k_z$ space. In brief, not a shred of evidence for instability has been found.

4.5.1 Details of the mode selection

I have selected a single set of initial conditions as follows: I set $\delta v_z = 1$ cm s^{-1} (the numerical value is arbitrary), $\delta v_\phi = 0$, $\delta\rho_0 = 0$, $\delta\boldsymbol{B}_0 = 0$. I assign to δv_R a different value for each mode, chosen as to satisfy equation (4.8). I have studied modes with initial wave vector components in the range:

$$k_{R0}, k_\phi, k_{z0} : \ \pm\frac{2\pi}{10^{-2}R_\odot} \rightarrow \pm\frac{2\pi}{10^{-14}R_\odot}, \tag{4.53}$$

The first limit guarantees that the wavelength of the perturbation is small compared to the typical scale height of the structural properties of the Sun ($\sim 10^{-1}R_\odot$), as required by the WKB approximation. The second limit guarantees that the wavelength is large compared to the mean free path of the particles in the radiative zone of the Sun (MBS04).

I focus here on the non-degenerate case in which the values of k_{R0}, k_ϕ, and k_{z0} are such that the absolute value of the ratio of any two of the wave vector components is not smaller than 10^{-3}. As a consequence, I cannot reproduce instabilities that would occur in the extreme degenerate case; but the axisymmetric limit can be addressed via the dispersion relation, as was done by MBS04. I select a value for the total integration time by the following considerations. From (4.42) - (4.44), k_R and k_z depend on time, while k_ϕ is constant, so that the behaviour of any perturbation becomes increasingly (large wavenumber) axisymmetric with time. The conditions for the perturbation to be approximately axisymmetric are:

$$Rk_\phi\frac{\partial\Omega}{\partial R}t \gg k_{R0}, \qquad Rk_\phi\frac{\partial\Omega}{\partial R}t \gg k_\phi, \tag{4.54}$$

$$Rk_\phi\frac{\partial\Omega}{\partial z}t \gg k_{z0}, \qquad Rk_\phi\frac{\partial\Omega}{\partial z}t \gg k_\phi. \tag{4.55}$$

With values of the derivatives of Ω typical of models A and B, and the requirement that $|k_\phi/k_{R0}|$ and $|k_\phi/k_{z0}|$ are not smaller than 10^{-3}, these conditions are satisfied if $t \gg 10^9$ s $\cong$ 30 y. I follow the evolution of the perturbations an order of magnitude beyond this, after which time the perturbations are very close to axisymmetric.

To solve equations (4.36) - (4.40), it is necessary to specify the strength and geometry of the background magnetic field in the upper radiative zone. I note here that $\boldsymbol{B}$ appears in equations (4.36) - (4.40) only via the term $\boldsymbol{k}\cdot\boldsymbol{v}_A$. This term may be treated as a constant parameter. Unfortunately, $\boldsymbol{k}\cdot\boldsymbol{v}_A$ is effectively a natural frequency of the system and, in the most interesting case in which it is comparable to (or higher than) the angular velocity Ω, its presence makes following the evolution of the system computationally more demanding. Both for this reason and because the magnetic field appears not to play a destabilising role, I focus

first on the hydrodynamic case. A magnetic field is introduced in a relatively small number of runs described in section 4.5.4.

4.5.2 Systematic approach

I study here the evolution of a sample of $\sim 10^4$ hydrodynamic modes for both model A and B. The wave vector components are given by the angles θ_k and ϕ_k describing the orientation of $\boldsymbol{k}$ in spherical wavenumber space:

$$k_{R0} = |\boldsymbol{k}| \sin(\theta_k) \cos(\phi_k), \tag{4.56}$$

$$k_{\phi} = |\boldsymbol{k}| \sin(\theta_k) \sin(\phi_k), \tag{4.57}$$

$$k_{z0} = |\boldsymbol{k}| \cos(\theta_k). \tag{4.58}$$

I follow perturbations at $r = 0.70$ R$_\odot$ for a variety of modes selected as follows. I choose 5 equally spaced values of the co-latitude θ in the interval $[5°, 85°]$; I assign values of $|\boldsymbol{k}|$ so that $\log_{10}(|\boldsymbol{k}|) = -10, -9, ..., 3$; I select 5 equally spaced values of θ_k in $(0°, 180°)$, and 10 equally spaced values of ϕ_k in $(0°, 360°)$. I also include all the relevant values of θ_k and ϕ_k that are $1°$ away from $0°, 90°, 180°, 270°$. For present purposes, a transient growth coefficient has been defined as the maximum of $\delta v^2(t)/\delta v^2(t = 0)$. For both models, this analysis has not revealed any mode that is unstable or shows significant transient growth.

4.5.3 Random selection - hydrodynamic case

In the $\boldsymbol{v}_A = 0$ case, I have selected 10^5 runs for each of 9 equally spaced values of the co-latitude θ in the interval $5° - 85°$, for both models A and B, for a total of 1.8×10^6 modes, and tracked the evolution of these modes. The modes have been generated from uniform distributions for $\log_{10}(|k_R|)$, $\log_{10}(|k_\phi|)$, $\log_{10}(|k_z|)$ with the additional constraint that the absolute value of the ratio of any two of the wave vector components is not smaller than 10^{-3}.

No unstable modes were found. The vast majority of modes were damped, with no traceable growth. A typical evolution is shown in figure 4.2 (see end of the chapter). The time-scale of the damping and, when present, the oscillations, vary significantly between different modes. The damping of the perturbations appears to be predominantly viscous. Figure 4.3, for example, shows the behaviour of the perturbation with the same wave vector as that of figure 4.2, but with an artificially reduced viscosity of $\nu = 0.1\nu_\odot$.

I have identified about 10^2 modes that present a moderate transient growth before eventually damping to zero. In all these cases, the maximum growth factor is of order unity. These modes have typically small wave number, $|\boldsymbol{k}| \lesssim 10^{-8}$ cm^{-1}, feature multiple time-scales

behaviour, and have a much longer damping time-scale than the others. I show one such displacement in figures 4.4 (the short time-scale oscillations) and 4.5 (the long term integral average of $\delta v^2(t)/\delta v_0^2$). Nevertheless, all perturbations are eventually damped to 0.

4.5.4 Random selection - magnetic case

As noted above, $\boldsymbol{B}$ appears in equations (4.36) - (4.40) only via the term $\boldsymbol{k}\cdot\boldsymbol{v}_A$, a natural frequency of the system and a constant parameter. Since my focus is on the stability of the differential rotation patterns, I examine a variety of cases with $\boldsymbol{k}\cdot\boldsymbol{v}_A \ll \Omega$, $\boldsymbol{k}\cdot\boldsymbol{v}_A \sim \Omega$, or $\boldsymbol{k}\cdot\boldsymbol{v}_A \gg \Omega$, studying the interplay between the magnetic and rotational effects.

I selected 10^4 random modes for each of 9 equally spaced values of the co-latitude θ in the interval $5^\circ - 85^\circ$, for both models A and B, for a total of 1.8×10^5 modes. As in section 4.5.3, I varied k_{R0}, k_ϕ, and k_{z0} in the range (4.53). Adopting a uniform distribution for $\log_{10}(|\boldsymbol{k}\cdot\boldsymbol{v}_A|)$, I independently assigned random values to $\boldsymbol{k}\cdot\boldsymbol{v}_A$ in the range:

$$\boldsymbol{k}\cdot\boldsymbol{v}_A : \ \pm 10^{-2}\Omega \rightarrow \pm 10^{2}\Omega. \tag{4.59}$$

As before, I found no unstable behaviour. The vast majority of modes being damped with no traceable growth. I have identified about 10 modes that present a transient growth before being eventually damped to zero, with maximum growth factor of order unity.

High values of $\boldsymbol{k}\cdot\boldsymbol{v}_A$ cause short time-scale oscillations of the perturbations, which are ultimately damped. Figure 4.6 shows the behaviour of a perturbation with the same wave vector used in figure 4.2, but with $\boldsymbol{k}\cdot\boldsymbol{v}_A = 10^2\Omega$. As might have been expected, given that $\eta_\odot \gg \nu_\odot$ (at this depth $\nu_\odot \cong 23$ cm^2 s^{-1}, $\eta_\odot \cong 6 \times 10^2$ cm^2 s^{-1}), in the case $\boldsymbol{k}\cdot\boldsymbol{v}_A \gg \Omega$ the damping is primarily due to the resistivity, not the viscosity, and it occurs on a shorter time-scale. While decreasing ν has only a minor effect on the results of figure 4.6, decreasing η lessens the amplitude decrease. For the selected rotation profiles, the effect of the magnetic field, in contrast to MRI vulnerable systems, is to render the system yet more stable. Figure 4.7 shows the behaviour of a perturbation with the same wave vector, with magnetic parameter $\boldsymbol{k}\cdot\boldsymbol{v}_A = 10^2\Omega$, and $\eta = 0.1\eta_\odot$.

4.6 Conclusions and limitations

The local stability of a differentially rotating medium is a subject of great importance in the study of astrophysical fluids, most notably in the fields of accretion discs and rotating stars. The effects of non-axisymmetry, diffusive processes, and magnetic fields are often subtle, but can be critical in many applications. I have presented here a very general analysis, using the local linearised equations of a weakly magnetized, differentially rotating fluid, with finite thermal conductivity, viscosity, and resistivity for non-axisymmetric WKB displacements. Locally

co-moving Lagrangian coordinates have been employed. In the non-axisymmetric case, the equations are non-modal and the problem cannot be reduced to a dispersion relation.

Differential rotation stratified on cylinders is often a favoured model profile for the interiors of stars and discs. This is of course inevitable when a barotropic equation of state is used, but it is often justified on the basis of the classical axisymmetric GSF criterion. Under conditions valid in the radiative zone of the Sun, my analysis shows that this is misleading, and the Sun evidently has little difficulty maintaining a GSF-violating profile. Realistic values of ν and baroclinic rotation models compatible with the data from helioseismology prevent the growth of the GSF instability. It should be noted that, while nominally tailored for solar rotation, the GSF study was carried out long before the rotation profile of the Sun was actually known. The rotation-on-cylinders stability criterion applies to much stronger differential shear (which was the target of investigation of those authors) than is actually present in the solar interior.

I have calculated the evolution of non-axisymmetric displacements in the upper radiative zone and the tachocline of the Sun, near $r = 0.7R_\odot$ at various latitudes. I have found neither unstable disturbances nor strong transient growth. Patterns of solar rotation featuring angular velocity gradients similar to those inferred from the helioseismology data are more stable than is commonly realised. The investigation described here was carried out on the rotation pattern proposed in chapter 3, which is in strict, static radiative equilibrium. The feasibility of this model may alleviate the problem of the circulation-induced spreading of the tachocline [Spiegel and Zahn, 1992].

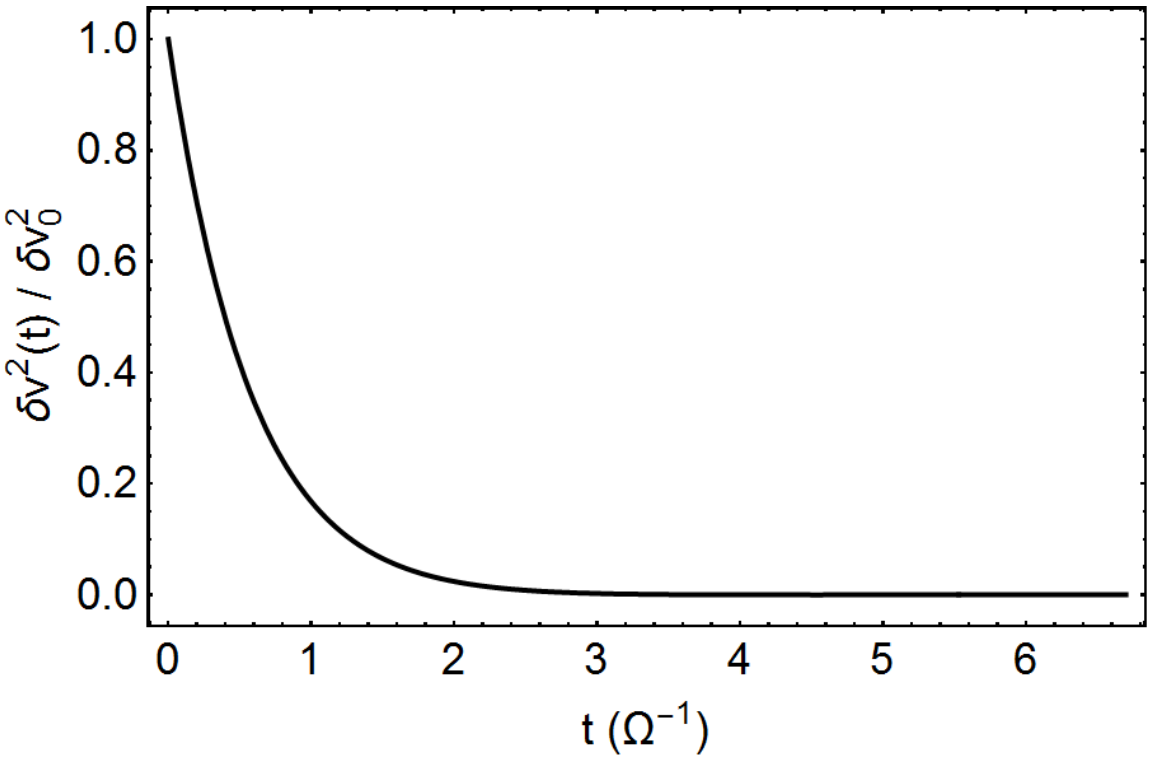

Figure 4.2: Typical behaviour of a perturbation. This particular solution was generated for the model A at $\theta = 45°$ with wave vector components $k_{R0} = 2.1 \times 10^{-4}$ cm^{-1}, $k_\phi = 4.2 \times 10^{-7}$ cm^{-1}, and $k_{z0} = 1.3 \times 10^{-5}$ cm^{-1}. The temporal axis is expressed in units of $\Omega^{-1} = 3.77 \cdot 10^5$ s, about 4.4 days.

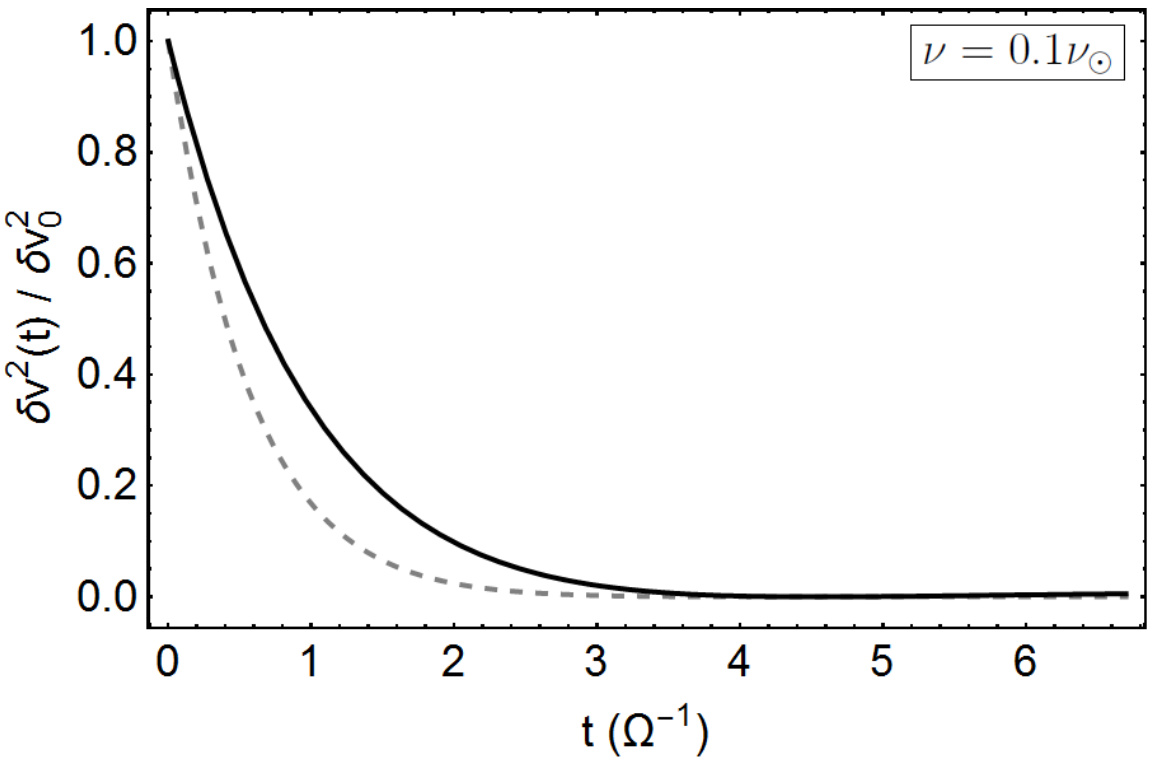

Figure 4.3: Behaviour of the same perturbation of figure 4.2 with $\nu = 0.1\nu_\odot$ (black line). The curve in the case $\nu = \nu_\odot$ is shown as a dashed gray line for comparison. The units are as in figure 4.2.

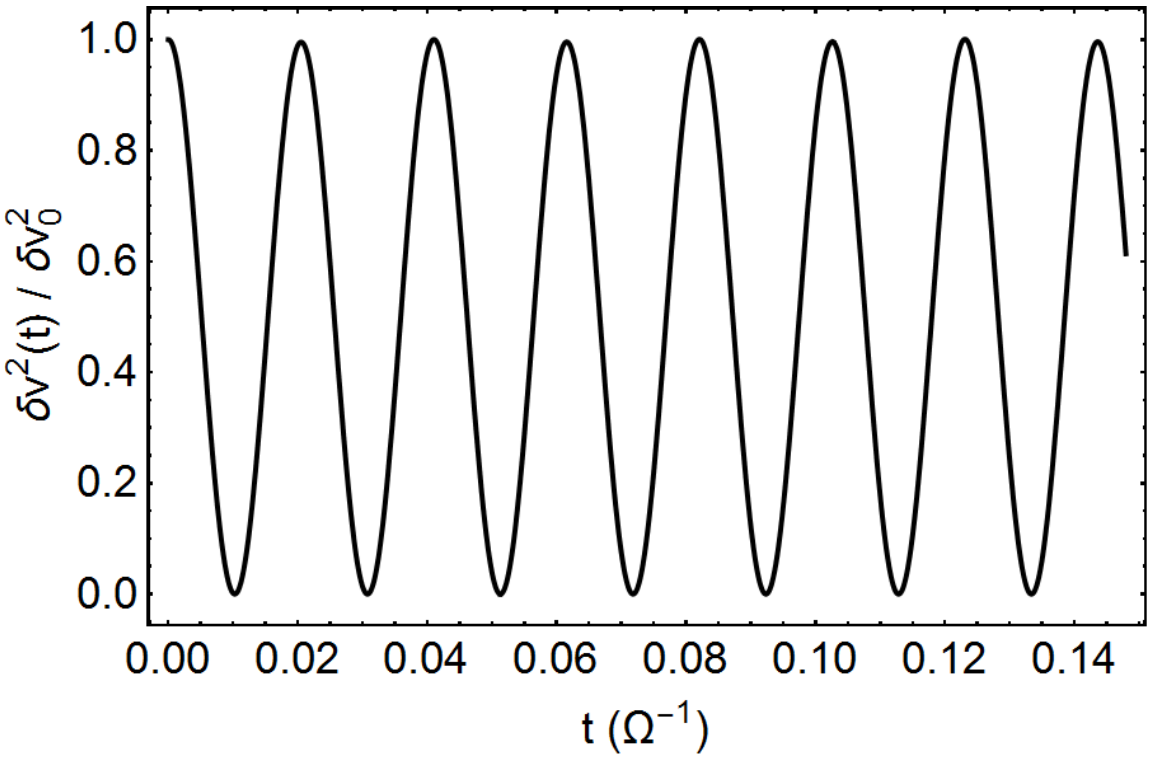

Figure 4.4: Very short time-scale oscillations of a perturbation featuring long term transient growth (figure 4.5 below). This particular solution was generated for the model A at $\theta = 85°$ and has wave vector components $k_{R0} = 8.7 \times 10^{-9}$ cm^{-1}, $k_\phi = 1.5 \times 10^{-10}$ cm^{-1}, and $k_{z0} = 4.9 \times 10^{-9}$ cm^{-1}.

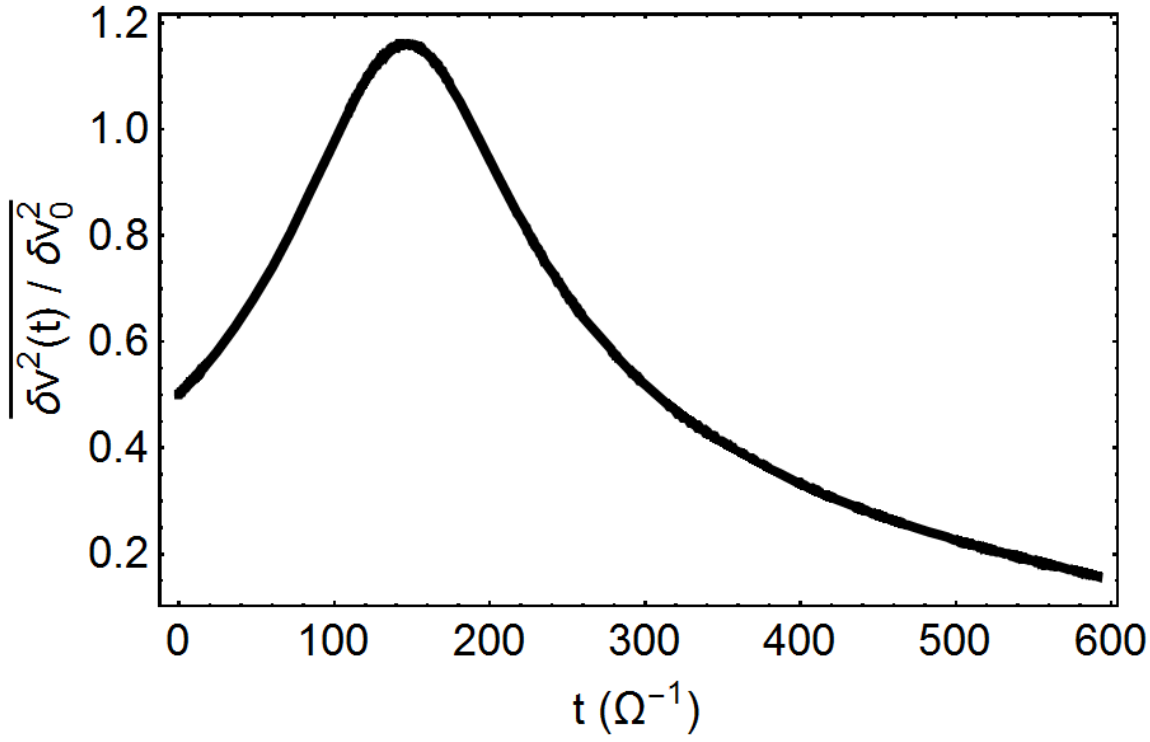

Figure 4.5: Integral average of $\delta v^2(t)/\delta v_0^2$ over a time of Ω^{-1} for the perturbation of figure 4.4. The maximum growth factor is approximately 2.4 and is reached at the peak of the short time-scale oscillations near $t \sim 140\Omega^{-1}$.

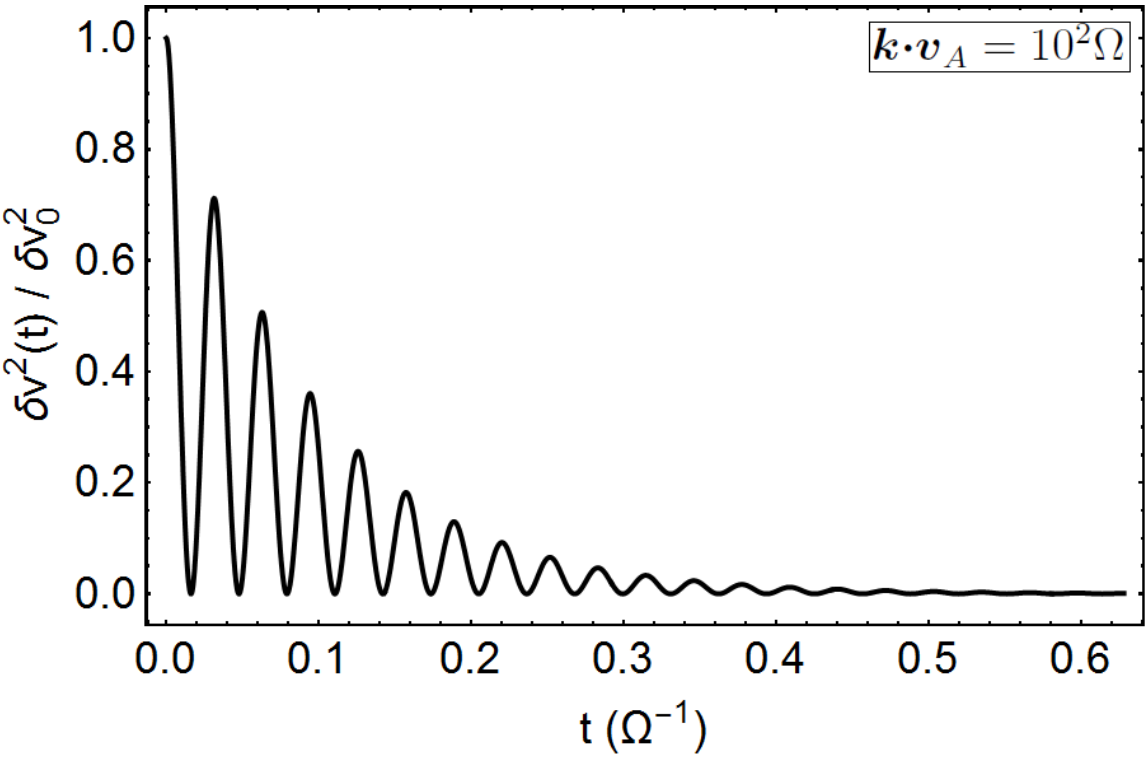

Figure 4.6: Behaviour of the same perturbation of figure 4.2 in the $\boldsymbol{k}\cdot\boldsymbol{v}_A = 10^2\Omega$ case. Note that the scale is different from that of figure 4.2.

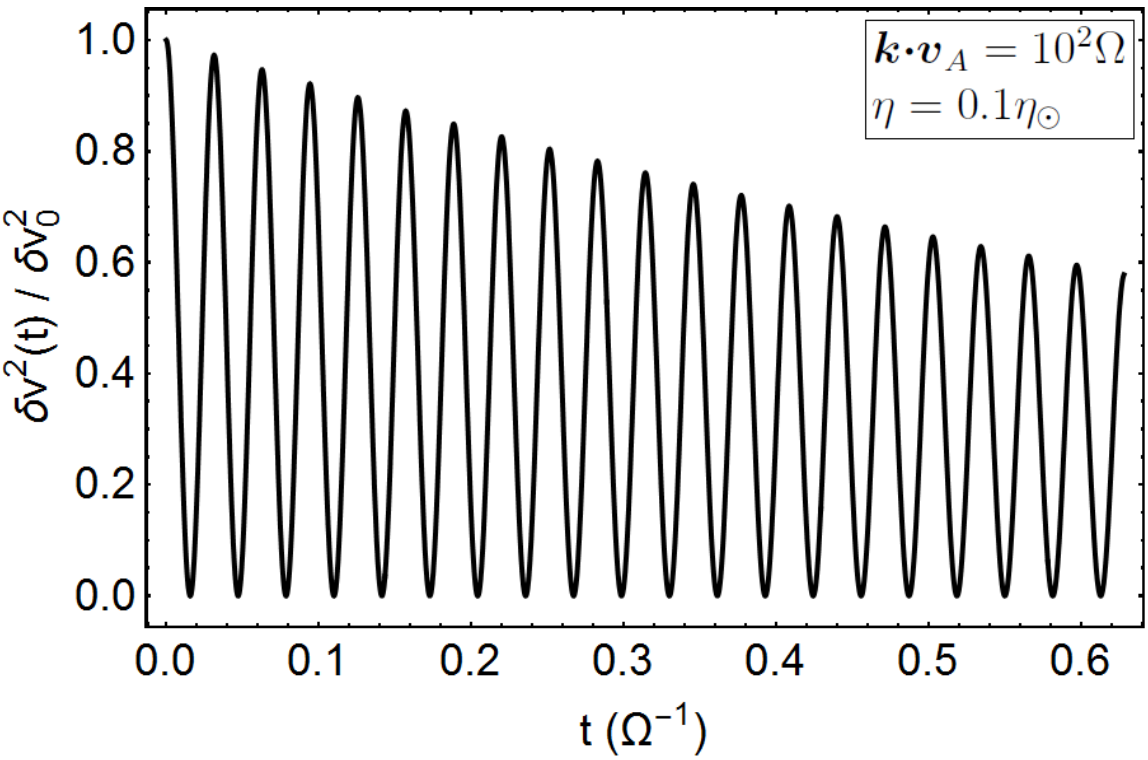

Figure 4.7: Behaviour of the same perturbation of figure 4.2 in the $\boldsymbol{k}\cdot\boldsymbol{v}_A = 10^2\Omega$, $\eta = 0.1\eta_\odot$ case. The units are as in figure 4.6.

Chapter 5

The Goldreich-Schubert-Fricke instability in stellar radiative zones

The Goldreich-Schubert-Fricke (GSF) instability is thought to contribute to the transfer of angular momentum in differentially rotating stars. As we have seen, it has been included in recent codes of stellar evolution in a diffusion-like approximation, under the assumption that the kinematic viscosity ν is unimportant for the development of the instability. However, for most stellar applications this is probably not a valid approximation. Here I discuss this issue in detail, solving the dispersion relation of the perturbed modes for realistic values of ν in the bulk of the radiative zone of the Sun and of three red giant stars at various evolutionary stages. I find that the GSF instability is triggered only in layers of very strong shear. In a simple case study, I also investigate the effect of a small deviation from axisymmetry or a small background magnetic field. I find that, like the viscosity, these have a stabilising effect. The conclusion is that this instability is probably far less efficient in transporting angular momentum than is often assumed. It may not even be present at all.

5.1 Introduction

We have seen that the GSF instability is an axisymmetric hydrodynamic instability that occurs in a shearing background when thermal diffusion from the displaced fluid elements counterbalances the stabilising effect of a positive entropy gradient. Since the advent of helioseismology and asteroseismology and their recent observational achievements, it has gained attention in the recent literature as one of the effects that are thought to contribute to the transfer of angular momentum (AM) inside stars.

Stellar evolution codes incorporate the GSF instability together with other hydrodynamic and magnetic processes, though not in the form of fundamental dynamics. These effects are

modelled as a diffusive term in the equation of the evolution of the AM distribution. The combined effect of these processes is still unable to reproduce the correct AM flux for subgiants and early RGs (red giants) [Cantiello et al., 2014]—at least in the current implementation. Codes are becoming more comprehensive, and other effects, including wave transport, may also soon be included. This approach holds promise, but the physics of the mechanisms that transport AM is often complicated. Increasingly constraining observations from asteroseismology motivate us to revisit these mechanisms and to re-examine with critical attention the approximations used in their modelling.

I have discussed in section 2.5.2 that the GSF instability is thought to cause a sort of meridional circulation, which I have referred to as GSF circulation [James and Kahn, 1970, 1971]. This circulation is also expected to play a role in the chemical evolution of stars on the asymptotic giant branch (AGB), see e.g. Herwig et al. [2003] and Siess et al. [2004]. These stars are known to be the main producers of elements heavier than iron, but theoretical models continue to struggle to reproduce the large spread in the heavy elements distribution observed among various AGB stars. Piersanti et al. [2013] attribute this phenomenon to rotational effects, and in particular to the mixing induced by the onset of the GSF instability at the top of the radiative zone. Revisiting the physics of the GSF instability will also have an impact on our understanding of the chemical evolution of evolved stars.

One of the approximations made by James and Kahn is that viscosity is ignored. However, an important but subtle feature of the GSF instability is that it can be suppressed by the presence of a very small kinematic viscosity ν, even if the Prandtl number $\mathrm{Pr} = \nu/\chi$, where χ is the thermal diffusion coefficient, is much smaller than unity [Acheson, 1978; Knobloch and Spruit, 1982; Menou et al., 2004]. In chapter 4 I have shown that it is likely that the GSF instability is suppressed in the upper radiative zone of the Sun, if the shear is comparable in value to that inferred from helioseismology. I explore here in greater detail the conditions under which the GSF instability occurs in differentially rotating stars. I find that when realistic values of ν are considered, the instability is triggered only in regions of very strong shear, and I determine the minimum shear required to trigger the instability in the radiative zone of the Sun and of three RGs at various evolutionary stages.

Recently, a similar study was conducted by Hirschi and Maeder [2010]. These authors have shown that the GSF instability would be suppressed by a turbulence-induced viscosity ν_{turb} in the radiative interior of a massive star. Here I consider instead a physical viscosity, i.e. the molecular viscosity and radiative viscosity. Our understanding of these processes is on a firmer footing than those underlying ν_{turb}.

In a particularly simple case, I also investigate what happens when two of the assumptions behind the work by Goldreich and Schubert are relaxed. I consider a generic GSF-unstable environment, and then include (a) a small deviation from axisymmetry in the form of a finite azimuthal component k_ϕ of the wave vector, and (b) a small background magnetic field.

Model	t (Myr)	$R/R_\odot$	$L/L_\odot$	$T_{\rm eff}$ (K)	$R_{\rm rad}/R$
Sun	4570	1.00	1.00	5776	0.72
RG1	3610	2.52	6.56	5822	0.70
RG2	3730	2.88	5.18	5133	0.42
RG3	3995	7.16	23.4	4744	0.08

Table 5.1: Main characteristics of the selected models: age, radius, luminosity, effective temperature, and location of the radiative-convective boundary.

5.2 The GSF instability in various stellar models

I discuss here the onset of the GSF instability in stellar environments, retaining the viscosity in the terms of equation (2.57). For the background states, I have used evolutionary tracks for the Sun and for a set of RGs. I have selected the models of a 1.3 $M_\odot$ star in three different evolutionary states on the RGB (red giant branch), corresponding to a subgiant, an early RG, and a more evolved RG, following the example by Belkacem et al. [2015a].

5.2.1 Stellar models

I have made use of a set of bespoke stellar models generated with the evolutionary code `PROSECCO` (see Tognelli et al. 2012). The main input physics adopted for the computations is detailed in Tognelli et al. [2015] and references therein. The code generates spherically symmetric stellar models in hydrostatic equilibrium. Convection in super adiabatic regions is treated by the Mixing Length scheme [Böhm-Vitense, 1958]. The models are computed adopting a solar-calibrated value of the mixing length parameter, namely $\alpha_{\rm ML} = 1.76$. A mild overshooting parameter $\lambda_{\rm ov} = 0.2$ for $M \geq 1.2$ $M_\odot$ has been adopted. All the models are calculated for [Fe/H]=+0.0, which translates into an initial helium abundance $Y = 0.274$ and a total metallicity $Z = 0.013$.

Figure 5.1 shows the evolutionary track of the 1.3 $M_\odot$ star in the effective temperature ($T_{\rm eff}$) - luminosity (L) plane, and the position of the three RG models in the HR diagram. The main properties of these structures are summarised in table 5.1. The last column of the table shows the radius of the radiative region of the star as a fraction of the total radius. In each case, the generation of energy via nuclear fusion, be it in the core (main sequence) or in shell (RGs), occurs entirely in a zone of radiative transport.

5.2.2 Diffusive processes

Whether or not the GSF instability occurs depends on the microscopic diffusion coefficients of the stellar material.

The heat flux in the radiative region of a star is of course due to diffusive radiative transfer.

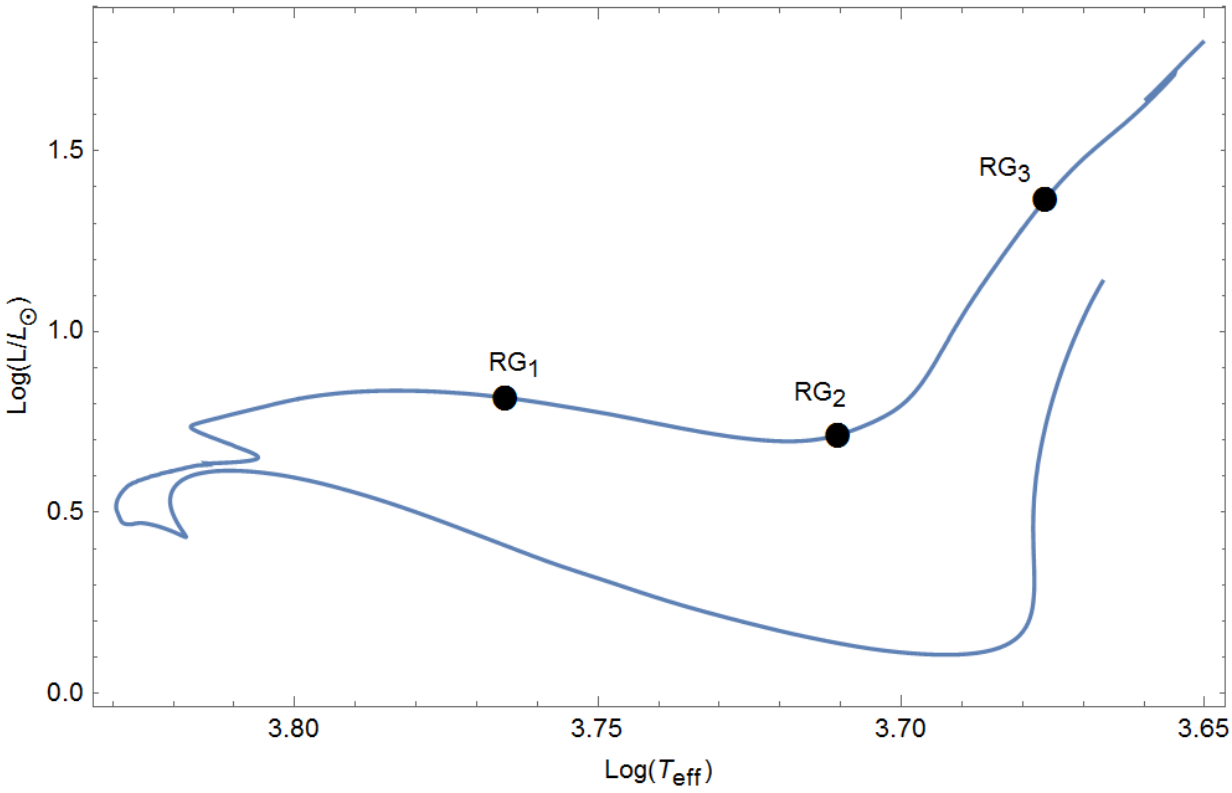

Figure 5.1: Evolutionary track of a 1.3 $M_\odot$ star in the HR diagram. The location of the three selected RG models is marked in the figure. $T_{\rm eff}$ is expressed in K.

Adopting the same notation of GS67, the thermal diffusivity for this process is:

$$\chi = \frac{16(\gamma-1)\bar{m}\sigma_{\rm SB}T^3}{3k_{\rm B}\kappa\rho^2}, \tag{5.1}$$

where $\sigma_{\rm SB}$ is the Stefan-Boltzmann constant, $k_{\rm B}$ is the Boltzmann constant, γ is the adiabatic index, $\bar{m}$ is the average particle mass, and κ is the opacity.

Two processes contribute to the viscosity in the star: the diffusion of particles and the diffusion of photons. I follow here the convention of referring to the first as "molecular" viscosity (though the particles are of course highly ionised atoms) and to the second as radiative viscosity. The molecular viscosity is given by [Spitzer, 1962]:

$$\nu_{\rm dyn} \cong 2.2\times10^{-15}\frac{T^{5/2}}{\log(\Lambda)\rho}\ {\rm cm}^2\ {\rm s}^{-1}, \tag{5.2}$$

where $\log(\Lambda)$ is the Coulomb logarithm. Values for $\log(\Lambda)$ given the physical properties of the plasma are tabulated by Spitzer [1962]. I adopt $\log(\Lambda) = 4$, an acceptable approximation throughout the radiative zone of the Sun and in the radiative zone of the RGs.

The radiative viscosity is given by (GS67; see also Thomas 1930):

$$\nu_{\rm rad} = \frac{16\sigma_{\rm SB}T^4}{15c^2\kappa\rho}, \tag{5.3}$$

where c is the speed of light. Inspection of equations (5.1) and (5.3) shows that the ratio between $\nu_{\rm rad}$ and χ is of order:

$$\frac{\nu_{\rm rad}}{\chi} \sim \left(\frac{c_{\rm s}}{c}\right)^2, \tag{5.4}$$

where $c_{\rm s}$ is the isothermal sound speed. The molecular viscosity $\nu_{\rm dyn}$ is usually more important than $\nu_{\rm rad}$ in stars. A notable exception, which is relevant to this paper, is given by the core of RGs. Equation (5.4) provides a lower limit for the Prandtl number, but in most cases it is not a good approximation for it.

For better readability, all the remaining figures of this chapter are reported at the end of the chapter itself. The thermal diffusivity and kinematic viscosity in the Sun are shown in figures 5.2 and 5.3; the same quantities are shown for the model RG1 in figures 5.4 and 5.5. The figures for the models RG2 and RG3 are similar to those for RG1 and are not reported here. The Prandtl number in the Solar radiative zone is at any point between 1×10^{-6} (the value near the outer boundary) and 2×10^{-5} (core); in the RG1 model it is between 1×10^{-7} and 5×10^{-7}. The noticeable spikes in figure 5.4 arise from the details of the opacity function.

5.2.3 Shear required to trigger the GSF instability

I wish to determine the minimum shear required to trigger the GSF instability in a rotating star. In the case at hand, this may be done rather simply by evaluating the sign of the last term of the dispersion relation by Goldreich & Schubert. At a given location, the result will depend on the structural variables of the star (e.g. ρ, T, χ, ν), the angular velocity Ω, and the shear. In the $\nu = 0$ case, of course, any shear in the $\hat{z}$ direction would suffice to induce instability.

In what follows, it is convenient to express the shear in dimensionless form. In cylindrical coordinates, this amounts to calculating $\partial \log \Omega / \partial \log R$ and $\partial \log \Omega / \partial \log z$. However, rotation in spherical shells is often assumed to be a good approximation in the radiative zone of a star, so that only the r-derivative $\partial \log \Omega / \partial \log r$ is required.

While the observations from asteroseismology provide estimates of Ω, the shear is much less precisely determined. The data on the radiative zone of the Sun are consistent with uniform rotation, with shear present only near the tachocline[1]. A straightforward interpolation of a the set of helioseismology data reported in chapter 1 gives, at $r = 0.70 \mathrm{R}_\odot$ (see chapter 3):

$$\frac{\partial \log \Omega}{\partial \log R} = -0.11, \qquad \frac{\partial \log \Omega}{\partial \log z} = -0.24. \tag{5.5}$$

The data are even less constraining for the RGs. Deheuvels et al. [2014] identified two subgiants for which the observations are significantly better reproduced by a curve with a discontinuity in Ω at a location near the H-burning shell, rather than by a smooth model. The smooth curve

[1] In this chapter, whenever I refer to the "shear", I refer to its absolute value. In all cases of interest to the work presented here, $\partial \log \Omega / \partial \log r$ is negative.

would correspond to a shear (inferred from their figure 10) of order: $\partial \log \Omega / \partial \log r \sim -1$. The shear near the discontinuity would obviously be larger than this, but it is not currently possible to estimate it with accuracy.

The structural quantities for our models have been interpolated from the PROSECCO models. For all models, I adopt an angular velocity value which is both a good approximation for the radiative zone of the Sun, and a reasonable average value for the radiative zone of a typical RG: $\Omega = 2.7 \times 10^{-6}$ rad s^{-1}. At about 20 radial locations in the radiative zone of each star, at low (20°), mid (45°), and high (70°) latitudes, I determine if the equation $C(\boldsymbol{k}) < 0$ has any solution for a range of values of k_R, k_z, for the 4 sign combinations of k_R, k_z, where $C(\boldsymbol{k})$ is given by equation (2.60) . In this way, I determine the minimum value of $\partial \log \Omega / \partial \log r$ for which there are solutions to the equation $C(\boldsymbol{k}) < 0$. I consider wave vector components in the range:

$$k_R, k_z : \ \pm \frac{2\pi}{10^{-2} R_\odot} \rightarrow \pm \frac{2\pi}{10^{-14} R_\odot}, \tag{5.6}$$

and limit the search to values of the shear in the interval:

$$0.1 < \left| \frac{\partial \log \Omega}{\partial \log r} \right| < 10. \tag{5.7}$$

The results are summarised in figure 5.6 for the Sun and figures 5.7 - 5.9 for the RGs. The main feature implied by these figures is that in all cases the onset of the GSF instability in the deep radiative interior is only possible for very strong shear, while it may occur more easily near the outer edge of the radiative zone. In the Sun, a shear of order unity is required even at the upper boundary of the radiative zone. This is consistent with the result of chapter 4 that the GSF instability does not occur in the upper radiative zone, for values of the shear given by equation (5.5). On the other hand, a small shear $\partial \log \Omega / \partial \log r \sim 0.1$ may be sufficient to induce instability in the upper radiative zone of the RG models, or in the very inner part of the nuclear core of the Sun.

5.3 Non-axisymmetric perturbations and introduction of a background magnetic field

The GSF instability is traditionally studied in the axisymmetric case. The evolution of non-axisymmetric displacements, i.e. displacements with a finite azimuthal component of the wave vector k_ϕ, is a much more complex problem. In this case, the perturbed equations cannot be reduced to a local dispersion relation. I adopt here the same techniques and notation as in chapter 4. There I have derived the set of non autonomous ordinary differential equations which describe the evolution of the perturbed quantities in the non-axisymmetric case, see equations (4.36) - (4.40). I also make use of the same standard, non-rotating background solar model as in that chapter [Bahcall et al., 2005].

The possible importance of non-axisymmetric perturbations is that they can be more unstable in a rotating system than axisymmetric disturbances. This happens, for example, in rotating convectively unstable systems in which a geostrophic balance eliminates rotational stabilisation, but only for non-axisymmetric modes [Balbus and Schaan, 2012]. I therefore discuss here an idealised case in which the GSF instability is not fully suppressed by the viscosity, and solve those equations to determine what happens when the assumptions of axisymmetry and non-magnetised background are relaxed, exploring the richness and complexity of the general, triple-diffusive problem. For this purpose, I consider an environment with the same properties of the upper radiative zone of the Sun (including the rotation), but an enhanced radiative thermal diffusion coefficient: $\xi_{\rm rad} = 10^3 \xi_{\rm rad\odot}$. For clarity, I note here that the coefficient $\xi_{\rm rad}$ of chapter 4 is related to the coefficient χ of the present discussion by $\xi_{\rm rad} = (\gamma - 1)\chi$.

5.3.1 Axisymmetric perturbations

The axisymmetric case is treated with the dispersion relation. I have solved equation (2.57) in the upper radiative zone of the Sun at $r = 0.70$ R$_\odot$, $\theta = 45°$, with the modification $\xi_{\rm rad} = 10^3 \xi_{\rm rad\odot}$. There are unstable modes only when k_R and k_z have opposite signs, and the results for $k_R > 0, k_z < 0$ are the same as those for $k_R < 0, k_z > 0$. Only modes in a relatively narrow region of the $k_R < 0, k_z > 0$ quadrant are unstable: I show this region and the growth time-scale of the instability in figure 5.10. The shortest growth time-scale is found to be given by $\log_{10}(T_{\rm gr}/s) \approx 6.7$, i.e. $T_{\rm gr} \approx 5 \times 10^6$ s, with a strong dependence of $T_{\rm gr}$ on the position in the $k_R - k_z$ plane.

5.3.2 Non-axisymmetric perturbations

As noted above, the evolution of perturbations with finite k_ϕ is not described by a plane wave dispersion relation, but rather determined by solving equations (4.36) - (4.40). However, a qualitative understanding of their behaviour can be obtained by noting that perturbations with a finite but small k_ϕ will still show a predominantly axisymmetric behaviour, albeit with values of k_R and k_z that are not constant in time. The classical dispersion relation by GS67 is therefore still of some use in understanding how these displacements behave, provided that the time dependence of k_R and k_z is correctly included in it.

At large times, all perturbations formally evolve towards a quasi-axisymmetric state with a wave vector of the form:

$$k_R(t) \to -R k_\phi t \frac{\partial \Omega}{\partial R}, \qquad k_z(t) \to -R k_\phi t \frac{\partial \Omega}{\partial z}, \tag{5.8}$$

Equivalently, they evolve towards a state with

$$\frac{k_R}{k_z} = \frac{\partial \Omega / \partial R}{\partial \Omega / \partial z}. \tag{5.9}$$

I have explored the stability of axisymmetric perturbations that adhere to the constraint (5.9) in the range of amplitudes $|\boldsymbol{k}| = 10^{-9} - 10^{-1}\text{cm}^{-1}$ and co-latitudes $\theta = 10° - 80°$. I have found no unstable modes: in this environment *all the non-axisymmetric modes are eventually stable*.

The next natural step of this analysis is to study the transient phase to assess the presence of large initial growths that occur before the perturbation moves out of the unstable region of the $k_R - k_z$ plane. The following empirical argument allows us to estimate a threshold for $|k_\phi|$ for the perturbation to grow by a large factor. We may visualize the position of the perturbation as a point in figure 5.10, which moves over the course of time. The perturbation will have a large growth phase if it remains in an unstable region of the plane for a time that is much longer than the growth time-scale in such region. The size of the unstable region of the plane is bounded by $|\Delta k| \lesssim 10^{-4}\text{cm}^{-1}$. The position of the perturbation in the region changes with constant wavenumber velocity:

$$\dot{k}_R = -k_\phi R \frac{\partial \Omega}{\partial R}, \qquad \dot{k}_z = -k_\phi R \frac{\partial \Omega}{\partial z}. \tag{5.10}$$

The condition that the perturbation remains in the region of close to maximum growth for a time much longer than the growth time-scale, say $\Delta t = 10 T_{\text{gr}}$, gives the constraint:

$$|k_\phi| < \frac{\Delta k}{R|\boldsymbol{\nabla}\Omega|} \frac{1}{\Delta t} \lesssim 10^{-6}\text{cm}^{-1}. \tag{5.11}$$

In fact, a detailed exploration of the modes in the unstable region shows that only modes with $|k_\phi| \lesssim 10^{-7}$ cm^{-1} are able to grow by many orders of magnitude. Since the most unstable region of the plane resides at $k_R > 10^{-5}$ cm^{-1}, only displacements that are strongly axisymmetric are found to be unstable enough for the GSF instability to have the time required to affect them.

It is possible to identify perturbations that grow by a large factor before becoming stable. I report in figure 5.11 the path of a perturbation with initial wave vector components $k_{R0} = -10^{-4.5}$ cm^{-1}, $k_\phi = 10^{-7}$ cm^{-1}, and $k_{z0} = 10^{-7}$ cm^{-1} in the $k_R - k_z$ plane. As the wave vector of the perturbation changes, it eventually moves out of the unstable region of the $k_R - k_z$ plane. Figure 5.12 shows the evolution of $\delta v_R(t)/\delta v_R(0)$ for this perturbation. Finally, I present in figure 5.13 the inverse growth rate T_{gr}^{-1} for the time interval in which the perturbation is in the unstable region. These results suggest that non-axisymmetric disturbances are not intrinsically unstable on their own; they show growth only to the extent that the instantaneous poloidal wavenumbers would be unstable in an axisymmetric calculation.

5.3.3 The stabilizing effect of $\boldsymbol{B}$

Finally, I discuss here the effect of a finite background magnetic field $\boldsymbol{B}$. $\boldsymbol{B}$ appears in equations (4.36) - (4.40) only via the constant term $\boldsymbol{k}\cdot\boldsymbol{v}_A$. It is convenient to compare $\boldsymbol{k}\cdot\boldsymbol{v}_A$

and Ω. As expected, I have found that the behaviour of the perturbation in figures 5.12 - 5.13 is unchanged for values of $\boldsymbol{k}\cdot\boldsymbol{v}_A \ll \Omega$. However, increasing $\boldsymbol{k}\cdot\boldsymbol{v}_A$ up to values greater than 0.1Ω, I have found that the growth is rapidly inhibited, disappearing for $\boldsymbol{k}\cdot\boldsymbol{v}_A \approx \Omega$. I report in figure 5.14 the evolution of $\delta v_R(t)/\delta v_R(0)$ for the same perturbation in the case $\boldsymbol{k}\cdot\boldsymbol{v}_A = \Omega$.

A qualitative understanding of the role of $\boldsymbol{B}$ is as follows. Once the effect of the background magnetic field becomes comparable to that of the rotation, the diffusivity term that most contributes to the damping is the resistivity η, rather than the viscosity. I have adopted the same value of η as in chapter 4, $\eta \sim 6 \times 10^2$ cm^2 s^{-1}, while $\nu \sim 2 \times 10^1$ cm^2 s^{-1}, so that η is at least one order of magnitude larger than ν in the problem at hand. This makes the damping more efficient in the magnetised case.

Interestingly, the condition $\boldsymbol{k}\cdot\boldsymbol{v}_A \geq \Omega$ for the wave vector of this perturbation gives $\boldsymbol{v}_A \gtrsim 0.1$ cm s^{-1}, a value many orders of magnitude smaller than the sound speed in the medium and the rotational velocity. The corresponding magnetic field is $|\boldsymbol{B}| \gtrsim 0.2$ G. Even if the radiative diffusion coefficient were much higher than in the Sun, a small magnetic field might be sufficient to suppress the GSF instability.

5.4 Conclusions

The GSF instability is often considered to be one of the sources of angular momentum transport in stellar interiors. It is thought to play a (modest) role in determining the time evolution the angular velocity $\Omega(r, \theta)$ in the star, and to affect the mixing of chemical elements in the upper radiative zone of stars in the AGB.

This instability is typically incorporated in codes of stellar evolution in a diffusion-like approximation assuming a non-viscous background. I have shown here that this approximation is not supported by a detailed analysis of the linear stability problem: when realistic values of the kinematic viscosity are accounted for, the GSF instability is suppressed in the bulk of the radiative zone of both the Sun and RGs at various evolutionary stages.

Finally, in a specific case of an environment which would normally be GSF-unstable, I have investigated the effect of a small deviation from axisymmetry and the presence of a small background magnetic field. Both these effects appear to have a stabilising influence.

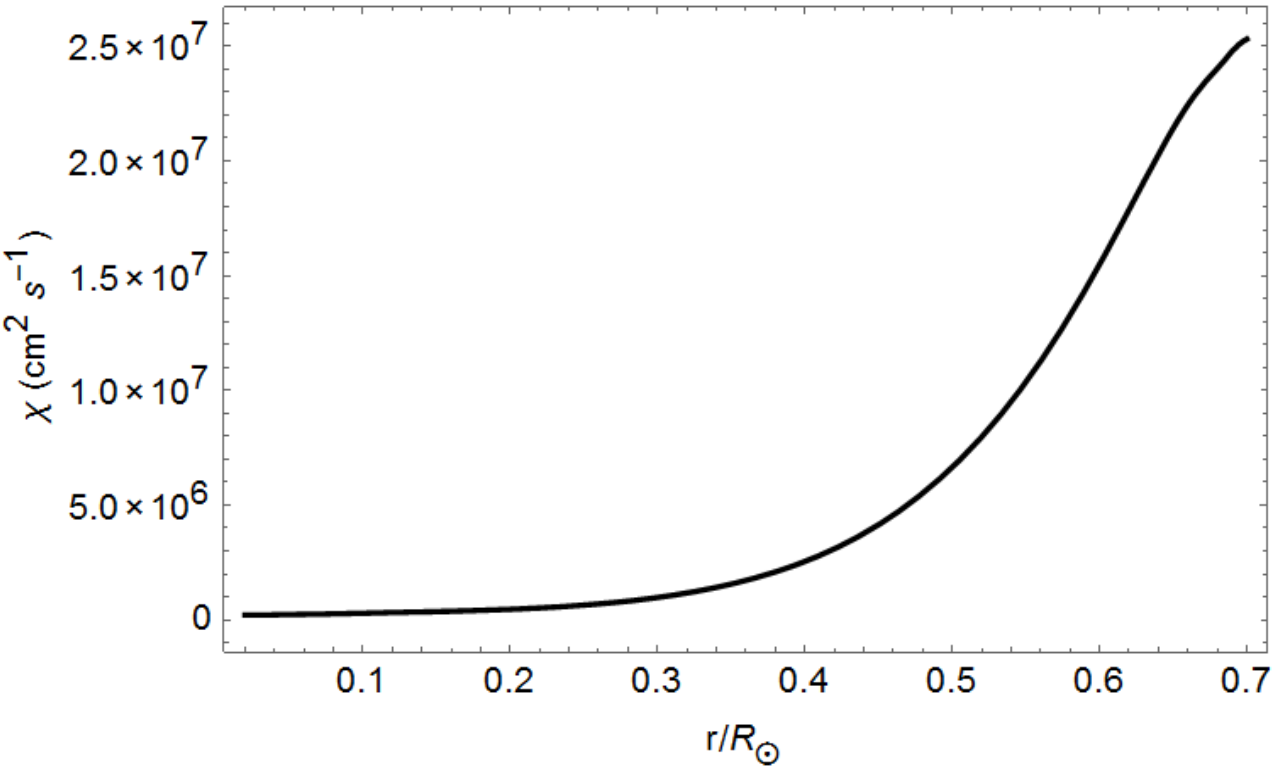

Figure 5.2: Thermal diffusivity χ in the radiative zone of the Sun.

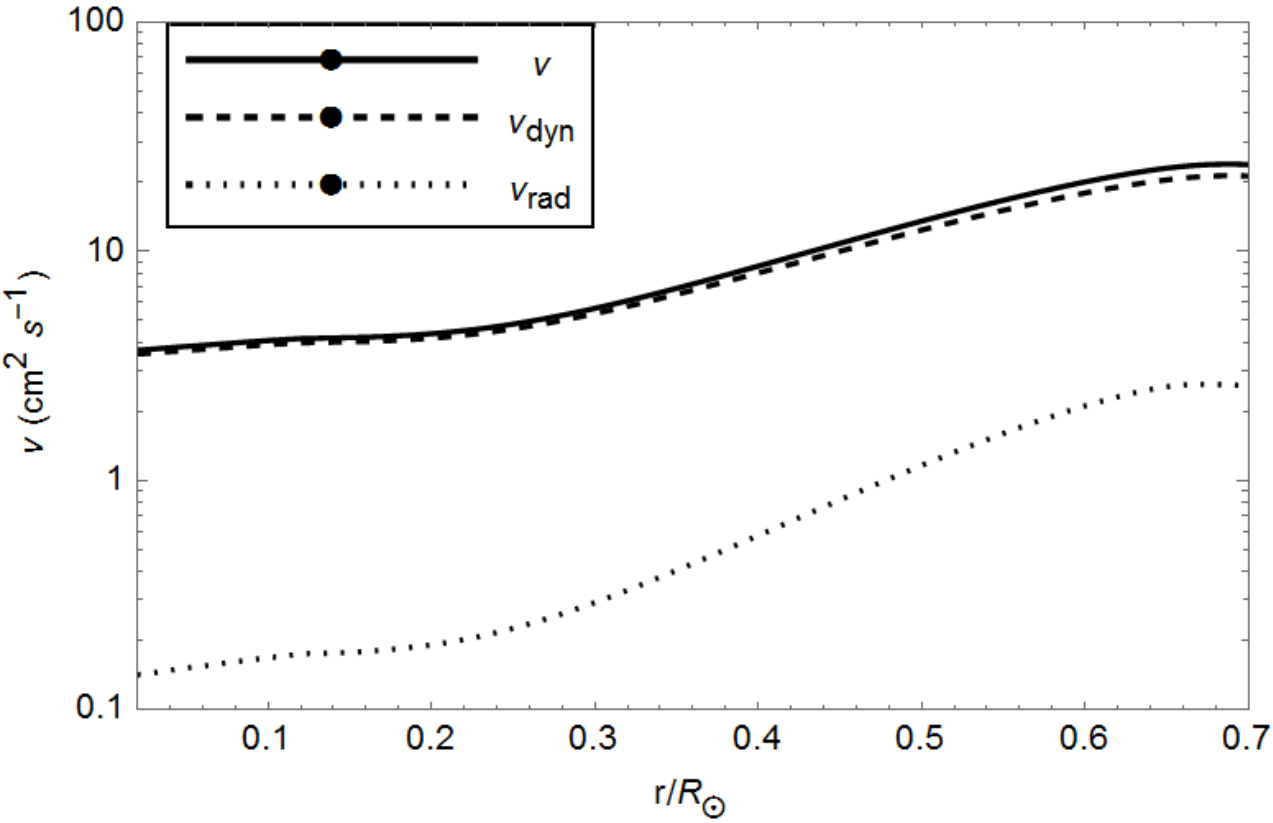

Figure 5.3: Kinematic viscosity ν in the radiative zone of the Sun.

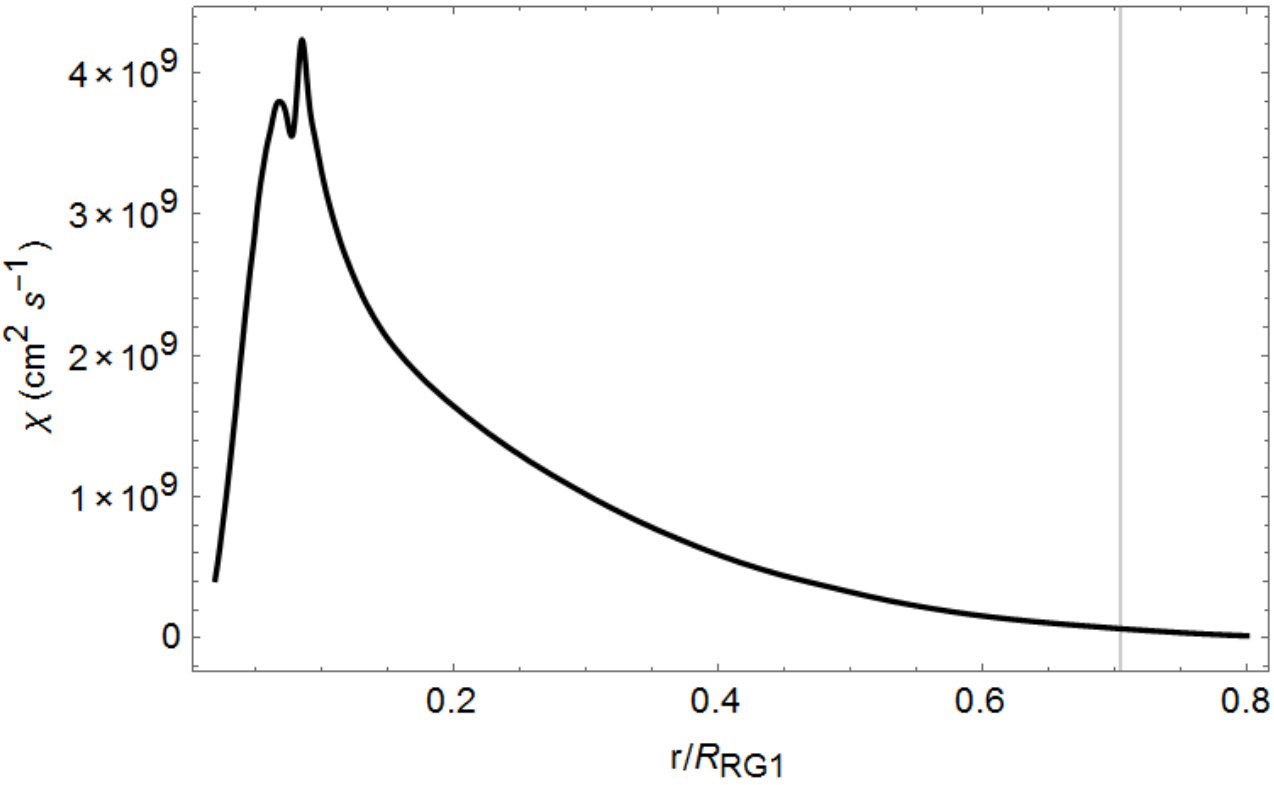

Figure 5.4: Thermal diffusivity χ in the RG1 model. The vertical grey line shows the boundary between the radiative and convective zones.

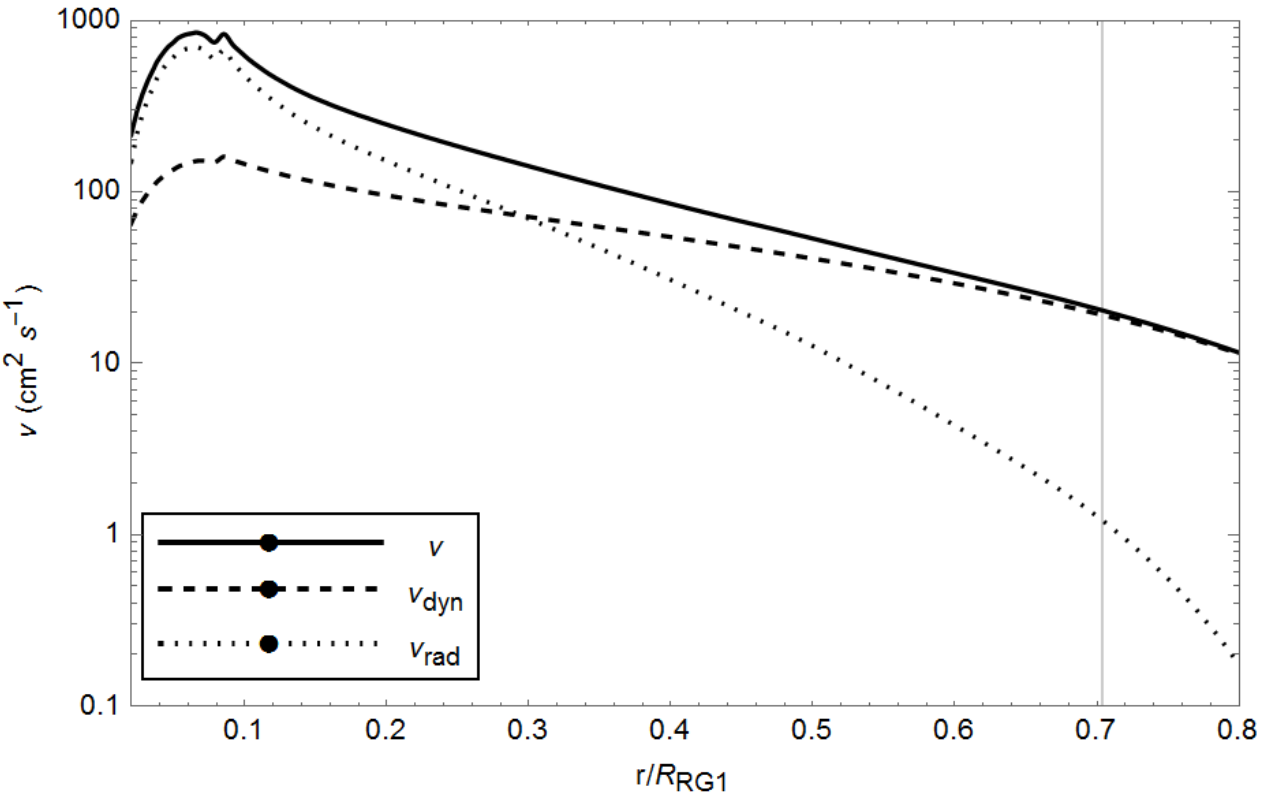

Figure 5.5: Kinematic viscosity ν in the interior of the RG1 model. The vertical grey line shows the boundary between the radiative and convective zones.

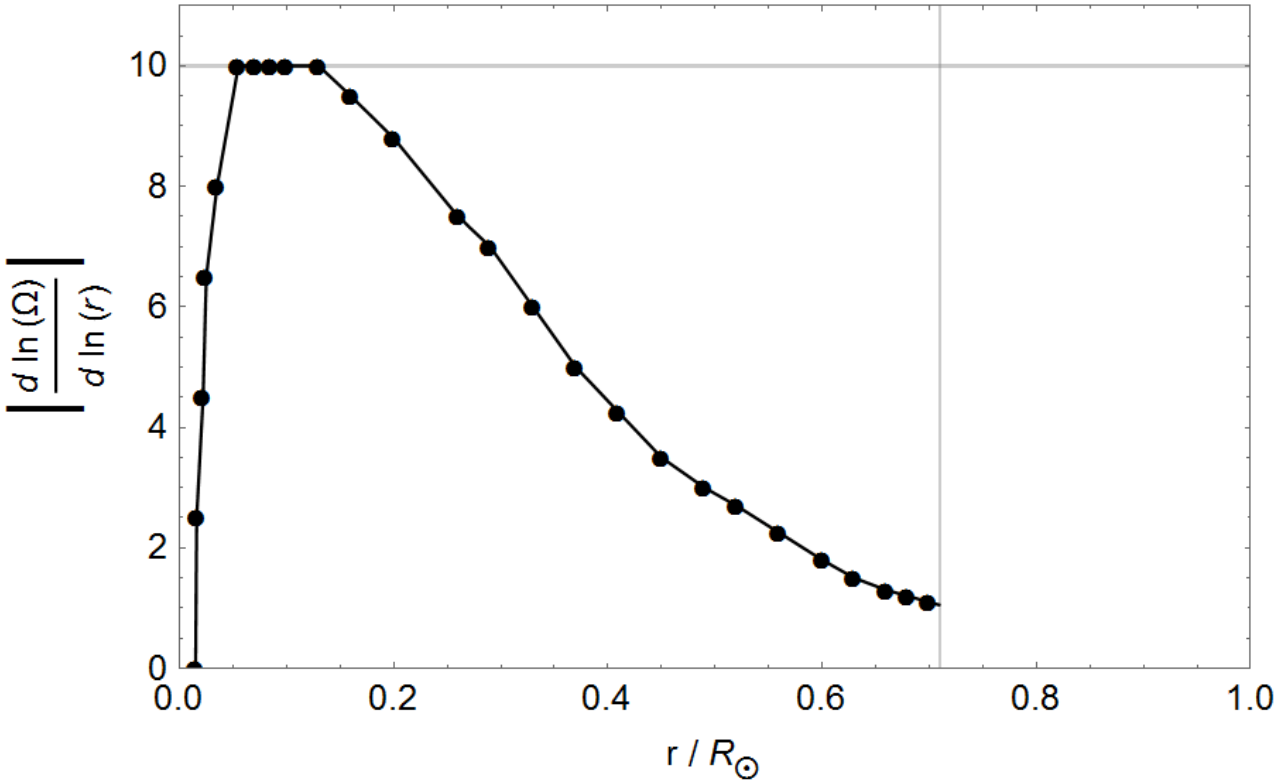

Figure 5.6: Minimum shear required for the onset of the GSF instability in the Sun, as a function of the distance from the centre of the star. The vertical grey line shows the boundary between the radiative and convective zones. The thin black line is a linear interpolation of the data points. The calculation is limited to the values of equation (5.7). The horizontal grey line shows the upper value $d\log\Omega/d(\log r) = 10$.

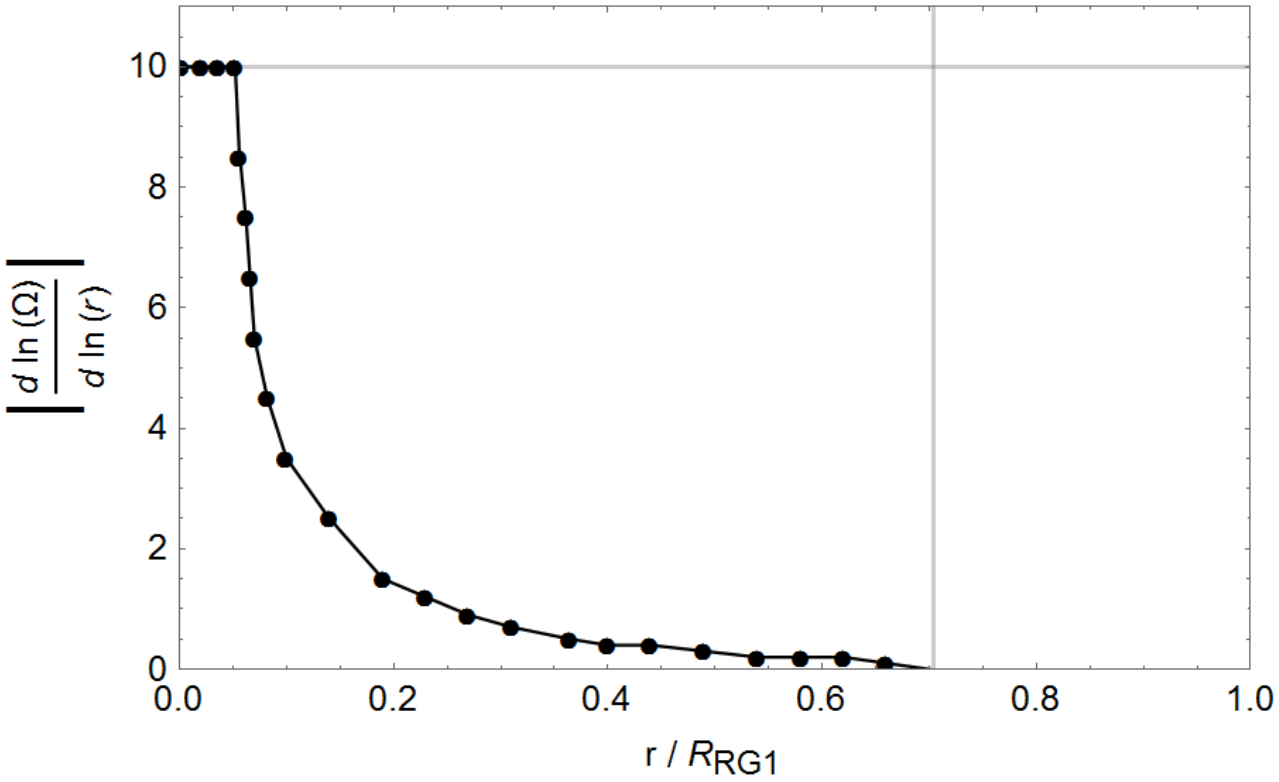

Figure 5.7: Minimum shear required for the onset of the GSF instability in the RG1 model. The vertical grey line shows the boundary between the radiative and convective zones.

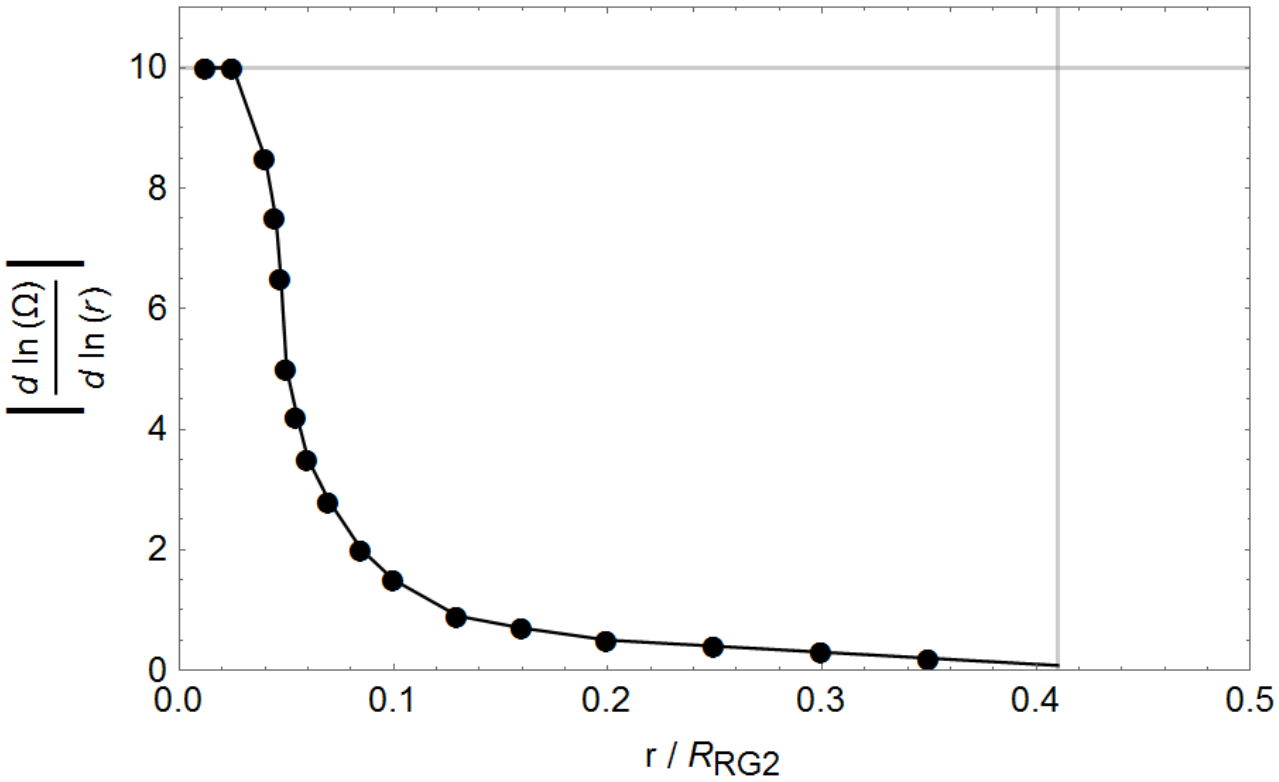

Figure 5.8: Minimum shear required for the onset of the GSF instability in the RG2 model. The vertical grey line shows the boundary between the radiative and convective zones.

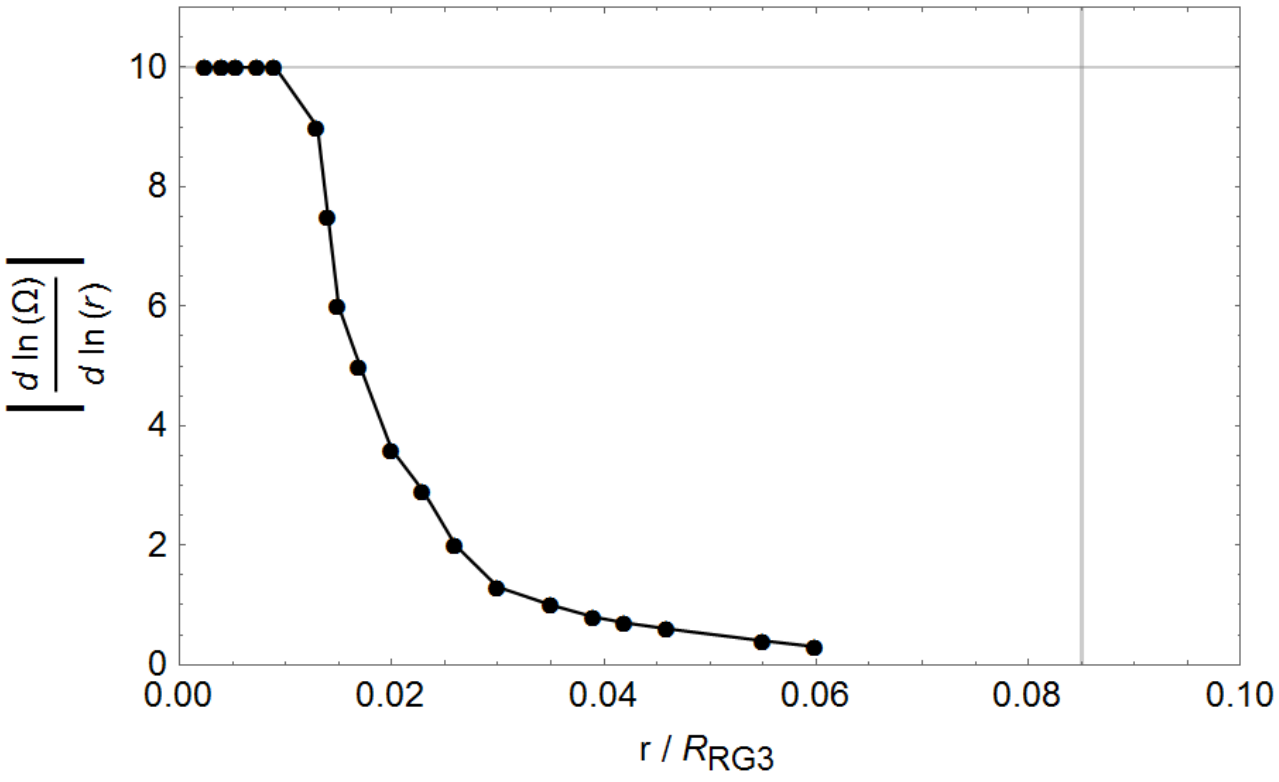

Figure 5.9: Minimum shear required for the onset of the GSF instability in the RG3 model. The vertical grey line shows the boundary between the radiative and convective zones.

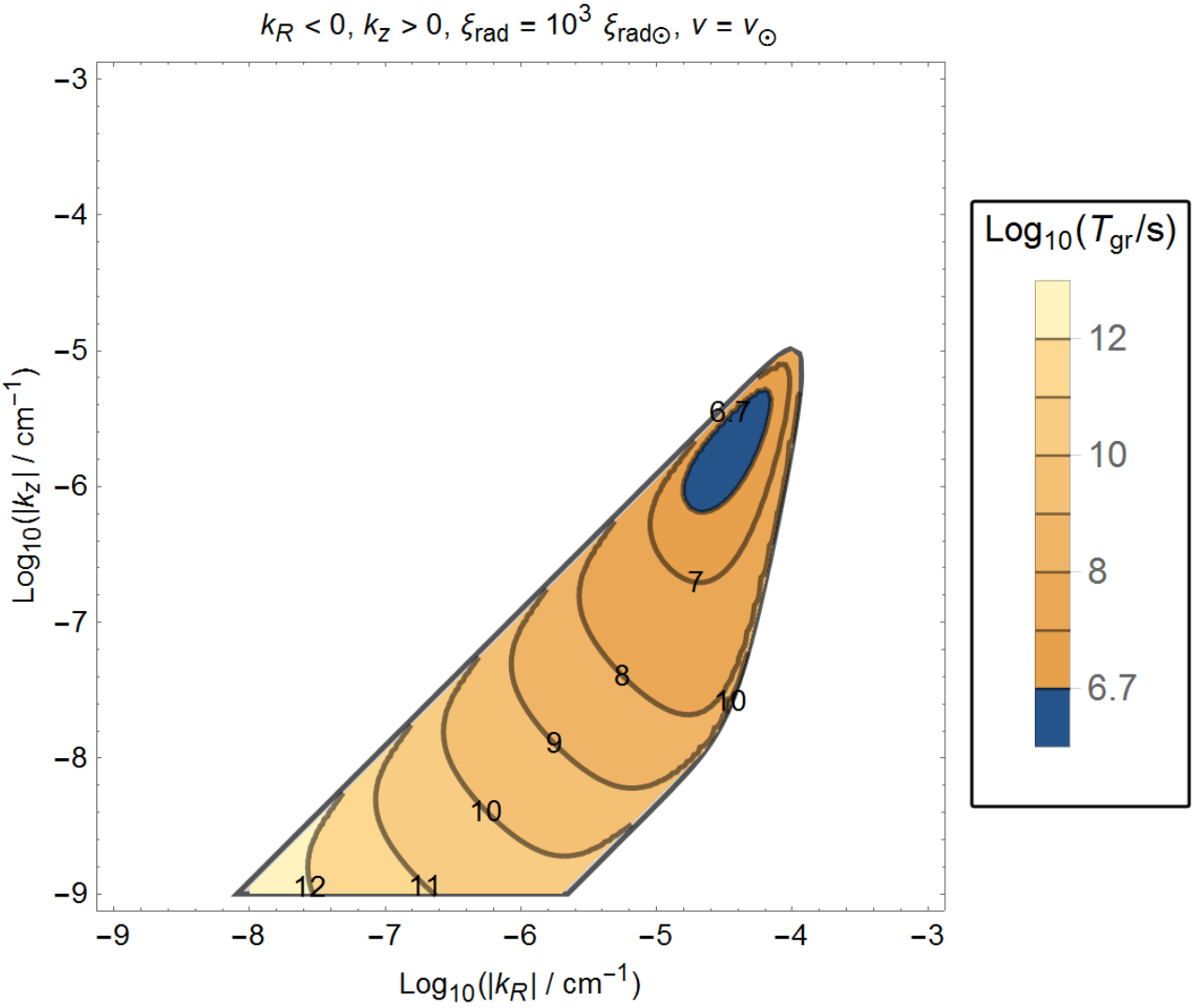

Figure 5.10: Region of the $k_R < 0, k_z > 0$ plane where the GSF instability occurs in a Solar-like environment and growth time-scale $T_{\rm gr}$ for the axisymmetric displacements, for $r = 0.7R_\odot$, $\theta = 45°$, with $\xi_{\rm rad} = 10^3\xi_{\rm rad\odot}$ and $\nu = \nu_\odot$. The numbers next to the iso-contours correspond to the value of $\log_{10}(T_{\rm gr})$ with $T_{\rm gr}$ expressed in seconds.

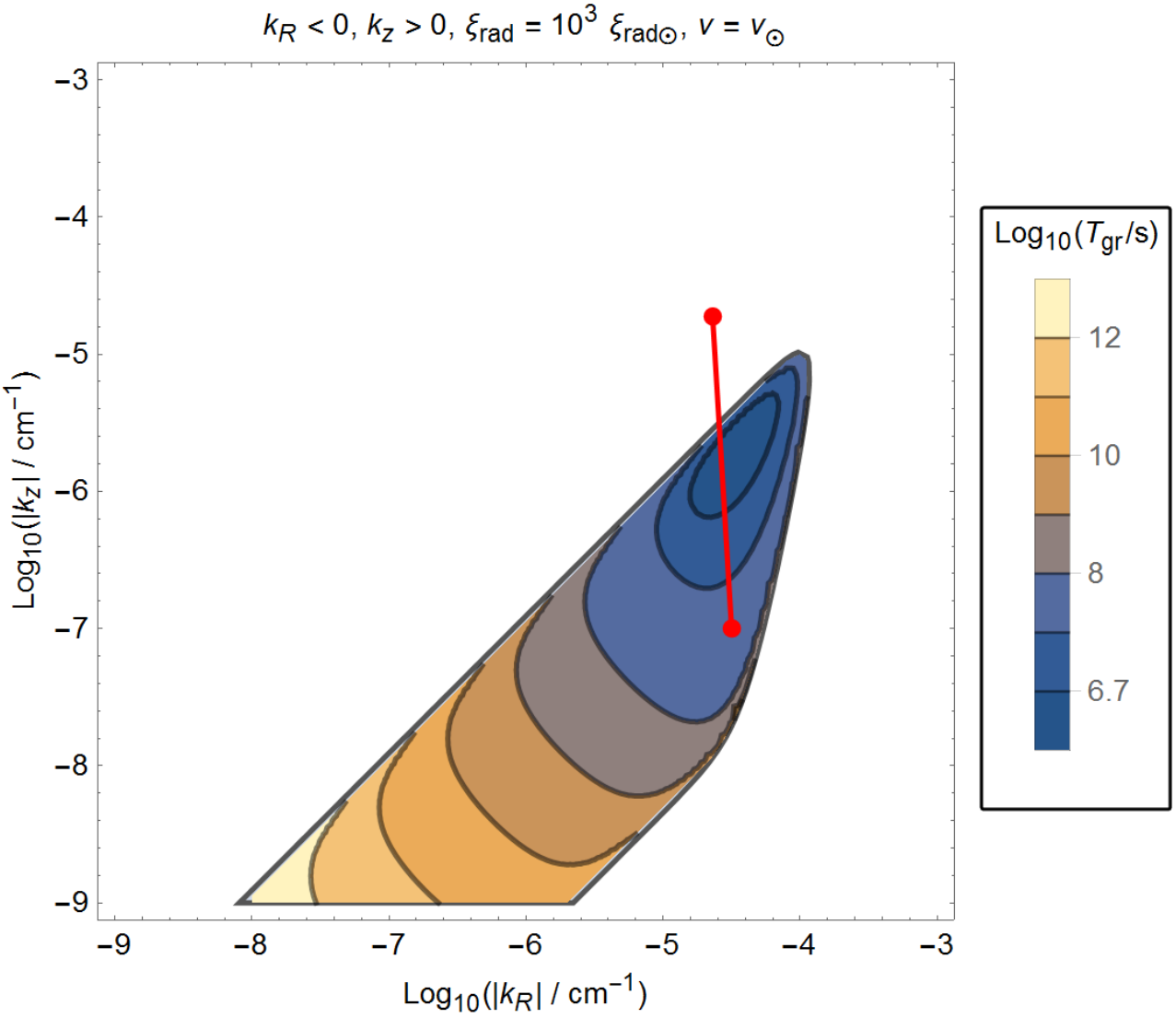

Figure 5.11: Path tracked by a perturbation with $k_{R0} = -10^{-4.5}$ cm^{-1}, $k_\phi = 10^{-7}$ cm^{-1}, and $k_{z0} = 10^{-7}$ cm^{-1} in the $k_R - k_z$ plane. The initial position of the perturbation is marked by the red dot in the unstable region of the plane, while the final position is marked by the other red dot. The position of the wave vector does not proceed linearly with time on the segment, due to the logarithmic scale adopted for the axes.

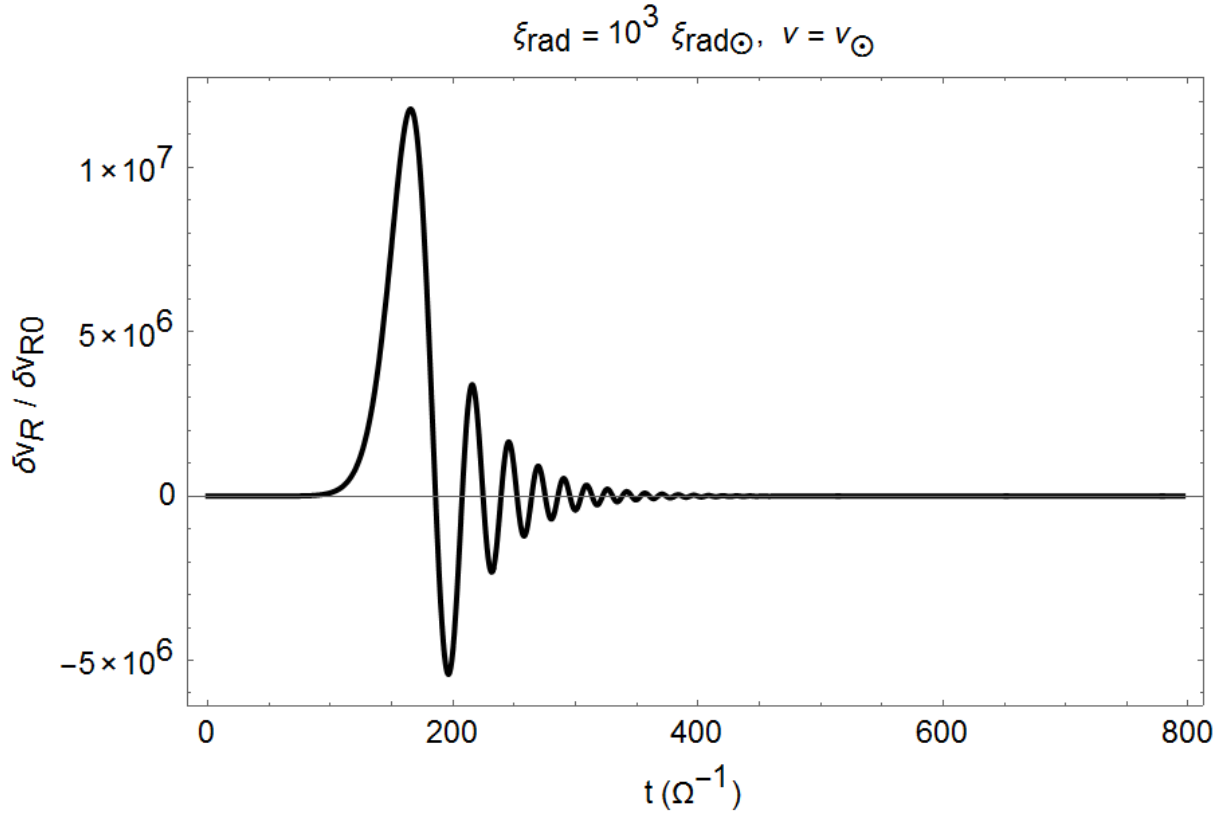

Figure 5.12: Evolution of $\delta v_R(t)$ for the perturbation of figure 5.11. The unit on the temporal axis is expressed in terms of $\Omega^{-1} = 3.77 \times 10^5$ s, corresponding to about 4.4 days.

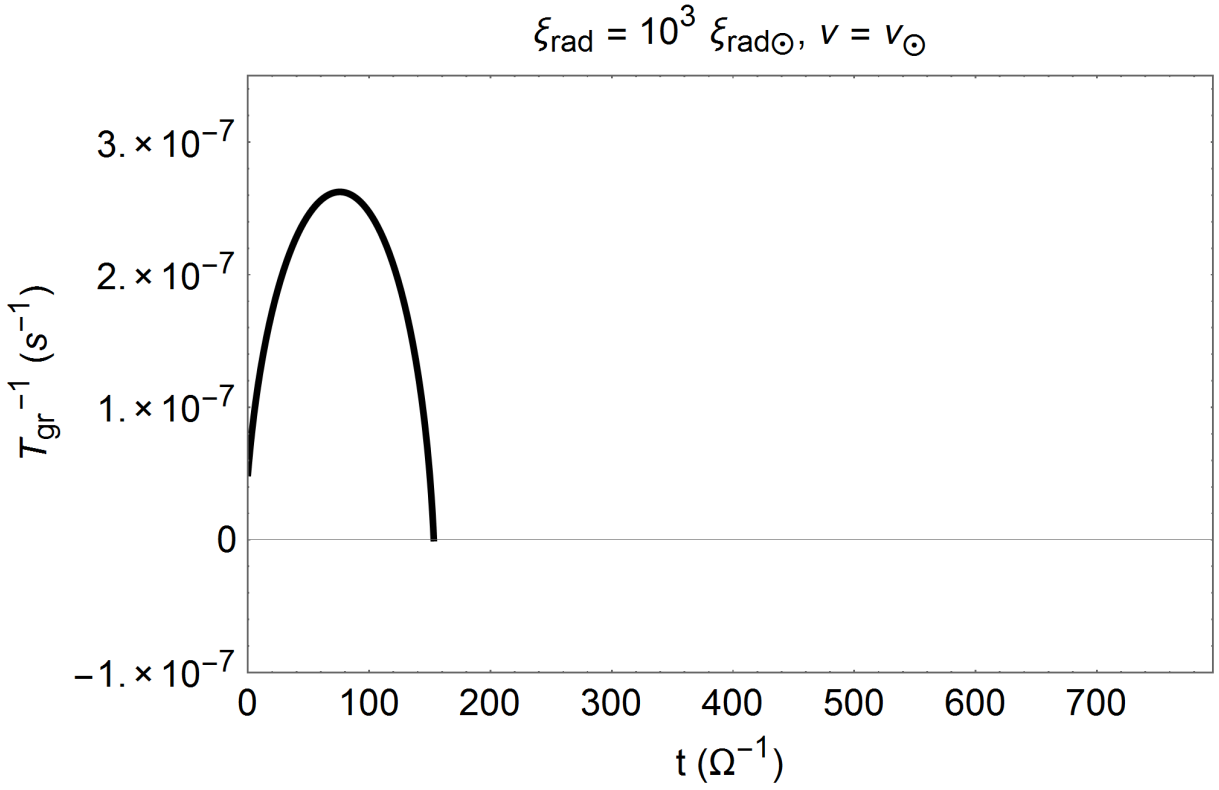

Figure 5.13: Growth rate $T_{\rm gr}^{-1}$ for the displacement of figure 5.11, reported for as long as it stays in the unstable region of the $k_R - k_z$ plane. The growth of the perturbation is halted when the growth rate reaches 0. The unit on the temporal axis is as in figure 5.12.

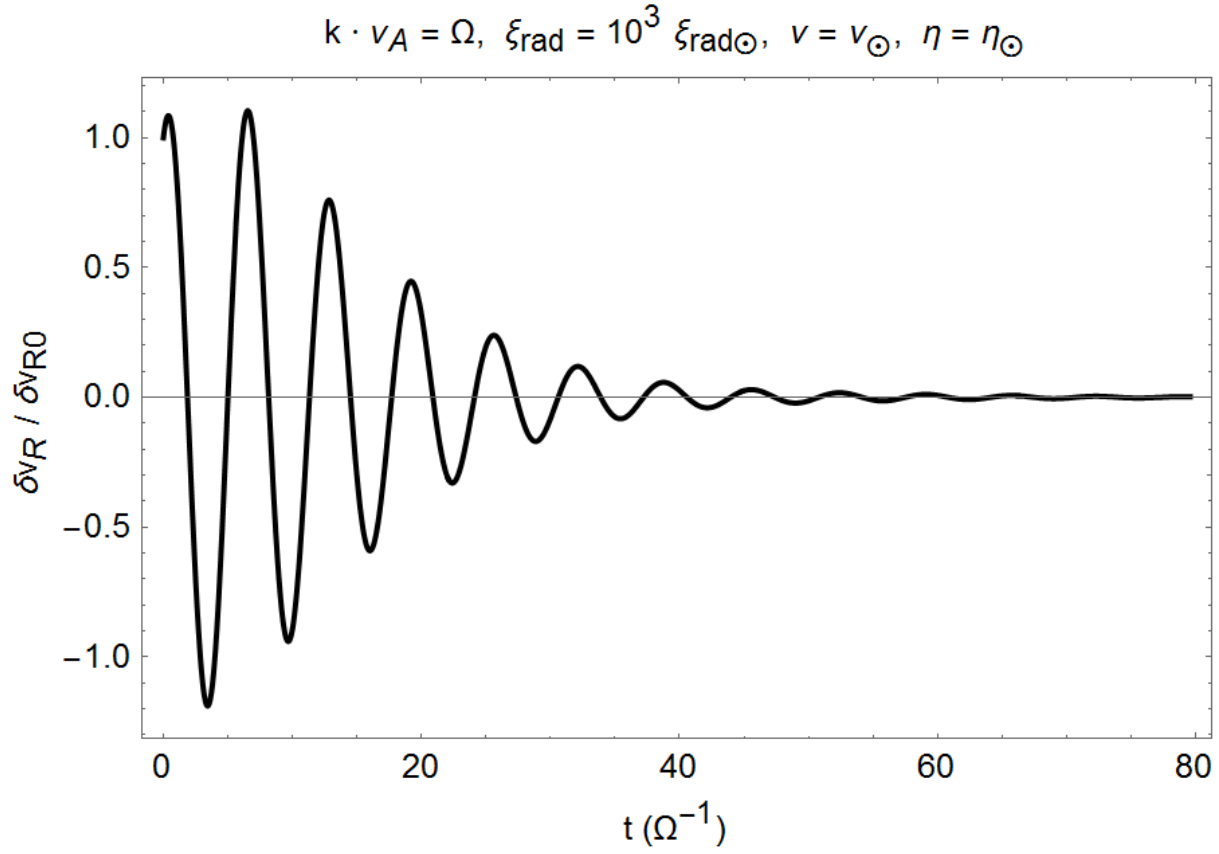

Figure 5.14: Evolution of $\delta v_R(t)$ for the perturbation with $k_{R0} = -10^{-4.5}$ cm^{-1}, $k_\phi = 10^{-7}$ cm^{-1}, and $k_{z0} = 10^{-7}$ cm^{-1} in the magnetic case $\boldsymbol{k}\cdot\boldsymbol{v}_A = \Omega$.

Chapter 6

Conclusions

6.1 Introduction

The aim of this thesis was to explore alternative models for the rotation of the Solar radiative zone and the tachocline. This was motivated in part by the complexity of the current models, which attempt to counter the phenomenon of the spreading of the tachocline by considering a large number of processes (including hydrodynamic turbulence, meridional flows, and magnetic effects). The literature on this subject has produced increasingly complicated scenarios, which have yet to be definitively validated by numerical simulations. In particular, in this thesis I set out to answer the following questions:

Q1. Is the observed baroclinic rotation pattern of the Solar radiative zone and the tachocline compatible with exact radiative equilibrium?

Q2. If this is the case, would such structure be dynamically stable?

In these conclusions, I discuss the answers to these questions that have been found here and the most important limitations of the analysis presented in this thesis, and elaborate on the opportunities for further research on this topic.

6.2 Summary of the results

The main findings of this thesis have been put forth in chapters 3 and 4. The work presented there allows us to answer the questions above as follows:

A1. Yes. I have studied models of rotation for the region of a star in perfect radiative equilibrium, i.e. with equation of energy transfer given by $\nabla \cdot \boldsymbol{F}_{\rm rad} = 0$, where $\boldsymbol{F}_{\rm rad}$ is the radiative flux and there is no contribution due to convective or advective fluid motions. I have described a procedure to construct differentially rotating models that are compatible with this condition, and in particular I have recalled that models in uniform rotation are not among these. I have demonstrated that some of these models provide a good fit to the data from helioseismology for the radiative zone of the Sun.

A2. Probably yes - these models are likely to be dynamically stable. Though absolute stability is an elusive goal, I have discussed a significant range of instabilities that could in principle affect a differentially rotating structure, and presented a general local analysis that incorporates all the effects that may be at play at the same time, including a background magnetic field, non-axisymmetry of the perturbations, and diffusion of heat, momentum, and magnetic field.

Having studied a wide range of modes at various locations in the upper Solar radiative zone, I have found that none of them are unstable. I have hence shown that the viscosity and resistivity, although apparently small, have a significant stabilising effect in the Solar radiative zone. In particular, all the models in exact radiative equilibrium violate the stability criterion by Goldreich-Schubert-Fricke (GSF); I have recalled that this criterion was derived in the non-viscous limit and demonstrated that a small viscosity is sufficient to suppress the instability.

It is immediately clear that the results obtained to answer the second question above may hold true for other stars as well, and not just for the Sun. In particular, very recent observational developments, some of which have been reported in the literature only after the beginning of this study, have allowed the astronomers to probe the internal rotation of subgiants and red giant stars, which have been confirmed to rotate differentially. A third question arises naturally as a consequence of this:

Q3. Would the differentially rotating red giant stars be affected by the GSF instability?

This question has been addressed in chapter 5, where I have used the same techniques described above to study the insurgence of the GSF instability in these structures. The answer is:

A3. Probably not. I have derived numerical limits on the shear required to trigger this instability in red giant stars. Very strong shear ($\partial \log(\Omega)/\partial \log(r) \sim 10$) would need to be present near the core of these stars. Although there is no observed value for the internal shear to date, this suggests that the GSF instability is not active in these environments.

The radiative zone of the Sun is often considered to be in exact uniform rotation, and it is thought to feature a complex advective motion known as the Eddington-Sweet (ES) circulation which contributes to the energy transfer equation. My result provides an arguably simpler alternative to this view: the rotation is differential and baroclinic, but there is no ES circulation. Moreover, differentially rotating stars are often thought to be affected by the GSF instability. I have shown that this may not be the case.

The results presented here therefore challenge the role of two hydrodynamic processes that have a long history in the literature, the ES circulation and the GSF instability. Although it has never been possible to observe them in action in stellar environments, these processes

are thought to contribute to the transport of angular momentum and the chemical mixing of elements inside stars, and they are often included in numerical codes of stellar evolution. The standard implementation of the ES circulation assumes that the star is in exact uniform rotation, and does not account for the fact that a small deviation from this state would be enough to dispense of the circulation. The standard implementation of the GSF instability does not account for the viscosity in the material. In this thesis I have shown that these approximations are problematic: if these processes are indeed suppressed (GSF instability), or just not present altogether (ES circulation), the current implementations are likely to be incorrect.

6.3 Limitations and future work

Some of the technical limitations of this work have been discussed alongside the results in chapters 3-5. I concentrate here on some more general shortcomings which I believe to be the strongest limitations of the results presented here.

I have studied models in quasi-uniform rotation that are devoid of ES circulation and in perfect radiative equilibrium, and I have presented evidence on their local stability. However, the global stability of the system has not been demonstrated. In particular, it would be important to reconsider the equations of chapter 3 maintaining the time-dependent terms, to determine whether a star initially without an ES circulation evolves towards a system with an advective motion, or whether the system remains in radiative equilibrium. This problem is clearly very complex. As illustrated in this thesis, diffusive terms (e.g. viscosity) would likely need to be included. Moreover, some of these effects, including the ES circulation itself, are so small that numerical simulations would not be able to reproduce them reliably. The solution to this problem would nevertheless be crucial to get to the root of the existence of the ES circulation.

Aside for the time-dependence of the model described in chapter 3, other effects not included in the local analysis of this thesis may be in action, including nonlinear destabilising shear processes discussed in the literature for either the local or global scales [Zahn, 1975]. While a full understanding of these remains elusive [Menou and Le Mer, 2006], some authors consider them to be of great importance for the transfer of angular momentum in stars.

Finally, I have always assumed a uniform chemical composition in the star. Although this is accurate in the bulk of the radiative zone, other venues and other problems might benefit from relaxing this hypothesis. If the tachocline of the Sun is characterised by strong compositional gradients, for example, this would aid in confining the magnetic field of the radiative zone (see e.g. Christensen-Dalsgaard and Thompson 2007, Wood and McIntyre 2011).

This is a crucial time for the field of stellar astrophysics, which is undergoing a revolution thanks to the advancements of asteroseismology. Although very few would have predicted this in the recent past, we have been able to probe the internal rotation of stars farther away than the Sun, and we are now even gathering information on their internal magnetic field

[Cantiello et al., 2016]. The challenge for the theorist is to update the current evolutionary models to explain the new data. This thesis suggests that this should be done with great care. Apparently negligible effects, including a small amount of shear and molecular viscosity, can have wide-ranging consequences.

Appendix A

Discussion of self-gravity

In this appendix I elaborate on the Cowling approximation adopted for the model presented in chapter 3. I will first estimate the magnitude of the terms δg_r and δg_θ that have been neglected in equations (3.8) and (3.9), showing that they are relatively small compared to other terms in the same relations. I will then illustrate why it is difficult to solve the problem self-consistently, and discuss a procedure to obtain a solution which is more refined, though still not entirely self-consistent.

A.1 Magnitude of the gravity perturbations

To estimate the magnitude of the δg_r, δg_θ terms that appear in equations (3.8), (3.9), I consider a star with uniform angular velocity Ω and determine the perturbation in the gravitational potential $\delta\Phi$ due to the rotation-induced structural change of the star.

For this purpose only, it is more convenient to expand the pressure and density perturbations in terms of Legendre polynomials $\mathrm{P}_l(\cos\theta)$ rather than in terms of powers of $\cos\theta$ as in equations (3.14), (3.15):

$$\delta P(r,\theta) = P_0(r) + P_2(r)\mathrm{P}_2(\mu), \qquad \delta\rho(r,\theta) = \rho_0(r) + \rho_2(r)\mathrm{P}_2(\mu), \tag{A.1}$$

with $\mu = \cos\theta$. The $P_0(r)$, $P_2(r)$, $\rho_0(r)$, $\rho_2(r)$ terms of this expansion differ from those of an expansion of the form (3.14), (3.15) by a numerical factor of order unity.

Plugging the expressions of equation (A.1) into equations (3.8), (3.9) neglecting the δg_r, δg_θ terms (hence the perturbation in the gravitational potential will not be self-consistent), and grouping the terms proportional to the same Legendre polynomials in each equation, it is possible to derive $P_2(r)$, $\rho_2(r)$. The procedure is analogous to that leading to equations (3.16),

(3.17). The result for the density perturbation is:

$$\rho_2(r) = \frac{1}{3}\frac{\Omega^2 r^2}{g}\frac{d\rho}{dr} \tag{A.2}$$

The perturbation to the gravitational potential in the star is[1]:

$$\delta\Phi(\boldsymbol{r}) = \int -\frac{G\delta\rho(\boldsymbol{r}')}{|\boldsymbol{r}-\boldsymbol{r}'|}d^3\boldsymbol{r}'. \tag{A.3}$$

Using equation (A.2) and retaining only the non spherically symmetric part, this is:

$$\delta\Phi(\boldsymbol{r}) = -\frac{G\Omega^2}{3}\int \frac{r'^2}{g}\frac{d\rho}{dr'}\frac{1}{|\boldsymbol{r}-\boldsymbol{r}'|}\mathrm{P}_2(\mu')d^3\boldsymbol{r}'. \tag{A.4}$$

The integral is calculated by expanding:

$$\frac{1}{|\boldsymbol{r}-\boldsymbol{r}'|} = \sum_{l\geq 0}\frac{r_<^l}{r_>^{l+1}}\Big(\mathrm{P}_l(\mu)\mathrm{P}_l'(\mu') + \mathrm{Q}_l\Big), \tag{A.5}$$

where $r_< = \min(r, r')$, $r_> = \max(r, r')$, and the terms

$$\mathrm{Q}_l = \sum_{m\neq 0}\frac{4\pi}{2l+1}\mathrm{Y}_{lm}^*(\theta,\phi)\mathrm{Y}_{lm}(\theta',\phi'), \tag{A.6}$$

do not contribute to the integral in (A.4). Plugging the expansion (A.5) in equation (A.4) the integral is computed by making use of the Legendre polynomials orthogonality properties as:

$$\delta\Phi = -\frac{4\pi G\Omega^2}{15}\mathrm{P}_2(\mu)\Big(\frac{1}{r^3}\int_0^r \frac{r'^6}{g}\frac{d\rho}{dr'}dr' + r^2\int_r^{R_\odot}\frac{r'}{g}\frac{d\rho}{dr'}dr'\Big). \tag{A.7}$$

I have determined the potential perturbation $\delta\Phi$ assuming the same Solar background structure as in chapter 3 and a uniform angular velocity $\Omega^2 = 7.5\cdot 10^{-12}$ rad s^{-2}. The amplitudes of the resulting gravity perturbations computed from the components of $\boldsymbol{\nabla}\delta\Phi$ at $r = 0.65$ R$_\odot$ and $\mu = 1$ are:

$$|\delta g_r(0.65R_\odot)| = \Big|\frac{\partial\delta\Phi}{\partial r}\Big| = 1.1\cdot 10^{-2}\text{cm s}^{-2}, \tag{A.8}$$

[1]Note: an additional term due to the deformation of the surface of the star would ordinarily contribute to the perturbation to the gravitational potential. This term can be neglected because the density $\rho(\boldsymbol{r})$ is very small at the surface of the star.

$$|\delta g_\theta(0.65R_\odot)| = \left|\frac{1}{r}\frac{\partial\delta\Phi}{\partial\theta}\right| = 1.5\cdot 10^{-2}\text{cm s}^{-2}. \tag{A.9}$$

The ratios of these terms to the penultimate terms in equations (3.8), (3.9) are:

$$\left|\frac{\delta g_r}{g\delta\rho/\rho}\right| = 1\%, \tag{A.10}$$

$$\left|\frac{\delta g_\theta}{(1/(r\rho))(\partial\delta P/\partial\theta)}\right| = 9\%. \tag{A.11}$$

This shows that while the radial self-gravity can safely be neglected, the horizontal one is small but not tiny. The Cowling approximation can be employed in the study of rotating stars, but precision work on their interior structure should be conducted retaining these additional terms.

A.2 Progress towards a self-consistent model

This section discusses the complications that arise when one attempts to solve the problem of chapter 3 self-consistently. I show here that a self-consistent model requires data on $\Omega(\boldsymbol{r})$ not just in the upper radiative zone, but also in the nuclear core of the Sun. Unfortunately, these data are not available. I then proceed to illustrate a procedure to obtain a first-order approximation to the results of chapter 3, building a model that includes a correction to the gravity, though it is still not fully self-consistent. The material presented here is meant to stimulate further thought on the issue of self-gravity; it is not meant to provide a definitive solution to this problem.

To solve the problem self-consistently, one needs to perturb Poisson's equation with the other relations of chapter 3, equations (3.4) - (3.7). Adopting here the same notation, the resulting set of equations is:

$$\Omega^2 r\sin^2\theta - \frac{1}{\rho}\frac{\partial\delta P}{\partial r} - \frac{g}{\rho}\delta\rho + \delta g_r = 0, \tag{A.12}$$

$$\Omega^2 r\sin\theta\cos\theta - \frac{1}{r\rho}\frac{\partial\delta P}{\partial\theta} + \delta g_\theta = 0, \tag{A.13}$$

$$\boldsymbol{\nabla}\cdot(\delta\boldsymbol{F}) = 0, \tag{A.14}$$

$$\frac{\delta T}{T} = \frac{\delta P}{P} - \frac{\delta\rho}{\rho}, \tag{A.15}$$

$$\boldsymbol{\nabla}^2(\delta\phi) = 4\pi G\delta\rho. \tag{A.16}$$

For ease of presentation, the expanded form of equation (A.14) has not been reported here; it is given by equation (3.10).

In order to solve equations (A.12) - (A.16), one needs boundary conditions on the variables $P(r,\theta)$, $\rho(r,\theta)$, $\phi(r,\theta)$, and the first derivatives of $\phi(r,\theta)$. In the solution of the non self-consistent problem in chapter 3 we have used the internal boundary conditions as free parameters to fit the model to the data from helioseismology. There we have seen that a good fit could be achieved. Introducing more free parameters would make the solution even more flexible and possibly render the problem moot. Moreover, it has to be noted that the most natural location in the star at which the boundary conditions on ϕ are imposed is the centre of the star: the gravity at the centre must be zero, so that:

$$\frac{\partial\phi(r,\theta)}{\partial r} = \frac{\partial\phi(r,\theta)}{\partial\theta} = 0. \tag{A.17}$$

There is no guarantee that this condition would be realised if boundary conditions were imposed elsewhere in the star. To assign the correct boundary conditions it would therefore be necessary to solve equations (A.12) - (A.16) in the entire Solar radiative zone, and not just in a shell near the tachocline. This is problematic, because equation (A.14) does not hold in the nuclear core of the Sun: this region is indeed not in radiative equilibrium, because energy is being generated by nuclear fusion. An additional energy generation term would need to be included in the equation. Additionally, the procedure of chapter 3 involves finding solutions for $\Omega_0^2(r)$ and $\Omega_2^2(r)$ that represent a good fit to the data from helioseismology. It is not sensible to do this from the centre of the star to the tachocline: as I have reported in chapter 1, the uncertainty on the observational data in the nuclear core of the Sun nears 100%.

For these reasons, I put forward a solution to this problem that, while not fully self-consistent, constitutes an improved approximation over that presented in chapter 3. I will first solve equations (A.12), (A.13), and (A.16) in the entire Solar radiative zone under the assumption that Ω is uniform and known. Since we have two fewer variables (Ω and δT), we do not need to use equations (A.14) and (A.15). The gravity perturbations δg_r and δg_θ so derived will then later be used to solve equations (A.12) - (A.15) as in chapter 3. This procedure is physically sensible: we know that Ω does not deviate much from its mean value in the Solar radiative zone. The error committed using values of δg_r and δg_θ derived under the assumption of uniform rotation will not be large, and this procedure constitutes an improvement over the simpler assumption $\delta g_r = \delta g_\theta = 0$.

For enhanced clarity, hereafter I express the explicit dependence on r and θ only for the variables for which the system of equations needs to be solved. I will therefore write e.g. Ω for the angular velocity, P for the background pressure, and $\delta P(r,\theta)$ for the pressure perturbation.

Since Ω uniform, the pressure and density need only be expanded to $\cos^2\theta$. I will therefore adopt the expansions:

$$\Omega^2 = \Omega_0^2, \qquad \delta P(r,\theta) = P_0(r) + P_2(r)\cos^2\theta, \qquad \delta\rho(r,\theta) = \rho_0(r) + \rho_2(r)\cos^2\theta. \tag{A.18}$$

The perturbation to the gravitational potential $\delta\phi(r,\theta)$ is also expanded in the same fashion:

$$\delta\phi(r,\theta) = \phi_0(r) + \phi_2(r)\cos^2\theta. \tag{A.19}$$

$\delta\phi(r,\theta)$ is of course related to $\delta g_r(r,\theta)$ and $\delta g_\theta(r,\theta)$ by:

$$\delta g_r(r,\theta) = -\frac{\partial\delta\phi(r,\theta)}{\partial r}, \qquad \delta g_\theta(r,\theta) = -\frac{1}{r}\frac{\partial\delta\phi(r,\theta)}{\partial\theta}. \tag{A.20}$$

Perturbing equation (A.12) and matching the angular terms gives:

$$\Omega_0^2 r - \frac{1}{\rho}P_0'(r) - \frac{g}{\rho}\rho_0(r) - \phi_0'(r) = 0, \tag{A.21}$$

$$-\Omega_0^2 r - \frac{1}{\rho}P_2'(r) - \frac{g}{\rho}\rho_2(r) - \phi_2'(r) = 0, \tag{A.22}$$

where $X'(r)$ is the radial derivative of the quantity X for any X.

Perturbing equation (A.13) and matching the angular terms gives:

$$\Omega_0^2 r + \frac{2}{r\rho}P_2(r) + \frac{2}{r}\phi_2(r) = 0. \tag{A.23}$$

To perturb equation (A.16) one uses the expression of the Laplacian in spherical coordinates, which in the azimuthally symmetric case reads:

$$\boldsymbol{\nabla}^2(\delta\phi(r,\theta)) = \frac{1}{r^2}\frac{\partial}{\partial r}\Big(r^2\frac{\partial(\delta\phi(r,\theta))}{\partial r}\Big) + \frac{1}{r^2\sin\theta}\frac{\partial}{\partial\theta}\Big(\sin\theta\frac{\partial(\delta\phi(r,\theta))}{\partial\theta}\Big). \tag{A.24}$$

Using this in equation (A.16) and matching the angular terms gives:

$$\phi_0''(r) + \frac{2}{r}\phi_0'(r) + \frac{2}{r^2}\phi_2(r) = 4\pi G\rho_0(r), \tag{A.25}$$

$$\phi_2''(r) + \frac{2}{r}\phi_2'(r) - \frac{6}{r^2}\phi_2(r) = 4\pi G\rho_2(r). \tag{A.26}$$

It must be noted that these equations cannot be solved in their entirety, because there are six variables (P_0, P_2, ρ_0, ρ_2, ϕ_0, ϕ_2) and only five equations (A.21 - A.26 excluding A.24). However, equations (A.22), (A.23), and (A.26) allow to solve for P_2, ρ_2, and ϕ_2 independently from the other variables. This is all that is needed here.

To proceed, one extracts $P_2(r)$ and $\rho_2(r)$ from equations (A.22) and (A.23) to reduce

equation (A.26) to an equation in $\phi_2(r)$. The result is:

$$\phi_2''(r) + \frac{2}{r}\phi_2'(r) + \left(\frac{4\pi G\rho'}{g} - \frac{6}{r^2}\right)\phi_2(r) = 2\pi G\rho'\frac{r^2\Omega_0^2}{g}, \tag{A.27}$$

where $\rho' = \rho'(r)$ is the derivative of the background density. It can be verified by explicit substitution that this seemingly complex differential equation has a simple solution:

$$\phi_2(r) = \frac{1}{2}\Omega_0^2 r^2. \tag{A.28}$$

This is the correct solution, because it satisfies the boundary conditions $\phi_2(0) = \phi_2'(0) = 0$, which need to be enforced because $\delta\phi(r,\theta)$ and $\delta\boldsymbol{g}(r,\theta)$ must be single-valued at $r = 0$.

It is now possible to return to the problem of chapter 3, using the potential perturbation we have just computed to calculate δg_r and δg_θ to be used in equations (3.8) and (3.9). From now on, I will label as $\overline{\Omega}$ the mean background angular velocity of rotation and as $\overline{\phi}_2 = \frac{1}{2}\overline{\Omega}^2 r^2$ the gravitational potential perturbation due to it. Matching the angular terms in equation (3.8) leads to:

$$r(\Omega_2^2(r) - \Omega_0^2(r)) - \frac{1}{\rho}P_2'(r) - \frac{g}{\rho}\rho_2(r) - \overline{\phi}_2' = 0, \tag{A.29}$$

$$-r\Omega_2^2(r) - \frac{1}{\rho}P_4'(r) - \frac{g}{\rho}\rho_4(r) = 0. \tag{A.30}$$

Doing the same for equation (3.9) leads to:

$$r\Omega_0^2(r) + \frac{2}{r\rho}P_2(r) + \frac{2}{r}\overline{\phi}_2 = 0, \tag{A.31}$$

$$r\Omega_2^2(r) + \frac{4}{r\rho}P_4(r) = 0. \tag{A.32}$$

Substituting the expression for $\overline{\phi}_2$ and solving for $P_2(r)$, $P_4(r)$, $\rho_2(r)$, and $\rho_4(r)$ gives:

$$P_2(r) = -\frac{1}{2}\rho r^2\Omega_0^2(r) - \frac{1}{2}\rho r^2\overline{\Omega}^2, \tag{A.33}$$

$$P_4(r) = -\frac{1}{4}\rho r^2\Omega_2^2(r), \tag{A.34}$$

$$\rho_2(r) = \frac{\rho r}{g}(\Omega_2^2(r) - \Omega_0^2(r)) - \frac{1}{g}(P_2'(r) + \rho\overline{\Omega}^2 r), \tag{A.35}$$

$$\rho_4(r) = -\frac{\rho r}{g}\Omega_2^2(r) - \frac{1}{g}P_4'(r). \tag{A.36}$$

	Best fit
$\Omega_0^2(r_0)$	$7.4 \cdot 10^{-12}$
$d\Omega_0^2(r_0)/dr$	$8.7 \cdot 10^{-23}$
$d^2\Omega_0^2(r_0)/dr^2$	$-1.8 \cdot 10^{-32}$
$\Omega_2^2(r_0)$	$-2.4 \cdot 10^{-13}$
$d\Omega_2^2(r_0)/dr$	$-5.9 \cdot 10^{-23}$
$d^2\Omega_2^2(r_0)/dr^2$	$-1.2 \cdot 10^{-32}$

Table A.1: Boundary conditions imposed at $r_0 = 0.60$ $R_\odot$ for the solutions of figures A.1 and A.2. The units are in cgs and have been omitted to aid readability.

These expressions replace equations (3.16) and (3.17); it is immediate to see that those equations are recovered in the limit $\overline{\Omega}^2 = 0$. Equation (3.19) still holds and the problem may now be solved exactly as in chapter 3.

I report here the results of such procedure. I have considered a mean background angular velocity $\overline{\Omega} = 2\pi/(27 \text{ days})$, a reasonable approximation for the Solar radiative zone. Just as in section 3.3, it is possible to set boundary conditions for Ω_0^2, Ω_2^2 and their derivatives at $r_0 = 0.60$ $R_\odot$ such that the solution constitutes a good approximation to the data from helioseismology. The fit has been executed by performing a χ^2 minimization around the solution of chapter 3. The resulting boundary conditions are not too dissimilar to those presented in the first column of table 3.1 and they are reported in table A.1. The angular velocity terms $\Omega_0^2(r)$ and $\Omega_2^2(r)$ for this radiative solution are shown as the dashed lines in figures A.1 and A.2 along with the GONG data.

The curves for Ω_0^2 and Ω_2^2 in the scenario with the gravity correction are very similar to those represented in figures 3.3 and 3.4. This again suggests that self-gravity does not play a crucial role in the solution of this problem. Nonetheless, it would be desirable to achieve a fully self-consistent solution.

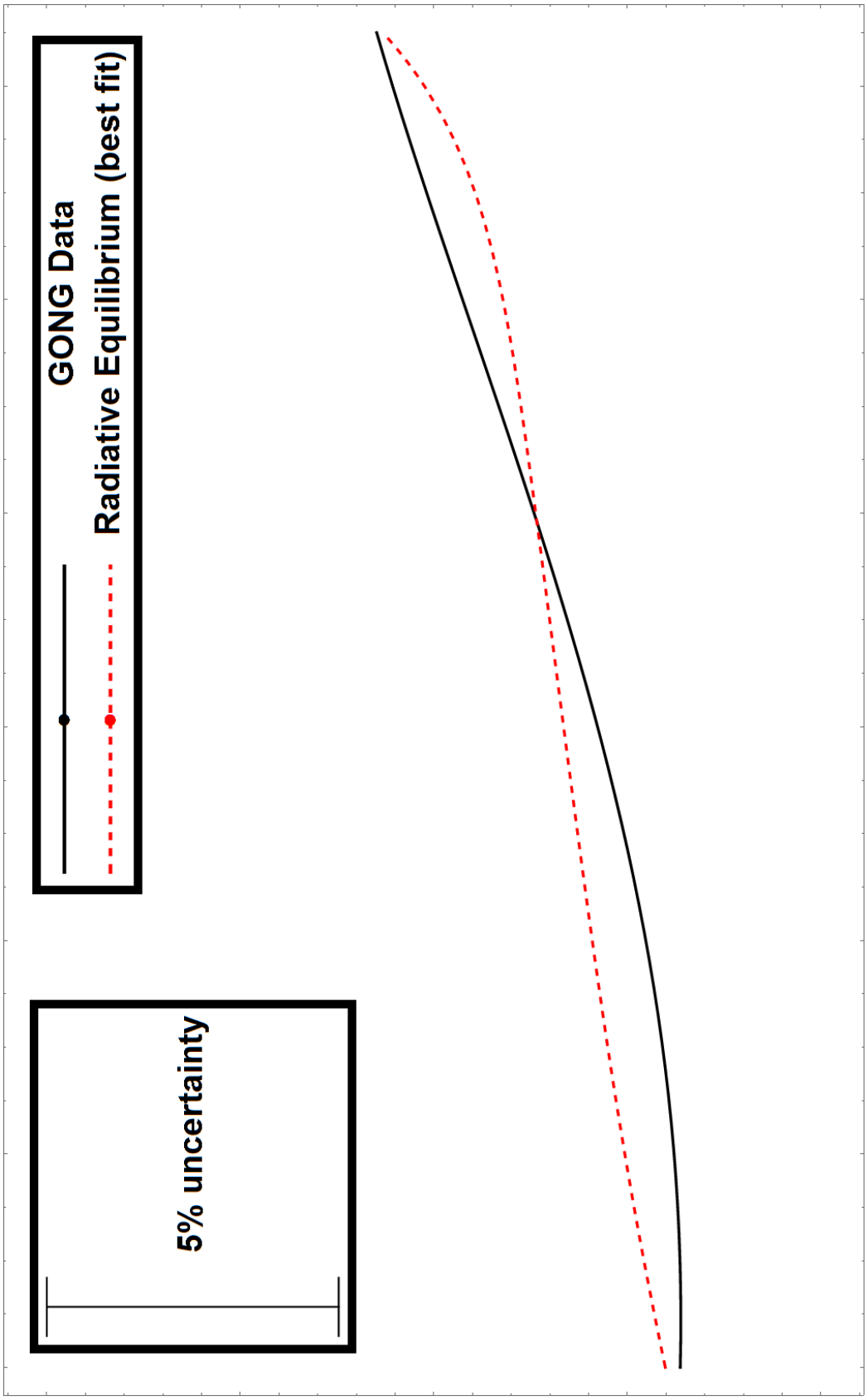

Figure A.1: Angular velocity term $\Omega_0^2(r)$ in the outer part of the radiative zone according to the GONG data (solid line) and to the gravity-corrected model in radiative equilibrium that best fits the data (dashed line). The boundary conditions at $r_0 = 0.60$ $R_\odot$ are illustrated in table A.1. An error bar corresponding to a relative uncertainty of about 5% at the tachocline is shown, although the actual error is probably larger.

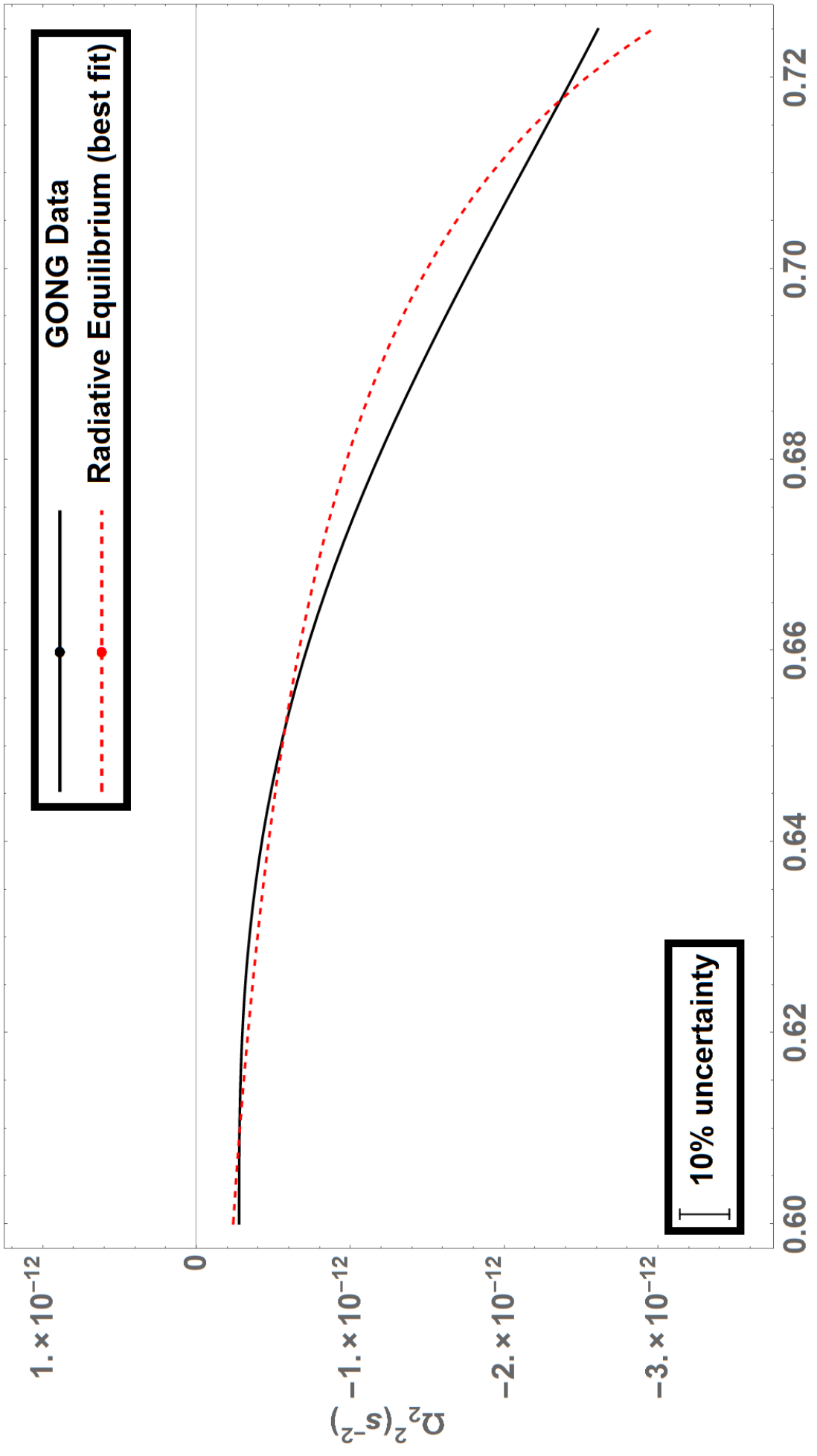

Figure A.2: Angular velocity term $\Omega_2^2(r)$ in the outer part of the radiative zone according to the GONG data (solid line) and to the gravity-corrected model in radiative equilibrium that best fits the data (dashed line). The boundary conditions at $r_0 = 0.60$ R$_\odot$ are illustrated in table A.1. An error bar corresponding to a relative uncertainty of about 10% at the tachocline is shown, although the actual error is probably larger.

References

L. A. Acevedo-Arreguin, P. Garaud, and T. S. Wood. Dynamics of the solar tachocline - III. Numerical solutions of the Gough and McIntyre model. *MNRAS*, 434:720–741, September 2013. doi: 10.1093/mnras/stt1065. 28

D. J. Acheson. On the instability of toroidal magnetic fields and differential rotation in stars. *Phil. Trans. R. Soc. Ser. A*, 289:459–500, June 1978. doi: 10.1098/rsta.1978.0066. 30, 32, 35, 46, 73

D. J. Acheson. *Elementary Fluid Dynamics*. Oxford University Press, 1990. 9, 24

C. Aerts, J. Christensen-Dalsgaard, and D. W. Kurtz. *Asteroseismology (Springer)*. 2010. 7

H. M. Antia and S. Basu. Revisiting the Solar Tachocline: Average Properties and Temporal Variations. *ApJL*, 735:L45, July 2011. doi: 10.1088/2041-8205/735/2/L45. 10, 39

G. Backus and F. Gilbert. Uniqueness in the Inversion of Inaccurate Gross Earth Data. *Philosophical Transactions of the Royal Society of London Series A*, 266:123–192, March 1970. doi: 10.1098/rsta.1970.0005. 7

J. N. Bahcall, A. M. Serenelli, and S. Basu. New Solar Opacities, Abundances, Helioseismology, and Neutrino Fluxes. *ApJL*, 621:L85–L88, March 2005. doi: 10.1086/428929. 44, 45, 59, 77

S. A. Balbus. General Local Stability Criteria for Stratified, Weakly Magnetized Rotating Systems. *ApJ*, 453:380, November 1995. doi: 10.1086/176397. 30, 34, 46, 59

S. A. Balbus and J. F. Hawley. A powerful local shear instability in weakly magnetized disks. I - Linear analysis. II - Nonlinear evolution. *ApJ*, 376:214–233, July 1991. doi: 10.1086/170270. 30

S. A. Balbus and E. Schaan. The stability of stratified, rotating systems and the generation of vorticity in the Sun. *MNRAS*, 426:1546–1557, October 2012. doi: 10.1111/j.1365-2966.2012.21729.x. 31, 32, 38, 42, 53, 78

S. A. Balbus, J. Bonart, H. N. Latter, and N. O. Weiss. Differential rotation and convection in the Sun. *MNRAS*, 400:176–182, November 2009. doi: 10.1111/j.1365-2966.2009.15464.x. 9, 37

P. G. Beck, T. R. Bedding, B. Mosser, D. Stello, R. A. Garcia, T. Kallinger, S. Hekker, Y. Elsworth, S. Frandsen, F. Carrier, J. De Ridder, C. Aerts, T. R. White, D. Huber, M.-A. Dupret, J. Montalbán, A. Miglio, A. Noels, W. J. Chaplin, H. Kjeldsen, J. Christensen-Dalsgaard, R. L. Gilliland, T. M. Brown, S. D. Kawaler, S. Mathur, and J. M. Jenkins. Kepler Detected Gravity-Mode Period Spacings in a Red Giant Star. *Science*, 332:205, April 2011. doi: 10.1126/science.1201939. 6, 11

P. G. Beck, J. Montalban, T. Kallinger, J. De Ridder, C. Aerts, R. A. García, S. Hekker, M.-A. Dupret, B. Mosser, P. Eggenberger, D. Stello, Y. Elsworth, S. Frandsen, F. Carrier, M. Hillen, M. Gruberbauer, J. Christensen-Dalsgaard, A. Miglio, M. Valentini, T. R. Bedding, H. Kjeldsen, F. R. Girouard, J. R. Hall, and K. A. Ibrahim. Fast core rotation in red-giant stars as revealed by gravity-dominated mixed modes. *Nature*, 481:55–57, January 2012. doi: 10.1038/nature10612. 12

T. R. Bedding, D. Huber, D. Stello, Y. P. Elsworth, S. Hekker, T. Kallinger, S. Mathur, B. Mosser, H. L. Preston, J. Ballot, C. Barban, A. M. Broomhall, D. L. Buzasi, W. J. Chaplin, R. A. García, M. Gruberbauer, S. J. Hale, J. De Ridder, S. Frandsen, W. J. Borucki, T. Brown, J. Christensen-Dalsgaard, R. L. Gilliland, J. M. Jenkins, H. Kjeldsen, D. Koch, K. Belkacem, L. Bildsten, H. Bruntt, T. L. Campante, S. Deheuvels, A. Derekas, M.-A. Dupret, M.-J. Goupil, A. Hatzes, G. Houdek, M. J. Ireland, C. Jiang, C. Karoff, L. L. Kiss, Y. Lebreton, A. Miglio, J. Montalbán, A. Noels, I. W. Roxburgh, V. Sangaralingam, I. R. Stevens, M. D. Suran, N. J. Tarrant, and A. Weiss. Solar-like Oscillations in Low-luminosity Red Giants: First Results from Kepler. *ApJL*, 713:L176–L181, April 2010. doi: 10.1088/2041-8205/713/2/L176. 6, 11

K. Belkacem, J. P. Marques, M. J. Goupil, B. Mosser, T. Sonoi, R. M. Ouazzani, M. A. Dupret, S. Mathis, and M. Grosjean. Angular momentum redistribution by mixed modes in evolved low-mass stars. II. Spin-down of the core of red giants induced by mixed modes. *A&A*, 579:A31, July 2015a. doi: 10.1051/0004-6361/201526043. 14, 28, 74

K. Belkacem, J. P. Marques, M. J. Goupil, T. Sonoi, R. M. Ouazzani, M. A. Dupret, S. Mathis, B. Mosser, and M. Grosjean. Angular momentum redistribution by mixed modes in evolved low-mass stars. I. Theoretical formalism. *A&A*, 579:A30, July 2015b. doi: 10.1051/0004-6361/201526042. 28

E. Böhm-Vitense. Über die Wasserstoffkonvektionszone in Sternen verschiedener Effektivtemperaturen und Leuchtkräfte. Mit 5 Textabbildungen. *ZAp*, 46:108, 1958. 74

J. Braithwaite. The stability of toroidal fields in stars. *A&A*, 453:687–698, July 2006. doi: 10.1051/0004-6361:20041282. 14

J. Braithwaite. Axisymmetric magnetic fields in stars: relative strengths of poloidal and toroidal components. *MNRAS*, 397:763–774, August 2009. doi: 10.1111/j.1365-2966.2008.14034.x. 62

I. Brott, S. E. de Mink, M. Cantiello, N. Langer, A. de Koter, C. J. Evans, I. Hunter, C. Trundle, and J. S. Vink. Rotating massive main-sequence stars. I. Grids of evolutionary models and isochrones. *A&A*, 530:A115, June 2011a. doi: 10.1051/0004-6361/201016113. 17

I. Brott, C. J. Evans, I. Hunter, A. de Koter, N. Langer, P. L. Dufton, M. Cantiello, C. Trundle, D. J. Lennon, S. E. de Mink, S.-C. Yoon, and P. Anders. Rotating massive main-sequence stars. II. Simulating a population of LMC early B-type stars as a test of rotational mixing. *A&A*, 530:A116, June 2011b. doi: 10.1051/0004-6361/201016114. 17

A. S. Brun and J.-P. Zahn. Magnetic confinement of the solar tachocline. *A&A*, 457:665–674, October 2006. doi: 10.1051/0004-6361:20053908. 28

A. S. Brun, M. S. Miesch, and J. Toomre. Modeling the Dynamical Coupling of Solar Convection with the Radiative Interior. *ApJ*, 742:79, December 2011. doi: 10.1088/0004-637X/742/2/79. 9, 39, 40

A. Caleo and S. A. Balbus. The radiative zone of the Sun and the tachocline: stability of baroclinic patterns of differential rotation. *MNRAS*, 457:1711–1721, April 2016. doi: 10.1093/mnras/stw098.

A. Caleo, S. A. Balbus, and W. J. Potter. Differential rotation and radiative equilibrium in the Sun: is the tachocline spreading? *MNRAS*, 448:2077–2084, April 2015. doi: 10.1093/mnras/stv115.

A. Caleo, S. A. Balbus, and E. Tognelli. The Goldreich-Schubert-Fricke instability in stellar radiative zones. *MNRAS*, 460:338–344, July 2016. doi: 10.1093/mnras/stw1002.

M. Cantiello, C. Mankovich, L. Bildsten, J. Christensen-Dalsgaard, and B. Paxton. Angular Momentum Transport within Evolved Low-mass Stars. *ApJ*, 788:93, June 2014. doi: 10.1088/0004-637X/788/1/93. 14, 15, 73

M. Cantiello, J. Fuller, and L. Bildsten. Asteroseismic Signatures of Evolving Internal Stellar Magnetic Fields. *ApJ*, 824:14, June 2016. doi: 10.3847/0004-637X/824/1/14. 92

C. Charbonnel and S. Talon. Influence of Gravity Waves on the Internal Rotation and Li Abundance of Solar-Type Stars. *Science*, 309:2189–2191, September 2005a. doi: 10.1126/science.1116849. 28

C. Charbonnel and S. Talon. Influence of Gravity Waves on the Internal Rotation and Li Abundance of Solar-Type Stars. *Science*, 309:2189–2191, September 2005b. doi: 10.1126/science.1116849. 14

S. Charpinet, G. Fontaine, and P. Brassard. Seismic evidence for the loss of stellar angular momentum before the white-dwarf stage. *Nature*, 461:501–503, September 2009. doi: 10.1038/nature08307. 6, 13

J. Christensen-Dalsgaard. *Lecture Notes on Stellar Oscillations.* Fifth edition. Aarhus University, 2003. 4

J. Christensen-Dalsgaard and M. J. Thompson. *Observational results and issues concerning the tachocline, in The Solar Tachocline, editors Hughes D., Rosner R., Weiss N., Cambridge Univ. Press, Cambridge, p. 53.* 2007. 9, 91

J. Christensen-Dalsgaard, J. Schou, and M. J. Thompson. A comparison of methods for inverting helioseismic data. *MNRAS*, 242:353–369, February 1990. doi: 10.1093/mnras/242.3.353. 7

T. G. Cowling. The non-radial oscillations of polytropic stars. *MNRAS*, 101:367, 1941. doi: 10.1093/mnras/101.8.367. 20, 41

S. Deheuvels, R. A. García, W. J. Chaplin, S. Basu, H. M. Antia, T. Appourchaux, O. Benomar, G. R. Davies, Y. Elsworth, L. Gizon, M. J. Goupil, D. R. Reese, C. Regulo, J. Schou, T. Stahn, L. Casagrande, J. Christensen-Dalsgaard, D. Fischer, S. Hekker, H. Kjeldsen, S. Mathur, B. Mosser, M. Pinsonneault, J. Valenti, J. L. Christiansen, K. Kinemuchi, and F. Mullally. Seismic Evidence for a Rapidly Rotating Core in a Lower-giant-branch Star Observed with Kepler. *ApJ*, 756:19, September 2012. doi: 10.1088/0004-637X/756/1/19. 12

S. Deheuvels, G. Doğan, M. J. Goupil, T. Appourchaux, O. Benomar, H. Bruntt, T. L. Campante, L. Casagrande, T. Ceillier, G. R. Davies, P. De Cat, J. N. Fu, R. A. García, A. Lobel, B. Mosser, D. R. Reese, C. Regulo, J. Schou, T. Stahn, A. O. Thygesen, X. H. Yang, W. J. Chaplin, J. Christensen-Dalsgaard, P. Eggenberger, L. Gizon, S. Mathis, J. Molenda-Żakowicz, and M. Pinsonneault. Seismic constraints on the radial dependence of the internal rotation profiles of six Kepler subgiants and young red giants. *A&A*, 564:A27, April 2014. doi: 10.1051/0004-6361/201322779. 12, 13, 76

F.-L. Deubner. Observations of low wavenumber nonradial eigenmodes of the sun. *A&A*, 44: 371–375, November 1975. 3

R. H. Dicke. The Sun's Rotation and Relativity. *Nature*, 202:432–435, May 1964. doi: 10.1038/202432a0. 33

M.-A. Dupret, K. Belkacem, R. Samadi, J. Montalban, O. Moreira, A. Miglio, M. Godart, P. Ventura, H.-G. Ludwig, A. Grigahcène, M.-J. Goupil, A. Noels, and E. Caffau. Theoretical amplitudes and lifetimes of non-radial solar-like oscillations in red giants. *A&A*, 506: 57–67, October 2009. doi: 10.1051/0004-6361/200911713. 11

A. S. Eddington. Circulating currents in rotating stars. *The Observatory*, 48:73–75, March 1925. 13, 22

A. Eff-Darwich and S. G. Korzennik. The Dynamics of the Solar Radiative Zone. *Solar Physics*, 287:43–56, October 2013. doi: 10.1007/s11207-012-0048-z. 11

J. R. Elliott. Aspects of the solar tachocline. *A&A*, 327:1222–1229, November 1997. 28

A. S. Endal and S. Sofia. The evolution of rotating stars. II - Calculations with time-dependent redistribution of angular momentum for 7- and 10-solar-mass stars. *ApJ*, 220:279–290, February 1978. doi: 10.1086/155904. 35

K. Fricke. Instabilität stationärer Rotation in Sternen. *Z. Astrophys.*, 68:317, 1968. 13, 30, 33

J. Fuller, D. Lecoanet, M. Cantiello, and B. Brown. Angular Momentum Transport via Internal Gravity Waves in Evolving Stars. *ApJ*, 796:17, November 2014. doi: 10.1088/0004-637X/796/1/17. 14, 28

G. Galilei, M. Welser, and A. de Filiis. *Istoria e dimostrazioni intorno alle macchie solari e loro accidenti*. 1613. 2

L. Gizon and A. C. Birch. Local Helioseismology. *Living Reviews in Solar Physics*, 2, November 2005. doi: 10.12942/lrsp-2005-6. 3

P. Goldreich and D. Lynden-Bell. II. Spiral arms as sheared gravitational instabilities. *MNRAS*, 130:125, 1965. 31

P. Goldreich and G. Schubert. Differential Rotation in Stars. *ApJ*, 150:571, November 1967. doi: 10.1086/149360. 13, 30, 33, 46, 61

D. O. Gough. Some Glimpses from Helioseismology at the Dynamics of the Deep Solar Interior. *SSR*, 196:15–47, December 2015. doi: 10.1007/s11214-015-0159-6. 27

D. O. Gough and M. E. McIntyre. Inevitability of a magnetic field in the Sun's radiative interior. *Nature*, 394:755–757, August 1998. doi: 10.1038/29472. 10, 28

J. W. Harvey, F. Hill, R. P. Hubbard, J. R. Kennedy, J. W. Leibacher, J. A. Pintar, P. A. Gilman, R. W. Noyes, A. M. Title, J. Toomre, R. K. Ulrich, A. Bhatnagar, J. A. Kennewell, W. Marquette, J. Patron, O. Saa, and E. Yasukawa. The Global Oscillation Network Group (GONG) Project. *Science*, 272:1284–1286, May 1996. doi: 10.1126/science.272.5266.1284. 4

A. Heger, N. Langer, and S. E. Woosley. Presupernova Evolution of Rotating Massive Stars. I. Numerical Method and Evolution of the Internal Stellar Structure. *ApJ*, 528:368–396, January 2000. doi: 10.1086/308158. 14

A. Heger, S. E. Woosley, and H. C. Spruit. Presupernova Evolution of Differentially Rotating Massive Stars Including Magnetic Fields. *ApJ*, 626:350–363, June 2005. doi: 10.1086/429868. 14

F. Herwig, N. Langer, and M. Lugaro. The s-Process in Rotating Asymptotic Giant Branch Stars. *ApJ*, 593:1056–1073, August 2003. doi: 10.1086/376726. 73

F. Hill and et al. The Solar Acoustic Spectrum and Eigenmode Parameters. *Science*, 272: 1292–1295, May 1996. doi: 10.1126/science.272.5266.1292. 4, 41, 60

R. Hirschi and A. Maeder. The GSF instability and turbulence do not account for the relatively low rotation rate of pulsars. *A&A*, 519:A16, September 2010. doi: 10.1051/0004-6361/201014222. 73

R. Howe. Solar Interior Rotation and its Variation. *Living Reviews in Solar Physics*, 6:1, February 2009. doi: 10.12942/lrsp-2009-1. 3, 4, 5, 8, 10

D. W. Hughes, R. Rosner, and N. O. Weiss. *The Solar Tachocline, Cambridge Univ. Press.* May 2007. 10, 27

C. A. Iglesias and F. J. Rogers. Updated Opal Opacities. *ApJ*, 464:943, June 1996. doi: 10.1086/177381. 44, 61

H. A. James and F. D. Kahn. Non-Linear Limiting of the Goidreich-Schubert Instability. *A&A*, 5:232, April 1970. 35, 73

R. A. James and F. D. Kahn. Angular Momentum Transport in Stars, Following the Goldreich-Schubert Instability. *A&A*, 12:332, June 1971. 35, 73

L. Jouve, T. Gastine, and F. Lignières. Three-dimensional evolution of magnetic fields in a differentially rotating stellar radiative zone. *A&A*, 575:A106, March 2015. doi: 10.1051/0004-6361/201425240. 14

D. Kagan and J. C. Wheeler. The Role of the Magnetorotational Instability in the Sun. *ApJ*, 787:21, May 2014. doi: 10.1088/0004-637X/787/1/21. 32, 64

R. Kippenhahn. Secularly Unstable Differential Rotation in Stars. *A&A*, 2:309, July 1969. 35

R. Kippenhahn. Circulation and Mixing. In R. J. Tayler and J. E. Hesser, editors, *Late Stages of Stellar Evolution*, volume 66 of *IAU Symposium*, 1974. 13, 35

R. Kippenhahn, A. Weigert, and A. Weiss. *Stellar Structure and Evolution, Springer-Verlag.* 2012. doi: 10.1007/978-3-642-30304-3. 18, 19, 22, 33

E. Knobloch and H. C. Spruit. Stability of differential rotation in stars. *A&A*, 113:261–268, September 1982. 35, 73

E. Knobloch and H. C. Spruit. The molecular weight barrier and angular momentum transport in radiative stellar interiors. *A&A*, 125:59–68, August 1983. 35

P. K. Kundu, I. M. Cohen, and D. R Dowling. *Fluid Mechanics (Elsevier).* 2012. 54

D. W. Kurtz, H. Saio, M. Takata, H. Shibahashi, S. J. Murphy, and T. Sekii. Asteroseismic measurement of surface-to-core rotation in a main-sequence A star, KIC 11145123. *MNRAS*, 444:102–116, October 2014. doi: 10.1093/mnras/stu1329. 13

N. Langer. Presupernova Evolution of Massive Single and Binary Stars. *ARA&A*, 50:107–164, September 2012. doi: 10.1146/annurev-astro-081811-125534. 15, 17

R. B. Leighton, R. W. Noyes, and G. W. Simon. Velocity Fields in the Solar Atmosphere. I. Preliminary Report. *ApJ*, 135:474, March 1962. doi: 10.1086/147285. 4

Y. Masada, T. Sano, and K. Shibata. The Effect of Neutrino Radiation on Magnetorotational Instability in Proto-Neutron Stars. *ApJ*, 655:447–457, January 2007. doi: 10.1086/509799. 32

M. E. McIntyre. *Solar tachocline dynamics: eddy viscosity, anti-friction, or something in between?, in Stellar Astrophysical Fluid Dynamics, editors Thompson, M. and Christensen-Dalsgaard, J., Cambridge Univ. Press.* 2003. 28

K. Menou and J. Le Mer. Magnetorotational Transport in the Early Sun. *ApJ*, 650:1208–1216, October 2006. doi: 10.1086/507022. 29, 31, 91

K. Menou, S. A. Balbus, and H. C. Spruit. Local Axisymmetric Diffusive Stability of Weakly Magnetized, Differentially Rotating, Stratified Fluids. *ApJ*, 607:564–574, May 2004. doi: 10.1086/383463. 30, 33, 35, 46, 53, 73

L. Mestel. *Stellar magnetism, second edition, Oxford University Press.* 1999. 25, 30

G. Meynet and A. Maeder. Stellar evolution with rotation. I. The computational method and the inhibiting effect of the μ-gradient. *A&A*, 321:465–476, May 1997. 34

M. S. Miesch, A. S. Brun, and J. Toomre. Solar Differential Rotation Influenced by Latitudinal Entropy Variations in the Tachocline. *ApJ*, 641:618–625, April 2006. doi: 10.1086/499621. 39

B. Mosser, K. Belkacem, M.-J. Goupil, A. Miglio, T. Morel, C. Barban, F. Baudin, S. Hekker, R. Samadi, J. De Ridder, W. Weiss, M. Auvergne, and A. Baglin. Red-giant seismic properties analyzed with CoRoT. *A&A*, 517:A22, July 2010. doi: 10.1051/0004-6361/201014036. 11

B. Mosser, C. Barban, J. Montalbán, P. G. Beck, A. Miglio, K. Belkacem, M. J. Goupil, S. Hekker, J. De Ridder, M. A. Dupret, Y. Elsworth, A. Noels, F. Baudin, E. Michel, R. Samadi, M. Auvergne, A. Baglin, and C. Catala. Mixed modes in red-giant stars observed with CoRoT. *A&A*, 532:A86, August 2011. doi: 10.1051/0004-6361/201116825. 11

B. Mosser, M. J. Goupil, K. Belkacem, J. P. Marques, P. G. Beck, S. Bloemen, J. De Ridder, C. Barban, S. Deheuvels, Y. Elsworth, S. Hekker, T. Kallinger, R. M. Ouazzani, M. Pinsonneault, R. Samadi, D. Stello, R. A. García, T. C. Klaus, J. Li, S. Mathur, and R. L. Morris. Spin down of the core rotation in red giants. *A&A*, 548:A10, December 2012. doi: 10.1051/0004-6361/201220106. 12, 15

Y. Osaki. Meridional Circulation in a Rotating Star. *PASJ*, 24:509, 1972. 25

K. P. Parfrey and K. Menou. The Origin of Solar Activity in the Tachocline. *ApJL*, 667: L207–L210, October 2007. doi: 10.1086/522426. 32

E. N. Parker. *Cosmical magnetic fields (New York: Oxford Univ. Press)*. 1979. 30

B. Paxton, M. Cantiello, P. Arras, L. Bildsten, E. F. Brown, A. Dotter, C. Mankovich, M. H. Montgomery, D. Stello, F. X. Timmes, and R. Townsend. Modules for Experiments in Stellar Astrophysics (MESA): Planets, Oscillations, Rotation, and Massive Stars. *ApJS*, 208:4, September 2013. doi: 10.1088/0067-0049/208/1/4. 14, 35

L. Piersanti, S. Cristallo, and O. Straniero. The Effects of Rotation on s-process Nucleosynthesis in Asymptotic Giant Branch Stars. *ApJ*, 774:98, September 2013. doi: 10.1088/0004-637X/774/2/98. 73

N. Przybilla, M. Firnstein, M. F. Nieva, G. Meynet, and A. Maeder. Mixing of CNO-cycled matter in massive stars. *A&A*, 517:A38, July 2010. doi: 10.1051/0004-6361/201014164. 16

G. Randers. Large-Scale Motion in Stars. *ApJ*, 94:109, July 1941. doi: 10.1086/144316. 25

T. M. Rogers. On Limiting the Thickness of the Solar Tachocline. *ApJ*, 733:12, May 2011. doi: 10.1088/0004-637X/733/1/12. 39, 40

H. Saio, D. W. Kurtz, M. Takata, H. Shibahashi, S. J. Murphy, T. Sekii, and T. R. Bedding. Asteroseismic measurement of slow, nearly uniform surface-to-core rotation in the main-sequence F star KIC 9244992. *MNRAS*, 447:3264–3277, March 2015. doi: 10.1093/mnras/stu2696. 13

J. Schou, J. Christensen-Dalsgaard, and M. J. Thompson. On comparing helioseismic two-dimensional inversion methods. *ApJ*, 433:389–416, September 1994. doi: 10.1086/174653. 6, 7

M. Schwarzschild. *Structure and Evolution of the Stars, Dover Publications*. 1958. 19, 20, 24, 61

G. Shajn and O. Struve. On the rotation of the stars. *MNRAS*, 89:222–239, January 1929. doi: 10.1093/mnras/89.3.222. 3

L. Siess, S. Goriely, and N. Langer. Nucleosynthesis of s-elements in rotating AGB stars. *A&A*, 415:1089–1097, March 2004. doi: 10.1051/0004-6361:20034281. 73

E. A. Spiegel and G. Veronis. On the Boussinesq Approximation for a Compressible Fluid. *ApJ*, 131:442, March 1960. doi: 10.1086/146849. 54

E. A. Spiegel and J.-P. Zahn. The solar tachocline. *A&A*, 265:106–114, November 1992. 10, 25, 26, 28, 39, 40, 45, 68

L. Spitzer. *Physics of Fully Ionized Gases (New York: Wiley)*. 1962. 61, 75

H. C. Spruit. Dynamo action by differential rotation in a stably stratified stellar interior. *A&A*, 381:923–932, January 2002. doi: 10.1051/0004-6361:20011465. 14

J. Squire and A. Bhattacharjee. Nonmodal Growth of the Magnetorotational Instability. *Physical Review Letters*, 113(2):025006, July 2014. doi: 10.1103/PhysRevLett.113.025006. 64

A. Strugarek , A. S. Brun, and J.-P. Zahn. Magnetic confinement of the solar tachocline: The oblique dipole. *Astronomische Nachrichten*, 332:891, December 2011. doi: 10.1002/asna.201111613. 28

P. A. Sweet. The importance of rotation in stellar evolution. *MNRAS*, 110:548, 1950. doi: 10.1093/mnras/110.6.548. 22

J.-L. Tassoul. *Stellar Rotation, Cambridge University Press*. April 2000. 3, 22, 25, 29

R. J. Tayler. The adiabatic stability of stars containing magnetic fields-I.Toroidal fields. *MNRAS*, 161:365, 1973. 14

L. H. Thomas. The radiation field in a fluid in motion. *The Quarterly Journal of Mathematics*, 1:239–251, 1930. doi: 10.1093/qmath/os-1.1.239. 75

M. J. Thompson, J. Christensen-Dalsgaard, M. S. Miesch, and J. Toomre. The Internal Rotation of the Sun. *ARA&A*, 41:599–643, 2003. doi: 10.1146/annurev.astro.41.011802.094848. 8

E. Tognelli, S. Degl'Innocenti, and P. G. Prada Moroni. ^{7}Li surface abundance in pre-main sequence stars. Testing theory against clusters and binary systems. *A&A*, 548:A41, December 2012. doi: 10.1051/0004-6361/201219111. 74

E. Tognelli, P. G. Prada Moroni, and S. Degl'Innocenti. Cumulative theoretical uncertainties in lithium depletion boundary age. *MNRAS*, 449:3741–3754, June 2015. doi: 10.1093/mnras/stv577. 74

L. N. Trefethen and M. Embree. *Spectra and Pseudospectra, The Behavior of Nonnormal Matrices and Operators (Princeton University Press)*. 2005. 64

R. K. Ulrich. The Five-Minute Oscillations on the Solar Surface. *ApJ*, 162:993, December 1970. doi: 10.1086/150731. 4

H. von Zeipel. The radiative equilibrium of a rotating system of gaseous masses. *MNRAS*, 84: 665–683, June 1924. doi: 10.1093/mnras/84.9.665. 19

T. S. Wood and M. E. McIntyre. Polar confinement of the Sun's interior magnetic field by laminar magnetostrophic flow. *Journal of Fluid Mechanics*, 677:445–482, June 2011. doi: 10.1017/jfm.2011.93. 91

J. P. Zahn. Differential Rotation and Turbulence in Stars. *Memoires of the Societe Royale des Sciences de Liege*, 8:31–34, 1975. 29, 91

J.-P. Zahn. *Hydrodynamic models of the tachocline, in The Solar Tachocline, editors Hughes D., Rosner R., Weiss N., Cambridge Univ. Press.* 2007. 25, 28, 39

J.-P. Zahn, A. S. Brun, and S. Mathis. On magnetic instabilities and dynamo action in stellar radiation zones. *A&A*, 474:145–154, October 2007. doi: 10.1051/0004-6361:20077653. 14